

International Telecommunication Union

ITU-R
Radiocommunication Sector of ITU

Report ITU-R M.2412-0
(10/2017)

**Guidelines for evaluation of radio interface
technologies for IMT-2020**

M Series
**Mobile, radiodetermination, amateur
and related satellite services**



International
Telecommunication
Union

Foreword

The role of the Radiocommunication Sector is to ensure the rational, equitable, efficient and economical use of the radio-frequency spectrum by all radiocommunication services, including satellite services, and carry out studies without limit of frequency range on the basis of which Recommendations are adopted.

The regulatory and policy functions of the Radiocommunication Sector are performed by World and Regional Radiocommunication Conferences and Radiocommunication Assemblies supported by Study Groups.

Policy on Intellectual Property Right (IPR)

ITU-R policy on IPR is described in the Common Patent Policy for ITU-T/ITU-R/ISO/IEC referenced in Annex 1 of Resolution ITU-R 1. Forms to be used for the submission of patent statements and licensing declarations by patent holders are available from <http://www.itu.int/ITU-R/go/patents/en> where the Guidelines for Implementation of the Common Patent Policy for ITU-T/ITU-R/ISO/IEC and the ITU-R patent information database can also be found.

Series of ITU-R Reports

(Also available online at <http://www.itu.int/publ/R-REP/en>)

Series	Title
BO	Satellite delivery
BR	Recording for production, archival and play-out; film for television
BS	Broadcasting service (sound)
BT	Broadcasting service (television)
F	Fixed service
M	Mobile, radiodetermination, amateur and related satellite services
P	Radiowave propagation
RA	Radio astronomy
RS	Remote sensing systems
S	Fixed-satellite service
SA	Space applications and meteorology
SF	Frequency sharing and coordination between fixed-satellite and fixed service systems
SM	Spectrum management

Note: This ITU-R Report was approved in English by the Study Group under the procedure detailed in Resolution ITU-R 1.

Electronic Publication
Geneva, 2017

© ITU 2017

All rights reserved. No part of this publication may be reproduced, by any means whatsoever, without written permission of ITU.

REPORT ITU-R M.2412-0

Guidelines for evaluation of radio interface technologies for IMT-2020

(2017)

TABLE OF CONTENTS

	<i>Page</i>
1 Introduction	3
2 Scope	4
3 Structure of the Report	5
4 Related ITU-R documents	5
5 Evaluation guidelines	5
6 Overview of characteristics for evaluation.....	6
7 Evaluation methodology.....	7
7.1 System simulation procedures	8
7.2 Analytical approach	13
7.3 Inspection approach	15
8 Test environments and evaluation configurations.....	16
8.1 Usage scenarios	16
8.2 Test environments.....	16
8.3 Network layout	17
8.4 Evaluation configurations.....	19
8.5 Antenna characteristics.....	30
9 Evaluation model approach	34
9.1 Channel model approach	34
10 List of acronyms and abbreviations.....	37
Annex 1 Test Environments and Channel Models.....	38
1 Test environments and mapping to channel model scenario.....	38
2 Overview of IMT-2020 channel modelling.....	39
2.1 Introduction.....	39
2.2 Advances in channel modelling.....	39
3 Path loss models, LOS probability, shadow fading.....	41

	<i>Page</i>
3.1 Path loss model	41
3.2 Outdoor to indoor (O-to-I) building penetration loss	48
3.3 Car penetration loss	49
3.4 LOS probability	50
4 Fast fading model	50
4.1 General parameter generation.....	53
4.2 Large scale parameter generation	53
4.3 Small scale parameter generation	54
4.4 Channel coefficient generation	58
4.5 Fast fading parameters	60
5 Advanced Modelling Components for IMT-2020 Channel Model	78
5.1 Oxygen absorption.....	79
5.2 Large bandwidth and large antenna array.....	80
5.3 Spatial consistency.....	81
5.4 Blockage	88
5.5 Modeling of inter-frequency correlation of large scale parameters.....	93
5.6 Time-varying Doppler shift	96
5.7 UT rotation.....	97
5.8 Modelling of Ground Reflection	97
5.9 Random cluster number	98
6 Channel models for link-level evaluations	100
6.1 Clustered Delay Line (CDL) models	100
6.2 Tapped Delay Line (TDL) models.....	106
6.3 Scaling of delays.....	108
6.4 Spatial filter for generating TDL channel model.....	109
6.5 Extension for MIMO simulations	110
6.6 K-factor for LOS channel models.....	112
Attachment 1 to Annex 1 Map-based hybrid channel model (alternative channel model methodology).....	115
Attachment 2 to Annex 1 Extension module below 6 GHz (alternative method of generating the channel parameters)	126

1	Large scale parameters	127
1.1	NLOS scenarios	127
1.2	LOS scenarios	128
1.3	XPD	129
1.4	Building penetration loss	129
1.5	Short-term variation	130
1.6	Spreads and their variations of PDP, AOD and AOA in large scale parameters	130
1.7	Threshold parameter	131
1.8	Time-spatial profile in cluster.....	131
2	Generation of reduced variability models based on TSP model	131
2.1	NLOS scenario.....	131
2.2	LOS scenario	134
3	<i>K</i> -factor.....	136
4	Cross polarization.....	136
5	Generation of small scale parameters in clusters.....	136
	Attachment 3 to Annex 1 Channel impulse response generation when using antenna arrays	137
	Annex 2 Linear cell layout configuration for high speed vehicular mobility at 500 km/h under Rural-eMBB test environment	140
1	Network layout	140
2	Additional configuration parameters	141

1 Introduction

Resolution ITU-R 56 defines a new term “IMT-2020” applicable to those systems, system components, and related aspects that provide far more enhanced capabilities than those described in Recommendation ITU-R M.1645.

In this regard, International Mobile Telecommunications-2020 (IMT-2020) systems are mobile systems that include the new capabilities of IMT that go beyond those of IMT-Advanced. Recommendation ITU-R M.2083 – IMT Vision – Framework and overall objectives of the future development of IMT for 2020 and beyond, identifies capabilities for IMT-2020 which would make IMT-2020 more efficient, fast, flexible, and reliable when providing diverse services in the intended usage scenarios.

The usage scenario of IMT-2020 will extend to enhanced mobile broadband (eMBB), massive machine type communications (mMTC) and ultra-reliable and low latency communications (URLLC).

IMT-2020 systems support low to high mobility applications and much enhanced data rates in accordance with user and service demands in multiple user environments. IMT-2020 also has capabilities for enabling massive connections for a wide range of services, and guarantee ultra-reliable and low latency communications for future deployed services even in critical environments.

The capabilities of IMT-2020 include:

- very high peak data rate;
- very high and guaranteed user experienced data rate;
- quite low air interface latency;
- quite high mobility while providing satisfactory quality of service;
- enabling massive connection in very high density scenario;
- very high energy efficiency for network and device side;
- greatly enhanced spectral efficiency;
- significantly larger area traffic capacity;
- high spectrum and bandwidth flexibility;
- ultra high reliability and good resilience capability;
- enhanced security and privacy.

These features enable IMT-2020 to address evolving user and industry needs.

The capabilities of IMT-2020 systems are being continuously enhanced in line with user and industry trends, and consistent with technology developments.

2 Scope

This Report provides guidelines for the procedure, the methodology and the criteria (technical, spectrum and service) to be used in evaluating the candidate IMT-2020 radio interface technologies (RITs) or Set of RITs (SRITs) for a number of test environments. These test environments are chosen to simulate closely the more stringent radio operating environments. The evaluation procedure is designed in such a way that the overall performance of the candidate RITs/SRITs may be fairly and equally assessed on a technical basis. It ensures that the overall IMT-2020 objectives are met.

This Report provides, for proponents, developers of candidate RITs/SRITs and independent evaluation groups, the common evaluation methodology and evaluation configurations to evaluate the candidate RITs/SRITs and system aspects impacting the radio performance.

This Report allows a degree of freedom to encompass new technologies. The actual selection of the candidate RITs/SRITs for IMT-2020 is outside the scope of this Report.

The candidate RITs/SRITs will be assessed based on those evaluation guidelines. If necessary, additional evaluation methodologies may be developed by each independent evaluation group to complement the evaluation guidelines. Any such additional methodology should be shared between independent evaluation groups and sent to the Radiocommunication Bureau as information in the consideration of the evaluation results by ITU-R and for posting under additional information relevant to the independent evaluation group section of the ITU-R IMT-2020 web page (<http://www.itu.int/en/ITU-R/study-groups/rsg5/rwp5d/imt-2020/Pages/submission-eval.aspx>).

3 Structure of the Report

Section 4 provides a list of documents related to this Report.

Section 5 describes the evaluation guidelines.

Section 6 lists the criteria chosen for evaluating the RITs.

Section 7 outlines the procedures and evaluation methodology for evaluating the criteria.

Section 8 defines the tests environments for envisaged usage scenarios for evaluation; the evaluation configurations which shall be applied when evaluating IMT-2020 candidate RITs/SRITs are also given in this section.

Section 9 describes modeling approach for the evaluation.

Section 10 provides a list of acronyms and abbreviations.

Annex 1 provides a description of the channel models used in this Report.

Annex 2 provides a description of linear cell layouts for high speed vehicular mobility at 500 km/h under Rural-eMBB test environment.

4 Related ITU-R documents

Recommendation ITU-R M.2083

Report ITU-R M.2135-1

Report ITU-R M.2320-0

Report ITU-R M.2370-0

Report ITU-R M.2376-0

Resolution ITU-R 56-2

Resolution ITU-R 65

Report ITU-R M.2410-0

Report ITU-R M.2411-0

Document IMT-2020/1

Document IMT-2020/2

5 Evaluation guidelines

IMT-2020 can be considered from multiple perspectives: users, manufacturers, application developers, network operators, service and content providers, and, finally, the usage scenarios – which are extensive. Therefore, candidate RITs/SRITs for IMT-2020 must be capable of being applied in a much broader variety of usage scenarios and supporting a much broader range of environments, significantly more diverse service capabilities as well as technology options. Consideration of every variation to encompass all situations is, however, not possible; nonetheless the work of the ITU-R has been to determine a representative view of IMT-2020 consistent with the process defined in Resolution ITU-R 65 – Principles for the process of future development of IMT-2020 and beyond, and the key technical performance requirements defined in Report ITU-R M.2410-0 – Minimum requirements related to technical performance for IMT-2020 radio interface(s).

The parameters presented in this Report are for the purpose of consistent definition, specification, and evaluation of the candidate RITs/SRITs for IMT-2020 in ITU-R in conjunction with the

development of Recommendations and Reports such as the framework, key characteristics and the detailed specifications of IMT-2020. These parameters have been chosen to be representative of a global view of IMT-2020 but are not intended to be specific to any particular implementation of an IMT-2020 technology. They should not be considered as the values that must be used in any deployment of any IMT-2020 system nor should they be taken as the default values for any other or subsequent study in ITU or elsewhere.

Further consideration has been given in the choice of parameters to balancing the assessment of the technology with the complexity of the simulations while respecting the workload of an evaluator or a technology proponent.

This procedure deals only with evaluating radio interface aspects. It is not intended for evaluating system aspects (including those for satellite system aspects).

The following principles are to be followed when evaluating radio interface technologies for IMT-2020:

- Evaluations of proposals can be through simulation, analytical and inspection procedures.
- The evaluation shall be performed based on the submitted technology proposals, and should follow the evaluation guidelines, using the evaluation methodology and the evaluation configurations defined in this Report.
- Evaluations through simulations contain both system-level and link-level simulations. Independent evaluation groups may use their own simulation tools for the evaluation.
- In case of evaluation through analysis, the evaluation is to be based on calculations which use the technical information provided by the proponent.
- In case of evaluation through inspection the evaluation is to be based on statements in the proposal.

The following options are foreseen for proponents and independent external evaluation groups doing the evaluations.

- Self-evaluation must be a complete evaluation (to provide a fully complete compliance template) of the technology proposal.
- An external evaluation group may perform complete or partial evaluation of one or several technology proposals to assess the compliance of the technologies with the minimum requirements of IMT-2020.
- Evaluations covering several technology proposals are encouraged.

6 Overview of characteristics for evaluation

The characteristics chosen for evaluation are explained in detail in § 3 of Report ITU-R M.[IMT-2020.SUBMISSION –Requirements, evaluation criteria and submission templates for the development of IMT-2020] including service aspect requirements, spectrum aspect requirements, and technical performance requirements, the last of which are based on Report ITU-R M.2410-0. These are summarized in Table 1, together with their high level assessment method:

- Simulation (including system-level and link-level simulations, according to the principles of the simulation procedure given in § 7.1 below).
- Analytical (via calculation or mathematical analysis).
- Inspection (by reviewing the functionality and parameterization of the proposal).

TABLE 1
Summary of evaluation methodologies

Characteristic for evaluation	High-level assessment method	Evaluation methodology in this Report	Related section of Reports ITU-R M.2410-0 and ITU-R M.2411-0
Peak data rate	Analytical	§ 7.2.2	Report ITU-R M.2410-0, § 4.1
Peak spectral efficiency	Analytical	§ 7.2.1	Report ITU-R M.2410-0, § 4.2
User experienced data rate	Analytical for single band and single layer; Simulation for multi-layer	§ 7.2.3	Report ITU-R M.2410-0, § 4.3
5 th percentile user spectral efficiency	Simulation	§ 7.1.2	Report ITU-R M.2410-0, § 4.4
Average spectral efficiency	Simulation	§ 7.1.1	Report ITU-R M.2410-0, § 4.5
Area traffic capacity	Analytical	§ 7.2.4	Report ITU-R M.2410-0, § 4.6
User plane latency	Analytical	§ 7.2.6	Report ITU-R M.2410-0, § 4.7.1
Control plane latency	Analytical	§ 7.2.5	Report ITU-R M.2410-0, § 4.7.2
Connection density	Simulation	§ 7.1.3	Report ITU-R M.2410-0, § 4.8
Energy efficiency	Inspection	§ 7.3.2	Report ITU-R M.2410-0, § 4.9
Reliability	Simulation	§ 7.1.5	Report ITU-R M.2410-0, § 4.10
Mobility	Simulation	§ 7.1.4	Report ITU-R M.2410-0, § 4.11
Mobility interruption time	Analytical	§ 7.2.7	Report ITU-R M.2410-0, § 4.12
Bandwidth	Inspection	§ 7.3.1	Report ITU-R M.2410-0, § 4.13
Support of wide range of services	Inspection	§ 7.3.3	Report ITU-R M.2411-0, § 3.1
Supported spectrum band(s)/range(s)	Inspection	§ 7.3.4	Report ITU-R M.2411-0, § 3.2

Section 7 defines the evaluation methodology for assessing each of these criteria.

7 Evaluation methodology

The submission and evaluation process is defined in Document IMT-2020/2 – Submission, evaluation process and consensus building for IMT-2020.

The evaluation should be performed in compliance with the technical parameters provided by the proponents and the evaluation configurations specified for the test environments in § 8.2 of this Report. Each requirement should be evaluated independently, except for the average spectral efficiency and 5th percentile user spectral efficiency – both of which criteria shall be assessed jointly using the same simulation; consequently, the candidate RITs/SRITs shall fulfil the corresponding

minimum requirements jointly. Furthermore, the evaluation parameters used for the system-level simulation used in the mobility evaluation should be the same as the parameters used for system-level simulation for average spectral efficiency and 5th percentile user spectral efficiency.

The evaluation methodology should include the following elements:

- 1 candidate RITs/SRITs should be evaluated using reproducible methods including computer simulation, analytical approaches and inspection of the proposal;
- 2 technical evaluation of the candidate RITs/SRITs should be made against each evaluation criterion for the required test environments;
- 3 candidate RITs/SRITs should be evaluated based on technical descriptions that are submitted using a technologies description template.

In order for the ITU to be in a position to assess the evaluation results of each candidate RIT/SRIT, the following points should be taken into account:

- use of unified methodology, software, and data sets by the evaluation groups wherever possible, e.g. in the area of channel modelling, link-level simulation, and link-to-system-level interface;
- evaluation of multiple proposals using a single simulation tool by each evaluation group.

Evaluations of average spectral efficiency, 5th percentile user spectral efficiency, peak spectral efficiency, user experienced data rate, area traffic capacity, peak data rate, mobility, reliability, and connection density of candidate RITs/SRITs should take into account the Layer 1 and Layer 2 overhead information provided by the proponents.

7.1 System simulation procedures

This sub-section provides detailed description of evaluation method for technical performance requirements that uses simulation.

System simulation is the simulation of the entire system which may be composed of link-level simulations and/or system-level simulations.

System-level simulation shall be based on the network layout defined in § 8.3 of this Report. The following principles shall be followed in system-level simulation:

- users are dropped independently with a certain distribution over the predefined area of the network layout throughout the system as described in § 8 of this Report;
- UEs (User Equipment) are randomly assigned LOS and NLOS channel conditions according to the applicable channel model defined in Annex 1 of this Report;
- cell assignment to a UE is based on the proponent's cell selection scheme, which must be described by the proponent;
- the applicable distances between a UE and a base station are defined in Annex 1 of this Report;
- signal fading and interference from each transmitter into each receiver are computed on an aggregated basis;
- the interference¹ over thermal parameter is an uplink design constraint that the proponent must take into account when designing the system such that the average interference over thermal value experienced in the evaluation is equal to or less than 10 dB;

¹ The interference means the effective interference received at the base station.

- in simulations based on the full-buffer traffic model, packets are not blocked when they arrive into the system (i.e. queue depths are assumed to be infinite);
- UEs with a required traffic characteristics shall be modelled according to the traffic models defined in Table 8-2 in § 8.4 of this Report;
- packets are scheduled with an appropriate packet scheduler(s), or with non-scheduled mechanism when applicable for full buffer and other traffic models separately. Channel quality feedback delay, feedback errors, PDU (protocol data unit) errors and real channel estimation effects inclusive of channel estimation error are modelled and packets are retransmitted as necessary;
- the overhead channels (i.e. the overhead due to feedback and control channels) should be realistically modelled;
- for a given drop, the simulation is run and then the process is repeated with UEs dropped at new random locations. A sufficient number of drops is simulated to ensure convergence in the UE and system performance metrics. The proponent should provide information on the width of confidence intervals of UE and system performance metrics of corresponding mean values, and evaluation groups are encouraged to use this information;²
- All cells in the system shall be simulated with dynamic channel properties and performance statistics are collected taking into account the wrap-around configuration in the network layout, noting that wrap-around is not considered in the indoor case.

In order to perform less complex system-level simulations, often the simulations are divided into separate ‘link-level’ and ‘system-level’ simulations with a specific link-to-system interface. Another possible way to reduce system-level simulation complexity is to employ simplified interference modelling. Such methods should be sound in principle, and it is not within the scope of this document to describe them.

Evaluation groups are allowed to use their own approaches provided that the used methodologies are:

- well described and made available to the Radiocommunication Bureau and other evaluation groups;
- included in the evaluation report.

Models for link-level and system-level simulations should include error modelling, e.g. for channel estimation, phase noise and for the errors of control channels that are required to decode the traffic channel (including the feedback channel and channel quality information). The overheads of the feedback channel and the control channel should be modelled according to the assumptions used in the overhead channels’ radio resource allocation.

7.1.1 Average spectral efficiency

Let $R_i(T)$ denote the number of correctly received bits by user i ($i = 1, \dots, N$) (downlink) or from user i (uplink) in a system comprising a user population of N users and M Transmission Reception Points (TRxPs). Further, let W denote the channel bandwidth and T the time over which the data bits are received. The average spectral efficiency may be estimated by running system-level simulations over number of drops N_{drops} . Each drop gives a value of $\sum_{i=1}^N R_i(T)$ denoted as:

$R^{(1)}(T), \dots, R^{(N_{drops})}(T)$ and the estimated average spectral efficiency resulting is given by:

² The confidence interval and the associated confidence level indicate the reliability of the estimated parameter value. The confidence level is the certainty (probability) that the true parameter value is within the confidence interval. The higher the confidence level the larger the confidence interval.

$$\widehat{SE}_{\text{avg}} = \frac{\sum_{j=1}^{N_{\text{drops}}} R_i^{(j)}(T)}{N_{\text{drops}} T.W.M} = \frac{\sum_{j=1}^{N_{\text{drops}}} \sum_{i=1}^N R_i^{(j)}(T)}{N_{\text{drops}} T.W.M}$$

where $\widehat{SE}_{\text{avg}}$ is the estimated average spectral efficiency and will approach the actual average with an increasing number of N_{drops} and $R_i^{(j)}(T)$ is the simulated total number of correctly received bits for user i in drop j .

The average spectral efficiency is evaluated by system level simulation using the evaluation configuration parameters of Indoor Hotspot-eMBB, Dense Urban-eMBB, and Rural-eMBB test environments as defined in this Report. It should be noted that the average spectral efficiency is evaluated only using a single-layer layout configuration even if a test environment comprises a multi-layer layout configuration.

The results from the system-level simulation are used to derive the average spectral efficiency as defined in Report ITU-R M.2410-0. The necessary information is the number of correctly received bits per UE during the active session time the UE is in the simulation. The effective bandwidth is the operating bandwidth normalized appropriately considering the uplink/downlink ratio for TDD system.

Layer 1 and Layer 2 overheads should be accounted for in time and frequency. Examples of Layer 1 overhead include synchronization, guard band and DC subcarriers, guard/switching time (for example, in TDD systems), pilots and cyclic prefix. Examples of Layer 2 overhead include common control channels, HARQ ACK/NACK signalling, channel feedback, random access, packet headers and CRC. It must be noted that in computing the overheads, the fraction of the available physical resources used to model control overhead in Layer 1 and Layer 2 should be accounted for in a non-overlapping way. Power allocation/boosting should also be accounted for in modelling resource allocation for control channels.

7.1.2 5th percentile user spectral efficiency

5th percentile user spectral efficiency is the 5th percentile point of the cumulative distribution function (CDF) of the normalized user throughput, estimated from all possible user locations.

Let user i in drop j correctly decode $R_i^{(j)}(T)$ accumulated bits in $[0, T]$. For non-scheduled duration of user i zero bits are accumulated. During this total time user i receives accumulated service time of $T_i \leq T$, where the service time is the time duration between the first packet arrival and when the last packet of the burst is correctly decoded. In case of full buffer, $T_i = T$. Hence the rate normalised by service time T_i and channel bandwidth W of user i in drop j , $r_i^{(j)}$, is:

$$r_i^{(j)} = \frac{R_i^{(j)}(T)}{T_i.W}$$

Running N_{drops} simulations leads to $N_{\text{drops}} \times N$ values of $r_i^{(j)}$ of which the lowest 5th percentile point of the CDF is used to estimate the 5th percentile user spectral efficiency.

The 5th percentile user spectral efficiency is evaluated by system level simulation using the evaluation configuration parameters of Indoor Hotspot-eMBB, Dense Urban-eMBB, and Rural-eMBB test environments. It should be noted that the 5th percentile user spectral efficiency is evaluated only using a single-layer layout configuration even if a test environment comprises a multi-layer layout configuration. The 5th percentile user spectral efficiency shall be evaluated using identical simulation assumptions as the average spectral efficiency for that test environment.

The results from the system-level simulation are used to derive the 5th percentile user spectral efficiency as defined in Report ITU-R M.2410-0. The necessary information is the number of correctly received bits per UE during the active session time the UE is in the simulation. The effective

bandwidth is the operating bandwidth normalized appropriately considering the uplink/downlink ratio for TDD system.

Layer 1 and Layer 2 overheads should be accounted for in time and frequency. Examples of Layer 1 and Layer 2 overheads can be found in § 7.1.1 for average spectral efficiency.

7.1.3 Connection density

There are two possible evaluation methods to evaluate connection density requirement defined in ITU-R M.2410-0:

- non-full buffer system-level simulation;
- full-buffer system-level simulation followed by link-level simulation.

The following steps are used to evaluate the connection density based on non-full buffer system-level simulation. Traffic model used in this method is defined in Table 8-2 in § 8.4 of this Report.

Step 1: Set system user number per TRxP as N .

Step 2: Generate the user packet according to the traffic model.

Step 3: Run non-full buffer system-level simulation to obtain the packet outage rate. The outage rate is defined as the ratio of the number of packets that failed to be delivered to the destination receiver within a transmission delay of less than or equal to 10s to the total number of packets generated in *Step 2*.

Step 4: Change the value of N and repeat *Step 2-3* to obtain the system user number per TRxP N' satisfying the packet outage rate of 1%.

Step 5: Calculate connection density by equation $C = N' / A$, where the TRxP area A is calculated as $A = \text{ISD}^2 \times \sqrt{3}/6$, and ISD is the inter-site distance.

The requirement is fulfilled if the connection density C is greater than or equal to the connection density requirement defined in Report ITU-R M.2410-0.

The simulation bandwidth used to fulfill the requirement should be reported. Additionally, it is encouraged to report the connection efficiency (measured as N' divided by simulation bandwidth) for the achieved connection density.

The following steps are used to evaluate the connection density based on full-buffer system-level simulation followed by link-level simulation. Traffic model used in this method is defined in Table 8-3 in § 8.4 of this Report.

Step 1: Perform full-buffer system-level simulation using the evaluation parameters for Urban Macro-mMTC test environment, determine the uplink $SINR_i$ for each percentile $i=1\dots99$ of the distribution over users, and record the average allocated user bandwidth W_{user} .

- In case UE multiplexing on the same time/frequency resource is modelled in this step, record the average number of multiplexed users N_{mux} . $N_{\text{mux}} = 1$ for no UE multiplexing.

Step 2: Perform link-level simulation and determine the achievable user data rate R_i for the recorded $SINR_i$ and W_{user} values.

- In case UE multiplexing on the same time/frequency resource is modelled in this step, record the average number of multiplexed users $n_{\text{mux},i}$ under $SINR_i$. The achievable data rate for this case is derived by $R_i = Z_i/n_{\text{mux},i}$, where aggregated bit rate Z_i is the summed bit rate of $n_{\text{mux},i}$ users on W_{user} . $n_{\text{mux},i} = 1$ for no UE multiplexing.

Step 3: Calculate the packet transmission delay of a user as $D_i = S/R_i$, where S is the packet size.

Step 4: Calculate the traffic generated per user as $T = S/T_{\text{inter-arrival}}$, where $T_{\text{inter-arrival}}$ is the inter-packet arrival time.

Step 5: Calculate the long-term frequency resource requested under $SINR_i$ as $B_i = T/(R_i/W_{\text{user}})$.

Step 6: Calculate the number of supported connections per TRxP, $N = W / \text{mean}(B_i)$. W is the simulation bandwidth. The mean of B_i may be taken over the best 99% of the $SINR_i$ conditions.

- In case UE multiplexing is modelled in *Step 1*, $N = N_{\text{mux}} \times W / \text{mean}(B_i)$. In case UE multiplexing is modelled in *Step 2*, $N = W / \text{mean}(B_i/n_{\text{mux},i})$.

Step 7: Calculate the connection density as $C = N / A$, where the TRxP area A is calculated as $A = \text{ISD}^2 \times \text{sqrt}(3)/6$, and ISD is the inter-site distance.

The requirement is fulfilled if the 99th percentile of the delay per user D_i is less than or equal to 10s, and the connection density is greater than or equal to the connection density requirement defined in Report ITU-R M.2410-0.

The simulation bandwidth used to fulfill the requirement should be reported. Additionally, it is encouraged to report the connection efficiency (measured as N divided by simulation bandwidth) for the achieved connection density.

7.1.4 Mobility

Mobility shall be evaluated under Indoor Hotspot-eMBB, Dense Urban-eMBB, and Rural-eMBB test environments using the same evaluation parameters and configuration selected for the evaluation of average spectral efficiency and 5th percentile user spectral efficiency. Under Rural-eMBB test environment, target values for both mobility of 120 km/h and 500 km/h in Table 4 of Report ITU-R M.2410-0 shall be achieved to fulfill mobility requirements of Rural-eMBB test environment.

The evaluator shall perform the following steps in order to evaluate the mobility requirement.

Step 1: Run uplink system-level simulations, identical to those for average spectral efficiency, and 5th percentile user spectral efficiency except for speeds taken from Table 4 of Report ITU-R M.2410-0, using link-level simulations and a link-to-system interface appropriate for these speed values, for the set of selected test environment(s) associated with the candidate RITs/SRITs and collect overall statistics for uplink $SINR$ values, and construct CDF over these values for each test environment.

Step 2: Use the CDF for the test environment(s) to save the respective 50th-percentile $SINR$ value.

Step 3: Run new uplink link-level simulations for the selected test environment(s) for either NLOS or LOS channel conditions using the associated speeds in Table 4 of Report ITU-R M.2410-0, as input parameters, to obtain link data rate and residual packet error ratio as a function of $SINR$. The link-level simulation shall use air interface configuration(s) supported by the proposal and take into account retransmission, channel estimation and phase noise impact.

Step 4: Compare the uplink spectral efficiency values (link data rate normalized by channel bandwidth) obtained from *Step 3* using the associated $SINR$ value obtained from *Step 2* for selected test environments, with the corresponding threshold values in the Table 4 of Report ITU-R M.2410-0.

Step 5: The proposal fulfils the mobility requirement if the spectral efficiency value is larger than or equal to the corresponding threshold value and if also the residual decoded packet error ratio is less than 1%, for all selected test environments. For the selected test environment it is sufficient if one of the spectral efficiency values (using either NLOS or LOS channel conditions) fulfils the threshold.

Similar methodology can be used for downlink in case this is additionally evaluated.

7.1.5 Reliability

The evaluator shall perform the following steps in order to evaluate the reliability requirement using system-level simulation followed by link-level simulations.

- Step 1:* Run downlink or uplink full buffer system-level simulations of candidate RITs/SRITs using the evaluation parameters of Urban Macro-URLLC test environment see § 8.4.1 below, and collect overall statistics for downlink or uplink *SINR* values, and construct CDF over these values.
- Step 2:* Use the CDF for the Urban Macro-URLLC test environment to save the respective 5th percentile downlink or uplink *SINR* value.
- Step 3:* Run corresponding link-level simulations for either NLOS or LOS channel conditions using the associated parameters in the Table 8-3 of this Report, to obtain success probability, which equals to $(1-P_e)$, where P_e is the residual packet error ratio within maximum delay time as a function of *SINR* taking into account retransmission.
- Step 4:* The proposal fulfils the reliability requirement if at the 5th percentile downlink or uplink *SINR* value of *Step 2* and within the required delay, the success probability derived in *Step 3* is larger than or equal to the required success probability. It is sufficient to fulfil the requirement in either downlink or uplink, using either NLOS or LOS channel conditions.

7.2 Analytical approach

For §§ 7.2.1 to 7.2.7 below, a straight forward calculation based on the definition in Report ITU-R M.2410-0 will be enough to evaluate them. The evaluation shall describe how this calculation has been performed. Evaluation groups should follow the calculation provided by proponents if it is justified properly.

7.2.1 Peak spectral efficiency calculation

The peak spectral efficiency is calculated as specified in § 4.2 of Report ITU-R M.2410-0. The proponent should report the assumed frequency band(s) of operation and channel bandwidth, for which the peak spectral efficiency value is achievable. For TDD, the channel bandwidth information should include the effective bandwidth, which is the operating bandwidth normalized appropriately considering the uplink/downlink ratio.

The antenna configuration to be used for peak spectral efficiency is defined in Table 8-4 of this Report. Layer 1 and Layer 2 overhead should be accounted for in time and frequency, in the same way as assumed for the “Average spectral efficiency”.

Proponents should demonstrate that the peak spectral efficiency requirement can be met for, at least, one of the carrier frequencies assumed in the test environments under the eMBB usage scenario.

7.2.2 Peak data rate calculation

The peak data rate is calculated as specified in § 4.1 of Report ITU-R M.2410-0, using peak spectral efficiency and maximum assignable channel bandwidth.

Peak spectral efficiency and maximum assignable channel bandwidth may have different values in different frequency bands. The peak data rate may be summed over multiple bands in case of bandwidth aggregated across multiple bands.

The proponent should report the peak data rate value achievable by the candidate RITs/SRITs and identify the assumed frequency band(s) of operation, the maximum assignable channel bandwidth in that band(s) and the main assumptions related to the peak spectral efficiency over the assumed frequency band(s) (e.g. antenna configuration).

Proponents should demonstrate that the peak data rate requirement can be met for, at least, one carrier frequency or a set of aggregated carrier frequencies (where it is the case), assumed in the test environments under the eMBB usage scenario

7.2.3 User experienced data rate calculation

The evaluation is conducted in Dense Urban-eMBB test environment.

For one frequency band and one TRxP layer, user experienced data rate is derived analytically from the 5th percentile user spectral efficiency according to equation (3) defined in Report ITU-R M.2410-0. The bandwidth used should be reported by the proponent.

In case of multi-layer configuration, system-level simulation is used. In this case, the single user data rate may be aggregated over layers and/or bands. The user experienced data rate is derived from the 5th percentile point of the CDF of single user data rate.

7.2.4 Area traffic capacity calculation

The evaluation is conducted in Indoor Hotspot-eMBB test environment where a single band is considered.

Area traffic capacity is derived based on the achievable average spectral efficiency, TRxP density and bandwidth.

Let W denote the channel bandwidth and ρ the TRxP density (TRxP/m²). The area traffic capacity C_{area} is related to average spectral efficiency SE_{avg} as follows:

$$C_{area} = \rho \times W \times SE_{avg}$$

7.2.5 Control plane latency calculation

The proponent should provide the elements and their values in the calculation of the control plane latency. Table 2 provides an example of the elements in the calculation of the control plane latency.

TABLE 2
Example of control plane latency analysis template

Step	Description	Value
1	Random access procedure	
2	UL synchronization	
3	Connection establishment + HARQ retransmission	
4	Data bearer establishment + HARQ retransmission	
	Total control plane latency	

7.2.6 User plane latency calculation

The proponent should provide the elements and their values in the calculation of the user plane latency, for both UL and DL. Table 3 provides an example of the elements in the calculation of the user plane latency.

TABLE 3
Example of user plane latency analysis template

Step	Description	Value
1	UE processing delay	
2	Frame alignment	
3	TTI for data packet transmission	
4	HARQ retransmission	
5	BS processing delay	
	Total one way user plane latency	

7.2.7 Mobility interruption time calculation

The procedure of exchanging user plane packets with base stations during transitions shall be described based on the proposed technology including the functions and the timing involved.

7.3 Inspection approach

Inspection is conducted by reviewing the functionality and parameterization of a proposal.

7.3.1 Bandwidth

The support of maximum bandwidth required in § 4.13 of Report ITU-R M.2410-0, is verified by inspection of the proposal.

The scalability requirement is verified by demonstrating that the candidate RITs/SRITs can support multiple different bandwidth values. These values shall include the minimum and maximum supported bandwidth values of the candidate RITs/SRITs.

The requirements for bandwidth or the bandwidth numbers demonstrated by the proponent do not pose any requirements or limitations for other Technical Performance Requirements that depend on bandwidth. If any other requirement requires a higher bandwidth, the capability to reach that bandwidth should be described as well.

7.3.2 Energy efficiency

The energy efficiency for both network and device is verified by inspection by demonstrating that the candidate RITs/SRITs can support high sleep ratio and long sleep duration as defined in Report ITU-R M.2410-0 when there is no data.

Inspection can also be used to describe other mechanisms of the candidate RITs/SRITs that improve energy efficient operation for both network and device.

7.3.3 Support of wide range of services

There are elements of the minimum technical performance requirements identified within Report ITU-R M.2410-0 that indicate whether or not the candidate RITs/SRITs are capable of enabling certain services and performance targets, as envisioned in Recommendation ITU-R M.2083.

The support of a wide range of services is verified by inspection of the candidate RITs/SRITs ability to meet the minimum technical performance requirements for various usage scenarios and their associated test environments.

7.3.4 Supported spectrum band(s)/range(s)

The spectrum band(s) and/or range(s) that the candidate RITs/SRITs can utilize is verified by inspection.

8 Test environments and evaluation configurations

This section describes the test environments and the related evaluation configurations (including simulation parameters) necessary to evaluate the performance criteria of candidate RITs/SRITs (details of test environments and channel models can be found in Annex 1 of this Report).

These predefined test environments are used in order to evaluate the requirements for the technology proposals. IMT-2020 is to cover a wide range of performance in a wide range of environments. Although it should be noted that thorough testing and evaluation is prohibitive, these test environments have therefore been chosen such that typical and different deployments are modelled and critical aspects in system design and performance can be investigated. Focus is thus on scenarios testing limits of performance.

8.1 Usage scenarios

As defined in Recommendation ITU-R M.2083, IMT-2020 is envisaged to expand and support diverse usage scenarios and applications that will continue beyond IMT-Advanced. There are three usage scenarios for IMT-2020 as follows:

- **Enhanced Mobile Broadband (eMBB):** This usage scenario will come with new application areas and requirements in addition to existing Mobile Broadband applications for improved performance and an increasingly seamless user experience. This usage scenario covers a range of cases, including wide-area coverage and hotspot, which have different requirements.
- **Massive machine type communications (mMTC):** This usage scenario is characterized by a very large number of connected devices typically transmitting a relatively low volume of non-delay-sensitive data.
- **Ultra-reliable and low latency communications (URLLC):** This usage scenario has stringent requirements for capabilities such as throughput, latency and availability. Some examples include wireless control of industrial manufacturing or production processes, remote medical surgery, distribution automation in a smart grid, transportation safety, etc.

8.2 Test environments

A test environment reflects a combination of geographic environment and usage scenario. There are five selected test environments for IMT-2020 as follows:

- **Indoor Hotspot-eMBB:** An indoor isolated environment at offices and/or in shopping malls based on stationary and pedestrian users with very high user density.
- **Dense Urban-eMBB:** An urban environment with high user density and traffic loads focusing on pedestrian and vehicular users.
- **Rural-eMBB:** A rural environment with larger and continuous wide area coverage, supporting pedestrian, vehicular and high speed vehicular users.
- **Urban Macro-mMTC:** An urban macro environment targeting continuous coverage focusing on a high number of connected machine type devices.
- **Urban Macro-URLLC:** An urban macro environment targeting ultra-reliable and low latency communications.

The mapping of the five test environments and the three usage scenarios is given in Table 4.

TABLE 4

Mapping of test environments and usage scenarios

Usage scenarios	eMBB			mMTC	URLLC
Test environments	Indoor Hotspot – eMBB	Dense Urban – eMBB	Rural – eMBB	Urban Macro – mMTC	Urban Macro – URLLC

8.3 Network layout

No specific topographical details are taken into account in Dense Urban - eMBB (macro layer) Rural-eMBB, Urban Macro-mMTC, and Urban Macro-URLLC test environments. In the above cases, base stations (BSs) / sites are placed in a regular grid, following hexagonal layout. The simulation will be a wrap-around configuration of 19 sites, each of 3 TRxPs (cells). A basic hexagon layout for the example of three TRxPs per site is the same as shown in Fig. 1 in § 8.3 of Report ITU-R M.2135-1, where also basic geometry (antenna boresight, cell range, and ISD) is defined. UEs are distributed uniformly over the whole area.

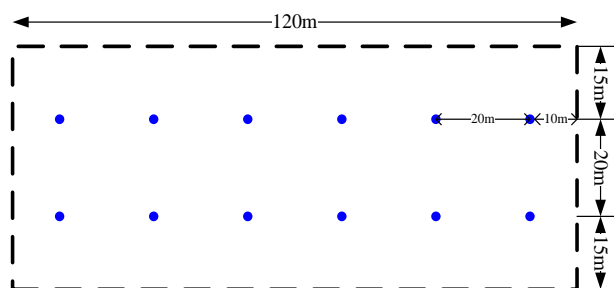
In the following network topology for the selected test environments is described.

8.3.1 Indoor Hotspot-eMBB

The Indoor Hotspot-eMBB test environment consists of one floor of a building. The height of the floor is 3 m. The floor has a surface of 120 m × 50 m and 12 BSs/sites which are placed in 20 meter spacing as shown in Fig. 1, with a LOS probability as defined by channel model in Annex 1, Table A1-9. In Fig. 1, internal walls are not explicitly shown but are modeled via the stochastic LOS probability model.

The type of site deployed (e.g. one TRxP per site or 3 TRxPs per site) is not defined and should be reported by the proponent.

FIGURE 1
Indoor Hotspot sites layout



8.3.2 Dense Urban-eMBB

The Dense Urban-eMBB test environment consists of two layers, a macro layer and a micro layer. The macro-layer base stations are placed in a regular grid, following hexagonal layout with three TRxPs each, as shown in Fig. 2 below. For the micro layer, there are 3 micro sites randomly dropped in each macro TRxP area (see Fig. 3). The micro-layer deployment (e.g. three micro sites per macro TRxP and there is either one or three TRxPs at each micro site) is not defined but should be reported by the proponent. The proponent should describe micro-layer base stations placement method.

FIGURE 2
Sketch of hexagonal site layout

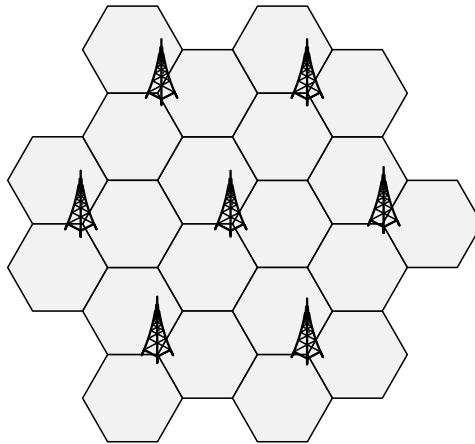
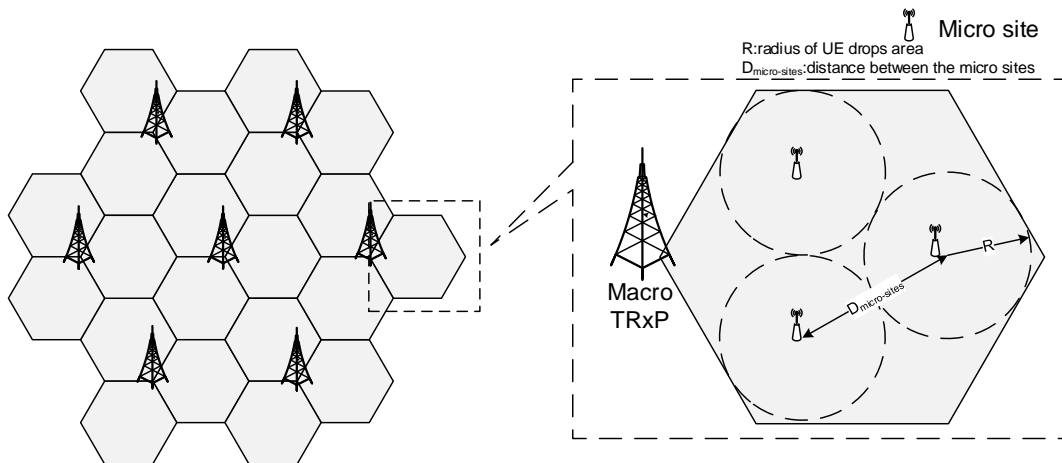


FIGURE 3
Example sketch of dense urban-eMBB layout



8.3.3 Rural-eMBB

In Rural-eMBB test environment, the BSs/sites are placed in a regular grid, following hexagonal layout with three TRxPs each, as in the macro layer of the Dense Urban-eMBB test environment, as shown in Fig. 2. For evaluation of the mobility, the same topographical details of hexagonal layout are applied to both 120 km/h and 500 km/h mobility.

For 500 km/h mobility, additional evaluations are encouraged using linear cell layout configuration(s) defined in Annex 2 of this Report.

8.3.4 Urban Macro-mMTC and Urban Macro-URLLC

In the Urban Macro-mMTC and Urban Macro-URLLC test environments, the BSs/sites are placed in a regular grid, following hexagonal layout with three TRxPs each, as in the Dense Urban-eMBB macro layer and Rural-eMBB test environment; this is shown in Fig. 2.

8.4 Evaluation configurations

Evaluation configurations are defined for the selected test environments. The configuration parameters shall be applied in analytical and simulation assessments of candidate RITs/SRITs. For the cases when there are multiple evaluation configurations under the selected test environment, one of the evaluation configurations under that test environment can be used to test the candidate RITs/SRITs. The technical performance requirement corresponding to that test environment is fulfilled if this requirement is met for one of the evaluation configurations under that specific test environment.

In addition, for the Rural-eMBB test environment, the average spectral efficiency value should meet the threshold values for the LMLC evaluation configuration with ISD of 6 000 m and either evaluation configuration with ISD of 1 732 m.

For system-level simulation, there are two channel model variants of primary module for IMT-2020 evaluation: (1) channel model A and (2) channel model B. Proponents can select either channel model A or B to evaluate the candidate RITs/SRITs. The technical performance requirement corresponding to a test environment is fulfilled if this requirement is met for either channel model A or B for that specific test environment. The same channel model variant should be used to evaluate all the test environments.

The configuration parameters (and also the propagation and channel models in Annex 1 of this Report) are solely for the purpose of consistent evaluation of the candidate RITs/SRITs and relate only to specific test environments designed for these evaluations. Therefore, the configuration parameters should not be considered as those that must be used in any deployment of any IMT-2020 system nor should they be taken as the default values for any other or subsequent study in ITU or elsewhere. They do not necessarily themselves constitute any requirements on the implementation of the system. Some configuration parameters are specified in terms of a range of values. This is done to provide some flexibility in the evaluation process. It should be noted that in such cases, meeting the technical performance requirements is not necessarily associated with the lowest/highest value in the range.

TABLE 5

a) Evaluation configurations for Indoor Hotspot-eMBB test environment

Parameters	Indoor Hotspot-eMBB		
	Spectral Efficiency, Mobility, and Area Traffic Capacity Evaluations		
	Configuration A	Configuration B	Configuration C
Baseline evaluation configuration parameters			
Carrier frequency for evaluation	4 GHz	30 GHz	70 GHz
BS antenna height	3 m	3 m	3 m
Total transmit power per TRxP	24 dBm for 20 MHz bandwidth 21 dBm for 10 MHz bandwidth	23 dBm for 80 MHz bandwidth 20 dBm for 40 MHz bandwidth e.i.r.p. should not exceed 58 dBm	21 dBm for 80 MHz bandwidth 18 dBm for 40 MHz bandwidth e.i.r.p. should not exceed 58 dBm
UE power class	23 dBm	23 dBm e.i.r.p. should not exceed 43 dBm	21 dBm e.i.r.p. should not exceed 43 dBm
Additional parameters for system-level simulation			
Inter-site distance	20 m	20 m	20 m
Number of antenna elements per TRxP	Up to 256 Tx/Rx	Up to 256 Tx/Rx	Up to 1024 Tx/Rx
Number of UE antenna elements	Up to 8 Tx/Rx	Up to 32 Tx/Rx	Up to 64 Tx/Rx
Device deployment	100% indoor Randomly and uniformly distributed over the area	100% indoor Randomly and uniformly distributed over the area	100% indoor Randomly and uniformly distributed over the area
UE mobility model	Fixed and identical speed $ v $ of all UEs, randomly and uniformly distributed direction	Fixed and identical speed $ v $ of all UEs, randomly and uniformly distributed direction	Fixed and identical speed $ v $ of all UEs, randomly and uniformly distributed direction
UE speeds of interest	100% indoor, 3 km/h	100% indoor, 3 km/h	100% indoor, 3 km/h
Inter-site interference modeling	Explicitly modelled	Explicitly modelled	Explicitly modelled
BS noise figure	5 dB	7 dB	7 dB
UE noise figure	7 dB	10 dB ³	10 dB ³
BS antenna element gain	5 dBi	5 dBi	5 dBi

³ 10 dB for 30 GHz / 70 GHz is assumed for high performance UE. Higher UE noise figure values can be considered by the proponent, e.g. 13 dB for 30 GHz / 70 GHz.

TABLE 5 (continued)

a) Evaluation configurations for Indoor Hotspot-eMBB test environment

Parameters	Indoor Hotspot-eMBB		
	Spectral Efficiency, Mobility, and Area Traffic Capacity Evaluations		
	Configuration A	Configuration B	Configuration C
UE antenna element gain	0 dBi	5 dBi	5 dBi
Thermal noise level	-174 dBm/Hz	-174 dBm/Hz	-174 dBm/Hz
Traffic model	Full buffer	Full buffer	Full buffer
Simulation bandwidth	20 MHz for TDD, 10 MHz+10 MHz for FDD	80 MHz for TDD, 40 MHz+40 MHz for FDD	80 MHz for TDD, 40 MHz+40 MHz for FDD
UE density	10 UEs per TRxP randomly and uniformly dropped throughout the geographical area	10 UEs per TRxP randomly and uniformly dropped throughout the geographical area	10 UEs per TRxP randomly and uniformly dropped throughout the geographical area
UE antenna height	1.5 m	1.5 m	1.5 m

b) Evaluation configurations for Dense Urban-eMBB test environment

Parameters	Dense Urban-eMBB		
	Spectral Efficiency and Mobility Evaluations		User Experienced Data Rate Evaluation
	Configuration A	Configuration B	Configuration C
Baseline evaluation configuration parameters			
Carrier frequency for evaluation	1 layer (Macro) with 4 GHz	1 layer (Macro) with 30 GHz	1 or 2 layers (Macro + Micro). 4 GHz and 30 GHz available in macro and micro layers
BS antenna height	25 m	25 m	25 m for macro sites and 10 m for micro sites

TABLE 5 (continued)

b) Evaluation configurations for Dense Urban-eMBB test environment

Parameters	Dense Urban-eMBB		
	Spectral Efficiency and Mobility Evaluations		User Experienced Data Rate Evaluation
	Configuration A	Configuration B	Configuration C
Total transmit power per TRxP	44 dBm for 20 MHz bandwidth 41 dBm for 10 MHz bandwidth	40 dBm for 80 MHz bandwidth 37 dBm for 40 MHz bandwidth e.i.r.p. should not exceed 73 dBm	Macro 4 GHz: 44 dBm for 20 MHz bandwidth 41 dBm for 10 MHz bandwidth Macro 30 GHz: 40 dBm for 80 MHz bandwidth 37 dBm for 40 MHz bandwidth e.i.r.p. should not exceed 73 dBm Micro 4 GHz: 33 dBm for 20 MHz bandwidth 30 dBm for 10 MHz bandwidth Micro 30 GHz: 33 dBm for 80 MHz bandwidth 30 dBm for 40 MHz bandwidth e.i.r.p. should not exceed 68 dBm
UE power class	23 dBm	23 dBm, e.i.r.p. should not exceed 43 dBm	4 GHz: 23 dBm 30 GHz: 23 dBm, e.i.r.p. should not exceed 43 dBm
Percentage of high loss and low loss building type	20% high loss, 80% low loss	20% high loss, 80% low loss	20% high loss, 80% low loss
Additional parameters for system-level simulation			
Inter-site distance	200 m	200 m	Macro layer: 200 m (NOTE – Density and layout of Micro layer are in § 8.3)
Number of antenna elements per TRxP	Up to 256 Tx/Rx	Up to 256 Tx/Rx	Up to 256 Tx/Rx
Number of UE antenna elements	Up to 8 Tx/Rx	Up to 32 Tx/Rx	4 GHz: Up to 8 Tx/Rx 30 GHz: Up to 32 Tx/Rx

TABLE 5 (continued)

b) Evaluation configurations for Dense Urban-eMBB test environment

Parameters	Dense Urban-eMBB		
	Spectral Efficiency and Mobility Evaluations		User Experienced Data Rate Evaluation
	Configuration A	Configuration B	Configuration C
Device deployment	80% indoor, 20% outdoor (in-car) Randomly and uniformly distributed over the area under Macro layer	80% indoor, 20% outdoor (in-car) Randomly and uniformly distributed over the area under Macro layer	80% indoor, 20% outdoor (in-car) Randomly and uniformly distributed over the area under Macro layer
UE mobility model	Fixed and identical speed $ v $ of all UEs of the same mobility class, randomly and uniformly distributed direction.	Fixed and identical speed $ v $ of all UEs of the same mobility class, randomly and uniformly distributed direction.	Fixed and identical speed $ v $ of all UEs of the same mobility class, randomly and uniformly distributed direction.
UE speeds of interest	Indoor users: 3 km/h Outdoor users (in-car): 30 km/h	Indoor users: 3 km/h Outdoor users (in-car): 30 km/h	Indoor users: 3 km/h Outdoor users (in-car): 30 km/h
Inter-site interference modeling	Explicitly modelled	Explicitly modelled	Explicitly modelled
BS noise figure	5 dB	7 dB	4 GHz: 5 dB 30 GHz: 7 dB
UE noise figure	7 dB	10 dB ⁴	4 GHz: 7 dB 30 GHz: 10 dB ⁴
BS antenna element gain	8 dBi	8 dBi	4 GHz: 8 dBi 30 GHz: Macro TRxP: 8 dBi
UE antenna element gain	0 dBi	5 dBi	4 GHz: 0 dBi 30 GHz: 5 dBi
Thermal noise level	-174 dBm/Hz	-174 dBm/Hz	-174 dBm/Hz
Traffic model	Full buffer	Full buffer	Full buffer
Simulation bandwidth	20 MHz for TDD, 10 MHz+10 MHz for FDD	80 MHz for TDD, 40 MHz+40 MHz for FDD	4 GHz: 20 MHz for TDD, 10 MHz+10 MHz for FDD 30 GHz: 80 MHz for TDD, 40 MHz+40 MHz for FDD

⁴ 10 dB for 30 GHz is assumed for high performance UE. Higher UE noise figure values can be considered by the proponent, e.g. 13 dB for 30 GHz.

TABLE 5 (continued)

b) Evaluation configurations for Dense Urban-eMBB test environment

Parameters	Dense Urban-eMBB		
	Spectral Efficiency and Mobility Evaluations		User Experienced Data Rate Evaluation
	Configuration A	Configuration B	Configuration C
UE density	10 UEs per TRxP Randomly and uniformly distributed over the area under Macro layer	10 UEs per TRxP Randomly and uniformly distributed over the area under Macro layer	10 UEs per TRxP for multi-layer case, randomly and uniformly dropped within a cluster. The proponent reports the size of the cluster
UE antenna height	Outdoor UEs: 1.5 m Indoor UTs: $3(n_{fl} - 1) + 1.5$; $n_{fl} \sim \text{uniform}(1, N_{fl})$ where $N_{fl} \sim \text{uniform}(4, 8)$	Outdoor UEs: 1.5 m Indoor UTs: $3(n_{fl} - 1) + 1.5$; $n_{fl} \sim \text{uniform}(1, N_{fl})$ where $N_{fl} \sim \text{uniform}(4, 8)$	Outdoor UEs: 1.5 m Indoor UTs: $3(n_{fl} - 1) + 1.5$; $n_{fl} \sim \text{uniform}(1, N_{fl})$ where $N_{fl} \sim \text{uniform}(4, 8)$

c) Evaluation configurations for Rural-eMBB test environment

Parameters	Rural-eMBB		
	Spectral Efficiency and Mobility Evaluations		Average Spectral Efficiency Evaluation
	Configuration A	Configuration B	Configuration C (LMLC)
Baseline evaluation configuration parameters			
Carrier frequency for evaluation	700 MHz	4 GHz	700 MHz
BS antenna height	35 m	35 m	35 m
Total transmit power per TRxP	49 dBm for 20 MHz bandwidth 46 dBm for 10 MHz bandwidth	49 dBm for 20 MHz bandwidth 46 dBm for 10 MHz bandwidth	49 dBm for 20 MHz bandwidth 46 dBm for 10 MHz bandwidth
UE power class	23 dBm	23 dBm	23 dBm
Percentage of high loss and low loss building type	100% low loss	100% low loss	100% low loss
Additional parameters for system-level simulation			
Inter-site distance	1732 m	1732 m	6000 m
Number of antenna elements per TRxP	Up to 64 Tx/Rx	Up to 256 Tx/Rx	Up to 64 Tx/Rx
Number of UE antenna elements	Up to 4 Tx/Rx	Up to 8 Tx/Rx	Up to 4 Tx/Rx

TABLE 5 (continued)

c) Evaluation configurations for Rural-eMBB test environment

Parameters	Rural-eMBB		
	Spectral Efficiency and Mobility Evaluations		Average Spectral Efficiency Evaluation
	Configuration A	Configuration B	Configuration C (LMLC)
Device deployment	50% indoor, 50% outdoor (in-car) Randomly and uniformly distributed over the area	50% indoor, 50% outdoor (in-car) Randomly and uniformly distributed over the area	40% indoor, 40% outdoor (pedestrian), 20% outdoor (in-car) Randomly and uniformly distributed over the area
UE mobility model	Fixed and identical speed $ v $ of all UEs, randomly and uniformly distributed direction	Fixed and identical speed $ v $ of all UEs, randomly and uniformly distributed direction	Fixed and identical speed $ v $ of all UEs, randomly and uniformly distributed direction
UE speeds of interest	Indoor users: 3 km/h; Outdoor users (in-car): 120 km/h; 500 km/h for evaluation of mobility in high-speed case	Indoor users: 3 km/h; Outdoor users (in-car): 120 km/h; 500 km/h for evaluation of mobility in high-speed case	Indoor users: 3 km/h; Outdoor users (pedestrian): 3 km/h; Outdoor users (in-car): 30 km/h
Inter-site interference modeling	Explicitly modelled	Explicitly modelled	Explicitly modelled
BS noise figure	5 dB	5 dB	5 dB
UE noise figure	7 dB	7 dB	7 dB
BS antenna element gain	8 dBi	8 dBi	8 dBi
UE antenna element gain	0 dBi	0 dBi	0 dBi
Thermal noise level	-174 dBm/Hz	-174 dBm/Hz	-174 dBm/Hz
Traffic model	Full buffer	Full buffer	Full buffer
Simulation bandwidth	20 MHz for TDD, 10 MHz+10 MHz for FDD	20 MHz for TDD, 10 MHz+10 MHz for FDD	20 MHz for TDD, 10 MHz+10 MHz for FDD
UE density	10 UEs per TRxP Randomly and uniformly distributed over the area	10 UEs per TRxP Randomly and uniformly distributed over the area	10 UEs per TRxP Randomly and uniformly distributed over the area
UE antenna height	1.5 m	1.5 m	1.5 m

TABLE 5 (continued)

d) Evaluation configurations for Urban Macro-mMTC test environments

Parameters	Urban Macro-mMTC	
	Connection Density Evaluation	
	Configuration A	Configuration B
Baseline evaluation configuration parameters		
Carrier frequency for evaluation	700 MHz	700 MHz
BS antenna height	25 m	25 m
Total transmit power per TRxP ⁵	49 dBm for 20 MHz bandwidth 46 dBm for 10 MHz bandwidth	49 dBm for 20 MHz bandwidth 46 dBm for 10 MHz bandwidth
UE power class	23 dBm	23 dBm
Percentage of high loss and low loss building type	20% high loss, 80% low loss	20% high loss, 80% low loss
Additional parameters for system-level simulation		
Inter-site distance	500 m	1732 m
Number of antenna elements per TRxP	Up to 64 Tx/Rx	Up to 64 Tx/Rx
Number of UE antenna elements	Up to 2 Tx/Rx	Up to 2 Tx/Rx
Device deployment	80% indoor, 20% outdoor Randomly and uniformly distributed over the area	80% indoor, 20% outdoor Randomly and uniformly distributed over the area
UE mobility model	Fixed and identical speed $ v $ of all UEs of the same mobility class, randomly and uniformly distributed direction.	Fixed and identical speed $ v $ of all UEs of the same mobility class, randomly and uniformly distributed direction.
UE speeds of interest	3 km/h for indoor and outdoor	3 km/h for indoor and outdoor
Inter-site interference modelling	Explicitly modelled	Explicitly modelled
BS noise figure	5 dB	5 dB
UE noise figure	7 dB	7 dB
BS antenna element gain	8 dBi	8 dBi
UE antenna element gain	0 dBi	0 dBi
Thermal noise level	-174 dBm/Hz	-174 dBm/Hz

⁵ This/these parameter(s) is/are used for cell association.

TABLE 5 (continued)

d) Evaluation configurations for Urban Macro-mMTC test environments

Parameters	Urban Macro-mMTC	
	Connection Density Evaluation	
	Configuration A	Configuration B
Traffic model	With layer 2 PDU (Protocol Data Unit) message size of 32 bytes: 1 message/day/device or 1 message/2 hours/device ⁶ Packet arrival follows Poisson arrival process for non-full buffer system-level simulation	With layer 2 PDU (Protocol Data Unit) message size of 32 bytes: 1 message/day/device or 1 message/2 hours/device ⁶ Packet arrival follows Poisson arrival process for non-full buffer system-level simulation
Simulation bandwidth	Up to 10 MHz	Up to 50 MHz
UE density	Not applicable for non-full buffer system-level simulation as evaluation methodology of connection density For full buffer system-level simulation followed by link-level simulation, 10 UEs per TRxP NOTE – this is used for SINR CDF distribution derivation	Not applicable for non-full buffer system-level simulation as evaluation methodology of connection density For full buffer system-level simulation followed by link-level simulation, 10 UEs per TRxP NOTE – this is used for SINR CDF distribution derivation
UE antenna height	1.5m	1.5 m

e) Evaluation configurations for Urban Macro-URLLC test environments

Parameters	Urban Macro-URLLC	
	Reliability Evaluation	
	Configuration A	Configuration B
Baseline evaluation configuration parameters		
Carrier frequency for evaluation	4 GHz	700 MHz
BS antenna height	25 m	25 m
Total transmit power per TRxP	49 dBm for 20 MHz bandwidth 46 dBm for 10 MHz bandwidth	49 dBm for 20 MHz bandwidth 46 dBm for 10 MHz bandwidth
UE power class	23 dBm	23 dBm
Percentage of high loss and low loss building type	100% low loss	100% low loss

⁶ Higher traffic loads are encouraged.

TABLE 5 (end)

e) Evaluation configurations for Urban Macro-URLLC test environments

Parameters	Urban Macro-URLLC	
	Reliability Evaluation	
	Configuration A	Configuration B
Additional parameters for system-level simulation		
Inter-site distance	500 m	500 m
Number of antenna elements per TRxP ¹	Up to 256 Tx/Rx	Up to 64 Tx/Rx
Number of UE antenna elements	Up to 8 Tx/Rx	Up to 4 Tx/Rx
Device deployment	80% outdoor, 20% indoor	80% outdoor, 20% indoor
UE mobility model	Fixed and identical speed $ v $ of all UEs, randomly and uniformly distributed direction	Fixed and identical speed $ v $ of all UEs, randomly and uniformly distributed direction
UE speeds of interest	3 km/h for indoor and 30 km/h for outdoor	3 km/h for indoor and 30 km/h for outdoor
Inter-site interference modelling	Explicitly modelled	Explicitly modelled
BS noise figure	5 dB	5 dB
UE noise figure	7 dB	7 dB
BS antenna element gain	8 dBi	8 dBi
UE antenna element gain	0 dBi	0 dBi
Thermal noise level	-174 dBm/Hz	-174 dBm/Hz
Traffic model	Full buffer NOTE – This is used for SINR CDF distribution derivation	Full buffer NOTE – This is used for SINR CDF distribution derivation
Simulation bandwidth	Up to 100 MHz NOTE – This value is used for SINR CDF distribution derivation	Up to 40 MHz NOTE – This value is used for SINR CDF distribution derivation
UE density	10 UEs per TRxP NOTE – This is used for SINR CDF distribution derivation	10 UEs per TRxP NOTE – This is used for SINR CDF distribution derivation
UE antenna height	1.5 m	1.5 m

Notes to Table 5:

NOTE 1 – High loss buildings are sometimes referred to as thermally efficient. Low loss buildings are sometimes referred to as traditional. Percentages of high loss and low loss building type can vary according to the actual distribution of building types. In the future, the percentage of high-loss building is expected to increase, so this factor would have to be taken into account in later evaluation activities. It is used only in the appropriate channel model variant as required.

NOTE 2 – The carrier frequency of 700 MHz represents frequency ranges of 450 MHz – 960 MHz; 4 GHz represents frequency ranges of 3 GHz – 6 GHz; 30 GHz represents frequency ranges of 24.25 GHz – 52.6 GHz; 70 GHz represents frequency ranges of 66 GHz – 86 GHz.

NOTE 3 –: For Rural-eMBB, the frequency ranges represented by 700 MHz, and its related configuration parameters, can also be assumed for a carrier frequency of 1.4 GHz. It is assumed that number of BS antenna elements is up to 256 Tx/Rx and number of UE antenna elements is up to 8 Tx/Rx.

NOTE 4 – The simulation bandwidth of TDD also applies to duplexing schemes other than FDD and TDD as total simulation bandwidth for uplink plus downlink. Detailed division of downlink and uplink shall be reported.

TABLE 6

**Additional parameters for link-level simulation
(for mobility, reliability, connection density requirements)**

Parameters	Indoor hotspot-eMBB	Dense Urban-eMBB	Rural-eMBB	Urban Macro-mMTC	Urban Macro-URLLC
Evaluated service profiles	Full buffer best effort	Full buffer best effort	Full buffer best effort	Full buffer best effort	Full buffer best effort
Simulation bandwidth	10 MHz	10 MHz	10 MHz	Up to 10 MHz (for ISD = 500 m) Up to 50 MHz (for ISD = 1732 m)	Up to 40 MHz (for carrier frequency of 700 MHz) Up to 100 MHz (for carrier frequency of 4 GHz)
Number of users in simulation	1	1	1	≥ 1	1
Packet size	N.A.	N.A.	N.A.	32 bytes at Layer 2 PDU	32 bytes at Layer 2 PDU
Inter-packet arrival time	N.A.	N.A.	N.A.	1 message/day/device or 1 message/2 hours/device	N.A.

TABLE 7

Evaluation configuration parameters for analytical assessment of peak data rate, peak spectral efficiency

Parameters	Values
Number of BS antenna elements	700 MHz: Up to 64 Tx/Rx 4 GHz / 30 GHz: Up to 256 Tx /Rx 70 GHz: Up to 1 024 Tx/Rx
Number of UE antenna elements	700 MHz / 4 GHz: Up to 8 Tx /Rx 30 GHz: Up to 32 Tx /Rx 70 GHz: Up to 64 Tx /Rx

TABLE 8

Additional channel model parameters for link-level simulation

Parameters	Indoor Hotspot-eMBB (for Mobility)	Dense Urban-eMBB (for Mobility)	Rural-eMBB (for Mobility)	Urban Macro-mMTC (for Connection density)	Urban Macro-URLLC (for Reliability)
Link-level Channel model	NLOS: CDL/ TDL-i LOS: CDL/TDL-iv	NLOS: CDL/ TDL-iii LOS: CDL/TDL-v	NLOS: CDL/ TDL-iii LOS: CDL/TDL-v	NLOS: TDL-iii LOS: TDL-v	NLOS: TDL-iii LOS: TDL-v
Delay spread scaling parameter $DS_{desired}$ (s)	$\text{Log}_{10}(DS_{desired})$ = μ_{gDS} in Table A4-7 (InH) in Annex 1	$\text{Log}_{10}(DS_{desired})$ = μ_{gDS} in Table A4-9 (UMa) in Annex 1	$\text{Log}_{10}(DS_{desired})$ = μ_{gDS} in Table A4-13 (RMa) in Annex 1	$\text{Log}_{10}(DS_{desired})$ = μ_{gDS} in Table A4-9 (UMa) in Annex 1	$\text{Log}_{10}(DS_{desired})$ = μ_{gDS} in Table A4-9 (UMa) in Annex 1
AoA, AoD, ZoA angular spreads scaling parameter $AS_{desired}$ (degree)	$\text{Log}_{10}(AS_{desired})$ = $\mu_{gASA} / \mu_{gASD} / \mu_{gZSA}$ in Table A4-7 (InH) in Annex 1	$\text{Log}_{10}(AS_{desired})$ = $\mu_{gASA} / \mu_{gASD} / \mu_{gZSA}$ in Table A4-9 (UMa) in Annex 1	$\text{Log}_{10}(AS_{desired})$ = $\mu_{gASA} / \mu_{gASD} / \mu_{gZSA}$ in Table A4-13 (RMa) in Annex 1	$\text{Log}_{10}(AS_{desired})$ = $\mu_{gASA} / \mu_{gASD} / \mu_{gZSA}$ in Table A4-9 (UMa) in Annex 1	$\text{Log}_{10}(AS_{desired})$ = $\mu_{gASA} / \mu_{gASD} / \mu_{gZSA}$ in Table A4-9 (UMa) in Annex 1
ZoD angular spreads scaling parameter $AS_{desired}$ (degree)	$\text{Log}_{10}(AS_{desired})$ = μ_{gZSD} in Table A4-8 (InH) in Annex 1	$\text{Log}_{10}(AS_{desired})$ = μ_{gZSD} in Table A4-10 (UMa) in Annex 1	$\text{Log}_{10}(AS_{desired})$ = μ_{gZSD} in Table A4-14 (RMa) in Annex 1	$\text{Log}_{10}(AS_{desired})$ = μ_{gZSD} in Table A4-10 (UMa) in Annex 1	$\text{Log}_{10}(AS_{desired})$ = μ_{gZSD} in Table A4-10 (UMa) in Annex 1

NOTE 1 – The use of TDL or CDL is up to the proponent/evaluator.

NOTE 2 – Delay spreads and angular spreads (for AoA, AoD, ZoA, and ZoD) in link-level channel model are scaled to the median values for the environment and channel type (LOS/NLOS) evaluated, and system-level channel model variant (model A or model B) selected.

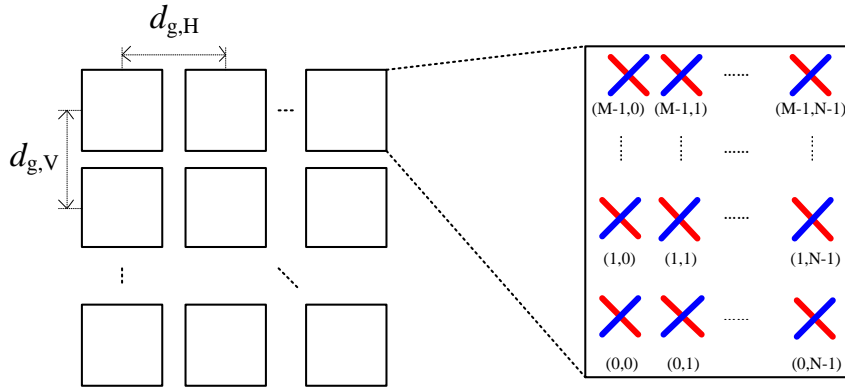
8.5 Antenna characteristics

This sub-section specifies the antenna characteristics, e.g. antenna pattern, gain, side-lobe level, orientation, etc., for antennas at the BS and the UE, which shall be applied for the evaluation in test environments with the hexagonal grid layouts and/or the non-hexagonal layouts. The characteristics do not form any kind of requirements and should be used only for the evaluation.

8.5.1 BS antenna

- BS antennas are modelled having one or multiple antenna panels, where an antenna panel has one or multiple antenna elements placed vertically, horizontally or in a two-dimensional array within each panel.
- An antenna panel has $M \times N$ antenna elements, where N is the number of columns and M is the number of antenna elements with the same polarization in each column. The antenna elements are uniformly spaced with a center-to-center spacing of d_H and d_V in the horizontal and vertical directions, respectively. The $M \times N$ elements may either be single polarized or dual polarized.
- When the BS has multiple antenna panels, a uniform rectangular panel array is modeled, comprising $M_g N_g$ antenna panels where M_g is number of panels in a column and N_g is number of panels in a row. Antenna panels are uniformly spaced with a center-to-center spacing of $d_{g,H}$ and $d_{g,V}$ in the horizontal and vertical direction respectively. See Fig. 4 for an illustration of the BS antenna model.

FIGURE 4
BS antenna model



The proponent and evaluator shall report the antenna polarization and the value of M , N , M_g , N_g , (d_H, d_V) and $(d_{g,H}, d_{g,V})$ in their evaluation, respectively.

For antenna element pattern, the general form of antenna element horizontal radiation pattern is specified as:

$$A_{E,H}(\varphi'') = -\min \left\{ 12 \left(\frac{\varphi''}{\varphi_{3dB}} \right)^2, SLA \right\}$$

where $-180^\circ \leq \varphi'' \leq 180^\circ$, $\min [.]$ denotes the minimum function, φ_{3dB} is the horizontal 3 dB beamwidth and SLA is the maximum side lobe level attenuation. The general form of antenna element vertical radiation pattern is specified as:

$$A_{E,V}(\theta'') = -\min \left\{ 12 \left(\frac{\theta'' - \theta_{tilt}}{\theta_{3dB}} \right)^2, SLA \right\}$$

where $0^\circ \leq \theta'' \leq 180^\circ$, θ_{3dB} is the vertical 3 dB beamwidth and θ_{tilt} is the tilt angle. Note that $\theta'' = 0^\circ$ points to the zenith and $\theta'' = 90^\circ$ points to the horizon. The combined vertical and horizontal antenna element pattern is then given as:

$$A''(\theta'', \varphi'') = -\min\{-[A_{E,V}(\theta'') + A_{E,H}(\varphi'')], SLA\}$$

where $A''(\theta'', \varphi'')$ is the the relative antenna gain (dB) of an antenna element in the direction (θ'', φ'') .

The BS side antenna element pattern for Dense Urban – eMBB (macro TRxP), Rural – eMBB, Urban Macro – mMTC and Urban Macro – URLLC test environments are provided in Table 9.

For Indoor Hotspot-eMBB test environment, the BS side antenna element pattern is provided in Table 10.

TABLE 9

3-TRxP BS antenna radiation pattern

Parameters	Values
Antenna element vertical radiation pattern (dB)	$A_{E,V}(\theta'') = -\min\left[12\left(\frac{\theta'' - 90^0}{\theta_{3dB}}\right)^2, SLA_V\right], \theta_{3dB} = 65^0, SLA_V = 30$
Antenna element horizontal radiation pattern (dB)	$A_{E,H}(\varphi'') = -\min\left[12\left(\frac{\varphi''}{\varphi_{3dB}}\right)^2, A_m\right], \varphi_{3dB} = 65^0, A_m = 30$
Combining method for 3D antenna element pattern (dB)	$A''(\theta'', \varphi'') = -\min\{-[A_{E,V}(\theta'') + A_{E,H}(\varphi'')], A_m\}$
Maximum directional gain of an antenna element $G_{E,max}$	8 dBi

TABLE 10

Indoor BS antenna radiation pattern – Ceiling-mount antenna pattern

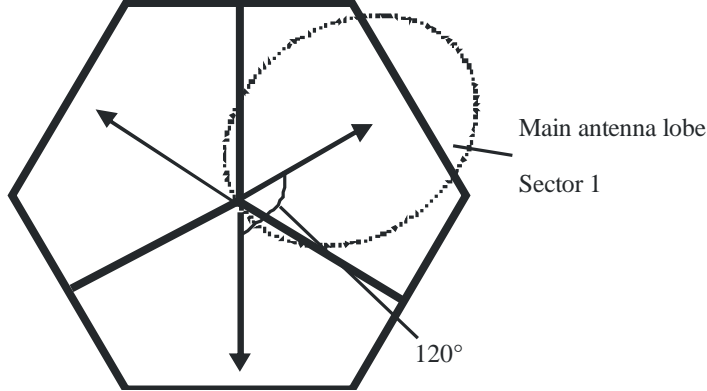
Parameters	Values
Antenna element vertical radiation pattern (dB)	$A_{E,V}(\theta'') = -\min\left[12\left(\frac{\theta'' - 90^0}{\theta_{3dB}}\right)^2, SLA_V\right], \theta_{3dB} = 90^0, SLA_V = 25$
Antenna element horizontal radiation pattern (dB)	$A_{E,H}(\varphi'') = -\min\left[12\left(\frac{\varphi''}{\varphi_{3dB}}\right)^2, A_m\right], \varphi_{3dB} = 90^0, A_m = 25$
Combining method for 3D antenna element pattern (dB)	$A''(\theta'', \varphi'') = -\min\{-[A_{E,V}(\theta'') + A_{E,H}(\varphi'')], A_m\}$
Maximum directional gain of an antenna element $G_{E,max}$	5 dBi

8.5.1.1 BS antenna orientation

The antenna bearing is defined as the angle between the main antenna lobe centre and a line directed due east given in degrees. The bearing angle increases in a clockwise direction. Figure 5 shows the hexagonal cell and its three TRxPs with the antenna bearing orientation proposed for the simulations

with three-TRxP sites. The centre directions of the main antenna lobe in each TRxP point to the corresponding side of the hexagon.

FIGURE 5
Antenna bearing orientation diagram



8.5.2 UE antenna

There are two options for UE side antenna element pattern. For 4 GHz and 700 MHz evaluation, Omni-directional antenna element is assumed.

For 30 GHz and 70 GHz evaluation, the directional antenna panel is assumed. In this case, the antenna pattern is defined in Table 11, and the $M_g N_g$ antenna panels may have different orientations. Introduce $(\Omega_{m_g, n_g}, \Theta_{m_g, n_g})$ as the orientation angles of the panel (m_g, n_g) $0 \leq m_g < M_g, 0 \leq n_g < N_g$, where the orientation of the first panel $(\Omega_{0,0}, \Theta_{0,0})$ is defined as the UE orientation, Ω_{m_g, n_g} is the array bearing angle and Θ_{m_g, n_g} is the array downtilt angle defined in Annex 1, § 4 (coordinate system).

TABLE 11

UE antenna radiation pattern model for 30 GHz and 70 GHz

Parameters	Values
Antenna element radiation pattern in θ'' dim (dB)	$A_{E,V}(\theta'') = -\min \left[12 \left(\frac{\theta'' - 90^0}{\theta_{3dB}} \right)^2, SLA_V \right], \theta_{3dB} = 90^0, SLA_V = 25$
Antenna element radiation pattern in φ'' dim (dB)	$A_{E,H}(\varphi'') = -\min \left[12 \left(\frac{\varphi''}{\varphi_{3dB}} \right)^2, A_m \right], \varphi_{3dB} = 90^0, A_m = 25$
Combining method for 3D antenna element pattern (dB)	$A''(\theta'', \varphi'') = -\min \left\{ - \left[A_{E,V}(\theta'') + A_{E,H}(\varphi'') \right], A_m \right\}$
Maximum directional gain of an antenna element $G_{E,max}$	5 dBi

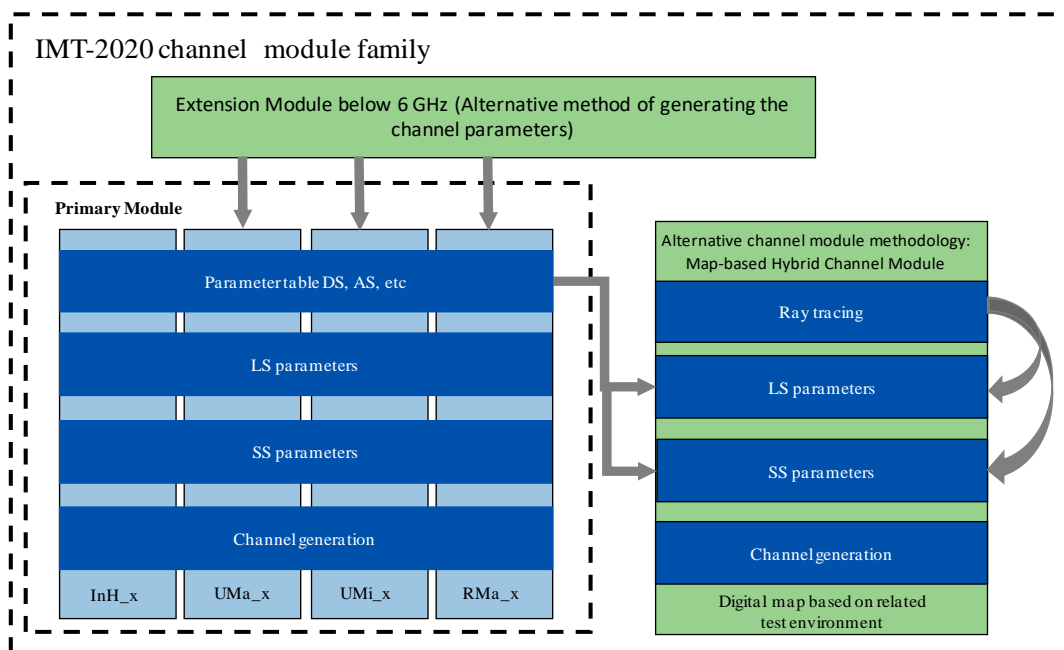
9 Evaluation model approach

9.1 Channel model approach

Channel models are needed in the evaluations of the IMT-2020 candidate RITs/SRITs to allow realistic modelling of the propagation conditions for the radio transmissions in the different environments. The channel model needs to cover all required test environments and usage scenarios of the IMT-2020 evaluations described in § 8.2.

The IMT-2020 channel model consists of a Primary Module, an Extension Module and a Map-based Hybrid Channel Module (last two of which provide optional means of generating fading parameters and optional channel modelling method), as shown in Fig. 6. Primary module parameters for evaluation of RITs for the test environments Indoor Hotspot-eMBB, Dense Urban-eMBB, Rural-eMBB, Urban Macro-URLLC, and Urban Macro-mMTC are described in detail in § 3 of Annex 1 for path loss, LOS probability and shadow fading, and § 4 of Annex 1 for fast fading.

FIGURE 6
The IMT-2020 channel model

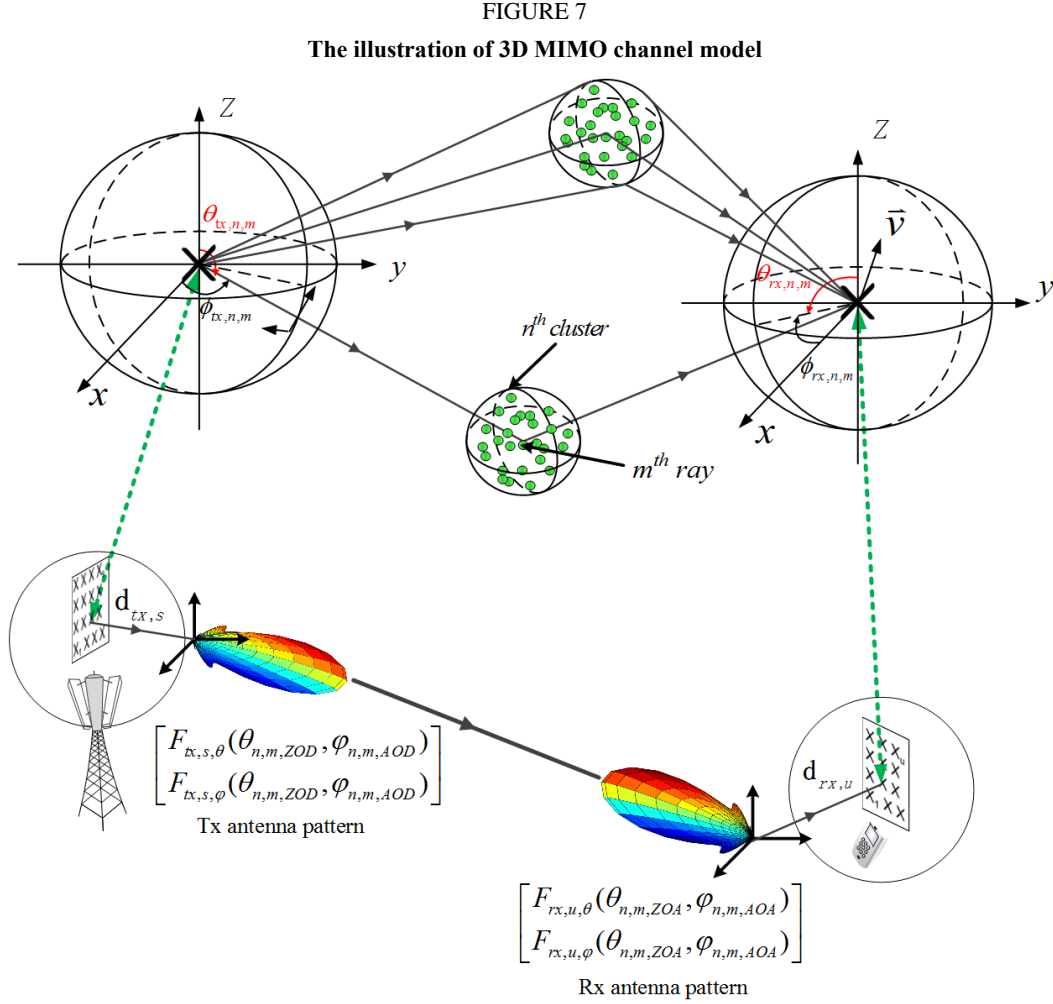


Primary Module

The IMT-2020 primary channel module is a geometry-based stochastic channel model. It does not explicitly specify the locations of the scatterers, but rather the directions of rays. Geometry based modelling of the radio channel enables separation of propagation parameters and antennas. The channel parameters for individual snapshots are determined stochastically based on statistical distributions extracted from channel measurements. Channel realizations are generated through the application of the geometrical principle by summing contributions of rays with specific small-scale parameters like delay, power, azimuth angles of arrival and departure, elevation angles of arrival and departure. Superposition results to correlation between antenna elements and temporal fading with geometry dependent Doppler spectrum.

The below section and equations aim to illustrate the principle of the model. The complete specification of the model is described in Annex 1 of this Report.

A single link channel model is shown in Fig. 7. Each circle with several dots represents scattering region causing one cluster, each cluster is constituted by M rays, and N clusters are assumed. S antennas are assumed for transmitter (Tx) and U antennas are assumed for receiver (Rx), respectively. The small-scale parameters like delay $\tau_{n,m}$, azimuth angle of arrival $\phi_{rx,n,m}$, elevation angle of arrival $\theta_{rx,n,m}$, azimuth angle of departure $\phi_{tx,n,m}$ and elevation angle of departure $\theta_{tx,n,m}$ are assumed to be different for each ray. Here the downlink is taken as one example to explain the principles of primary module.



The time-variant impulse matrix of $U \times S$ MIMO channel is given by:

$$\mathbf{H}(t; \tau) = \sum_{n=1}^N \mathbf{H}_n(t; \tau)$$

where:

- t : time
- τ : delay
- N : number of cluster
- n : cluster index.

It is composed of the antenna array response matrices \mathbf{F}_{tx} and \mathbf{F}_{rx} for the Tx and the Rx respectively, and the dual-polarized propagation channel response matrix.

The channel from the Tx antenna element, s , to the Rx element, u , for the cluster, n , is expressed as:

$$\begin{aligned} \mathbf{H}_{u,s,n,m}(t; \tau) = & \sqrt{\frac{P_n}{M}} \sum_{m=1}^M \begin{bmatrix} \mathbf{F}_{rx,u,\theta}(\theta_{n,mZOA}, \phi_{n,mAOA}) \\ \mathbf{F}_{rx,u,\phi}(\theta_{n,mZOA}, \phi_{n,mAOA}) \end{bmatrix}^T \begin{bmatrix} \exp(j \Phi_{n,m}^{\theta\theta}) & \sqrt{\kappa_{n,m}^{-1}} \exp(j \Phi_{n,m}^{\theta\phi}) \\ \sqrt{\kappa_{n,m}^{-1}} \exp(j \Phi_{n,m}^{\phi\theta}) & \exp(j \Phi_{n,m}^{\phi\phi}) \end{bmatrix} \\ & \times \begin{bmatrix} \mathbf{F}_{tx,s,\theta}(\theta_{n,mZOD}, \phi_{n,mAOD}) \\ \mathbf{F}_{tx,s,\phi}(\theta_{n,mZOD}, \phi_{n,mAOD}) \end{bmatrix} \exp(j 2\pi\lambda_0^{-1} (\mathbf{r}_{rx,n,m}^T \mathbf{d}_{rx,u})) \exp(j 2\pi\lambda_0^{-1} (\mathbf{r}_{tx,n,m}^T \mathbf{d}_{tx,s})) \\ & \times \exp(j 2\pi V_{n,m} t) \delta(\tau - \tau_{n,m}) \end{aligned}$$

where:

$\Phi_{n,m}^{\theta\theta}$, $\Phi_{n,m}^{\phi\phi}$, $\Phi_{n,m}^{\theta\phi}$ and $\Phi_{n,m}^{\phi\theta}$: random initial phase for each ray m of each cluster n and for four different polarisation combinations

$\mathbf{F}_{rx,u,\theta}$ and $\mathbf{F}_{rx,u,\phi}$: receive antenna element u field patterns in direction of the spherical basis vectors, θ and Φ , respectively

$\mathbf{F}_{tx,s,\theta}$ and $\mathbf{F}_{tx,s,\phi}$: transmit antenna element s field patterns in direction of the spherical basis vectors, θ and Φ , respectively

$\mathbf{r}_{rx,n,m}$ and $\mathbf{r}_{tx,n,m}$: spherical unit vector with azimuth arrival angle $\phi_{n,mAOA}$, elevation arrival angle $\theta_{n,mZOA}$ and azimuth departure angle $\phi_{n,mAOD}$, elevation departure angle $\theta_{n,mZOD}$

$\mathbf{d}_{rx,u}$ and $\mathbf{d}_{tx,s}$: location vector of receive antenna element u and transmit antenna element s

$\kappa_{n,m}$: cross polarisation power ratio in linear scale

λ_0 : wave length of the carrier frequency

$V_{n,m}$: Doppler frequency component of ray n, m .

If the radio channel is modelled as dynamic, all the above mentioned small-scale parameters are time variant, i.e. they are functions of t . The primary module, which covers the mathematical framework, a set of parameters as well as path loss models, comprehensively describes the channel characteristics as Annex 1 §§ 3 and 4.

The channel impulse response procedure given above is from a single antenna element to another antenna element. When antenna arrays are deployed at the Tx and Rx, the impulse response of such an arrangement results in the vector channel. An example of this is given for the case of a two-dimensional antenna array in Attachment 3 to Annex 1.

Extension Module below 6 GHz

The Extension Module below 6 GHz provides an alternative method of generating the channel parameters below 6 GHz in the primary module. It provides additional level of parameter variability. In the Primary Module, small-scale and large-scale parameters are variables, and the Extension Module provides new parameter values for the Primary Module based on environment-specific parameters. It still maintains the model framework.

The Extension Module is based on the time-spatial propagation model (i.e. TSP model) which is a geometry-based double directional channel model with closed-form functions. It calculates the large-

scale parameters for the channel realization by taking into account the following key parameters such as city structures (street width, average building height), BS height, bandwidth and the distance between the BS and the UE.

Map-based Hybrid Channel Module

The Map-based Hybrid Channel Module is an optional module, which is based on a digital map, and consists of a deterministic component following, e.g. METIS work and a stochastic component and can be used if:

- The system performance is desired to be evaluated or predicted with the adoption of digital map to take into account the impacts from environmental structures and materials.

The implementation of the Map-based Hybrid Channel Module starts with the definitions of scenario and digitized map. Based on the imported configurations, the Ray-tracing is applied to each pair of link Tx/Rx end with the output including LOS state/deterministic power, delay, angular information etc. Then, the large-scale parameters except for shadow fading, are adopted to generate the delay and virtual power for random clusters based on the similar procedures of primary model, where the threshold of probability for cluster inter-arrival interval is considered in the selection of random clusters. The real powers of the selected random clusters are calculated based on deterministic results. After merging the random and deterministic clusters, the generations of the channel coefficients are conducted through the similar procedures as the primary module except for the inherited mean value of cross polarization ratio (XPR) for dominant paths from the corresponding deterministic results.

10 List of acronyms and abbreviations

BS	Base station
CDF	Cumulative distribution function
eMBB	Enhanced Mobile Broadband
ISD	Inter-site distance
LMLC	Low mobility large cell
mMTC	Massive machine type communications
PDU	Protocol data unit
RIT	Radio interface technology
SRIT	Set of radio interface technologies
TRxP	Transmission reception point
UE	User equipment
URLLC	Ultra-reliable and low latency communications.

Annex 1

Test Environments and Channel Models

1 Test environments and mapping to channel model scenario

This Annex provides the reference channel models for test environment needed to evaluate IMT-2020 technical performance. The test environments are intended to cover the range of IMT-2020 radio operating environments.

The test environments are considered as a basic factor in the evaluation process of the candidate RITs. The reference models are used to estimate the critical aspects, such as spectrum, coverage and power efficiencies.

Test environment reflects geographic environment and usage scenario which is used for entire evaluation process and corresponding to technical performance requirements to be met.

- **Indoor hotspot-eMBB**: an indoor isolated environment at offices and/or in shopping malls based on stationary and pedestrian users with very high user density.
- **Dense Urban-eMBB**: an urban environment with high user density and traffic loads focusing on pedestrian and vehicular users.
- **Rural-eMBB**: a rural environment with larger and continuous wide area coverage, supporting pedestrian, vehicular and high speed vehicular users.
- **Urban Macro-mMTC**: an urban macro environment targeting continuous coverage focusing on a high number of connected machine type devices.
- **Urban Macro-URLLC**: an urban macro environment targeting ultra-reliable and low latency communications.

IMT-2020 is to cover a wide range of performance in a wide range of environments comprising the three usage scenarios. IMT-2020 primary module includes channel model A and B, which are both based on field measurements and are equally valid for IMT-2020 evaluation. Either of them can be used for the evaluation.

The channel models here described are InH_x (Indoor Hotspot), UMa_x (Urban Macro), UMi_x (Urban Micro), and RMa_x (Rural Macro). For each environment, the corresponding channel models to be used are specified in Table A1-1.

In this Annex, whenever a channel model is referred to with the _x suffix, this is meant to include both variants of the model, e.g. InH_x is taken to mean both InH_A and InH_B. Similarly, whenever a variant is referred to as “model A” or “model B” this is meant to include all instances of this variant, e.g. model A is taken to mean all of InH_A, UMa_A, UMi_A, and RMa_A.

TABLE A1-1

The mapping of channel models to the test environments

Test environment	Indoor Hotspot – eMBB	Dense urban – eMBB	Rural – eMBB	Urban macro - mMTC	Urban macro - URLLC
Channel model	InH_A, InH_B	Macro layer: UMa_A, UMa_B Micro layer: UMi_A, UMi_B	RMa_A, RMa_B	UMa_A, UMa_B	UMa_A, UMa_B

2 Overview of IMT-2020 channel modelling**2.1 Introduction**

The IMT-2020 channel model is established to meet the requirements of evaluating IMT-2020 candidate radio interface technologies (RITs) by allowing realistic modelling of the propagation conditions for the radio transmissions in different environments. Many organizations, groups and projects have made a great effort on channel model research for IMT-2020, e.g. 3rd Generation Partnership Project (3GPP), Mobile and wireless communications Enabler for the Twenty-twenty Information Society (METIS), Millimetre-wave Evolution for Backhaul and Access (MiWEBA), COST2100, IEEE802.11, and 5G Promotion Association in China, etc.

In order to meeting the technical requirements of IMT-2020 technologies, new features are captured in IMT-2020 channel model compared to IMT-Advanced channel model, such as supporting frequencies up to 100 GHz and large bandwidth, three dimensional (3D) modelling, supporting large antenna array, blockage modelling, and spatial consistency, etc.

2.2 Advances in channel modelling

This sub-section motivates some new capabilities of the channel model for IMT-2020 evaluations compared to previous models. For instance, higher frequencies, wider bandwidths and larger antenna arrays set new requirements to the channel models. Therefore, new features in the IMT-2020 channel model are needed. These new features include, e.g. 3D modelling, spatial consistency and clusters, large bandwidth and large antenna arrays, blockage modelling, gaseous absorption, ground reflection, vegetation, and channel sparsity, are introduced below.

3D modelling

3D modelling describes the channel propagation both in azimuth and elevation dimensions at both Tx and Rx. It is more complete and accurate compared with two-dimensional (2D) modelling which only considers the propagation characteristics in the azimuth dimension. Multi-antenna techniques capable of exploiting the elevation dimension are expected to be very important in IMT-2020, so that 3D channel model is required, which includes the elevation angles of departure and arrival, and their correlation with other parameters [1].

Spatial consistency and clusters

The spatial consistency of channel, on one hand, means that the channel evolves smoothly without discontinuities when the Tx and/or Rx moves or turns; on the other hand, means that channel characteristics are highly correlated in closely located links, e.g. two close-by mobile stations seen by the same base station. The spatial consistency covers various aspects including not only large scale

parameters and small scale parameters of delay, Angle of Arrival (AOA) and Angle of Departure (AOD), but also outdoor/indoor state, Line of Sight (LOS)/non-LOS (NLOS) state, blockage and shadowing which are also very important for evaluating the system performance, and finally facilitates the evaluations of beam tracking and Multi-user MIMO (MU-MIMO) performance.

Large bandwidth and large antenna arrays

To support the evaluation of large bandwidth and large antenna array, the channel model should be specified with sufficiently high resolution in the delay and angular domain. Large antenna arrays here contain two aspects. One is the very large size of the antenna array, the other is the large number of antenna elements of antenna array, referred as massive MIMO. These require the high angular resolution in channel model, which means more accurate modelling of AOA/AOD, and possibly higher number of multi-paths as well. In addition, different structures of antenna array could affect the performance of IMT-2020 technology. Since the elevation dimension can be used, the antenna elements are not only distributed in the azimuth plane but also in elevation, so that the antenna structure could be more complicated. Various types of antenna array like uniform linear array (ULA), uniform rectangle antenna array (URA) and uniform cylinder array (UCA) need to be considered and evaluated.

Blockage modelling

The blockage model describes the phenomenon where the stationary or moving objects standing between the transmitter and receivers dramatically changes the channel characteristics when the signal is blocked, especially for high frequency bands, since mm-waves do not effectively penetrate or diffract around human bodies [2] and other objects (such as cars, trucks, etc.). Shadowing by these objects is an important factor in the link budget and the time variation of the channel, and such dynamic blocking may be important to capture in evaluations of technologies that include beam-finding and beam-tracking capabilities. The effect of the blockage should be considered not only on the total received power, but also on the angle or power of multipath due to different size, location and direction of the blocker [3].

Gaseous absorption

The electromagnetic wave may be partially or totally absorbed by an absorbing medium due to atomic and molecular interactions. This gaseous absorption causes additional loss to the radio wave propagation [4]. The effect of gaseous absorption may not be neglected in the high frequency band. For frequencies around 60 GHz, additional loss of gaseous absorption is applied to the cluster responses for different centre frequency and bandwidth correspondingly.

Ground reflection

Measurements in millimetre wave frequency bands have shown that ground reflection in millimetre wave has significant effect which can produce a strong propagation path that superimposes with the direct LOS path and induces severe fading effects. In order to accurately capture the impact of ground reflection on future IMT-2020 systems, it is recommended to include ground reflection as an optional feature in the IMT-2020 channel model.

Vegetation effects

Radio waves are affected by foliage and this effect increases with frequency. The main propagation phenomena involved are: attenuation of the radiation through the foliage, diffraction above/below and sideways around the canopy, and diffuse scattering by the leaves. The vegetation effects are captured implicitly in the path loss equations.

Channel sparsity

It is often claimed that mm-wave channels are ‘sparse’ (i.e. have few entries in the delay angle bins), though experimental verification of this may be limited due to the resolution of rotating horn antennas used for such measurements. However, a lower bound on the channel sparsity can still be established from existing measurements, and in many environments the percentage of delay/angle bins with significant energy is rather low but not necessarily lower than at centimeter wave frequencies.

Random Cluster Number

In the Primary Module, the number of clusters are fixed and frequency independent. The typical number of clusters reported in the literature is often small, random, and can be modeled as a Poisson distribution. By choosing an appropriate mean value of the Poisson distribution, the events with a larger number of clusters with a low probability may also be produced.

3 Path loss models, LOS probability, shadow fading

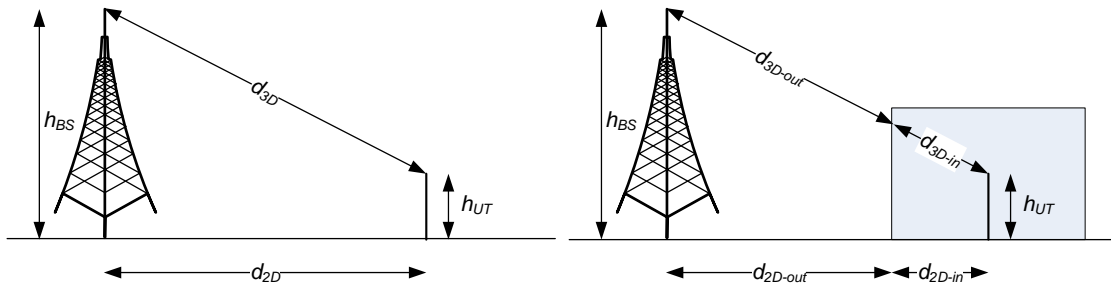
This section will give the detailed pathloss models, LOS probability and shadow fading for primary module. These are developed based on measurement results carried out in references [5] to [14], as well as results from the literature.

3.1 Path loss model

The pathloss models and their applicability, including frequency ranges, are summarized in Tables A1-2 to A1-5 and the distance definitions are indicated in Fig. A1-1.

Note that the distribution of the shadow fading is modelled as log-normal, and its standard deviation for each scenario is given in Tables A1-2 to A1-5.

FIGURE A1-1
Definition of d_{2D} and d_{3D} for outdoor UTs (left), definition of d_{2D-out} , d_{2D-in} , d_{3D-out} , and d_{3D-in} for indoor UTs (right)



Note that:

$$d_{3D} = d_{3D-out} + d_{3D-in} = \sqrt{(d_{2D-out} + d_{2D-in})^2 + (h_{BS} - h_{UT})^2} \quad (1)$$

In the Tables A1-2 to A1-5, the following applies:

- Note 1 – f_c in GHz denotes the center frequency normalized by 1 GHz, distance related values in meters are normalized by 1 m, unless it is stated otherwise.
- Note 2 – h_{UT} and h_{BS} are the antenna height at BS and UT, respectively. h and W are the average building height and average street width.
- Note 3 – For UMa_x, UMi_x, break point distance $d'_{BP} = 4 h'_{BS} h'_{UT} f_c / c$, where f_c is the centre frequency in Hz, $c = 3.0 \times 10^8$ m/s is the propagation velocity in free space, and h'_{BS} and h'_{UT}

are the effective antenna heights at the BS and the UT, respectively. The effective antenna heights h'_{BS} and h'_{UT} are computed as follows: $h'_{BS} = h_{BS} - h_E$, $h'_{UT} = h_{UT} - h_E$, where h_{BS} and h_{UT} are the actual antenna heights, and h_E is the effective environment height. For UMi_x $h_E=1$ m. For UMa_x $h_E=1$ m with a probability equal to $1/(1+C(d_{2D}, h_{UT}))$ and chosen from a discrete uniform distribution $\text{uniform}(12, 15, \dots, (h_{UT}-1.5))$ otherwise. Here $C(d_{2D}, h_{UT})$ given by:

$$C(d_{2D}, h_{UT}) = \begin{cases} 0 & , h_{UT} < 13\text{m} \\ \left(\frac{h_{UT} - 13}{10}\right)^{1.5} g(d_{2D}) & , 13\text{m} \leq h_{UT} \leq 23\text{m} \end{cases}$$

where:

$$g(d_{2D}) = \begin{cases} 0 & , d_{2D} \leq 18\text{m} \\ \frac{5}{4} \left(\frac{d_{2D}}{100}\right)^3 \exp\left(\frac{-d_{2D}}{150}\right) & , 18\text{m} < d_{2D} \end{cases}$$

- Note 4 – For RMa_x, break point distance $d_{BP} = 2\pi h_{BS} h_{UT} f_c / c$, where f_c is the centre frequency in Hz, $c = 3.0 \times 10^8$ m/s is the propagation velocity in free space, and h_{BS} and h_{UT} are the antenna heights at the BS and the UT, respectively.

3.1.1 InH_x

TABLE A1-2
Path loss and shadow fading for InH_x

InH_A	InH_B
LOS	LOS
$0.5 \text{ GHz} \leq f_c \leq 6 \text{ GHz}$ $PL_{\text{InH-LOS}} = 16.9 \log_{10}(d_{3D}) + 32.8 + 20 \log_{10}(f_c), \sigma_{SF} = 3 \text{ dB}, 0 \text{ m} \leq d_{2D} \leq 150 \text{ m},$	$0.5 \text{ GHz} \leq f_c \leq 100 \text{ GHz}$ $PL_{\text{InH-LOS}} = 32.4 + 17.3 \log_{10}(d_{3D}) + 20 \log_{10}(f_c), \sigma_{SF} = 3 \text{ dB}, 1 \text{ m} \leq d_{3D} \leq 150 \text{ m}$
$6 \text{ GHz} < f_c \leq 100 \text{ GHz}$ $PL_{\text{InH-LOS}} = 32.4 + 17.3 \log_{10}(d_{3D}) + 20 \log_{10}(f_c), \sigma_{SF} = 3, 1 \text{ m} \leq d_{3D} \leq 150 \text{ m}$	
NLOS	NLOS
$0.5 \text{ GHz} \leq f_c \leq 6 \text{ GHz}$ $PL_{\text{InH-NLOS}} = 43.3 \log_{10}(d_{3D}) + 11.5 + 20 \log_{10}(f_c), \sigma_{SF} = 4 \text{ dB}, 0 \text{ m} \leq d_{2D} \leq 150 \text{ m}$	$0.5 \text{ GHz} \leq f_c \leq 100 \text{ GHz}$ $PL_{\text{InH-NLOS}} = \max(PL_{\text{InH-LOS}}, PL'_{\text{InH-NLOS}})$ $PL'_{\text{InH-NLOS}} = 38.3 \log_{10}(d_{3D}) + 17.30 + 24.9 \log_{10}(f_c), \sigma_{SF} = 8.03 \text{ dB}, 1 \text{ m} \leq d_{3D} \leq 150 \text{ m}$ Optional: $PL'_{\text{InH-NLOS}} = 32.4 + 20 \log_{10}(f_c) + 31.9 \log_{10}(d_{3D}), \sigma_{SF} = 8.29 \text{ dB}$
$6 \text{ GHz} < f_c \leq 100 \text{ GHz}$ $PL_{\text{InH-NLOS}} = \max(PL_{\text{InH-LOS}}, PL'_{\text{InH-NLOS}})$ $PL'_{\text{InH-NLOS}} = 38.3 \log_{10}(d_{3D}) + 17.30 + 24.9 \log_{10}(f_c), \sigma_{SF} = 8.03 \text{ dB}, 1 \text{ m} \leq d_{3D} \leq 150 \text{ m}$ Optional: $PL'_{\text{InH-NLOS}} = 32.4 + 20 \log_{10}(f_c) + 31.9 \log_{10}(d_{3D}), \sigma_{SF} = 8.29 \text{ dB}$	
$3 \text{ m} \leq h_{\text{BS}} \leq 6 \text{ m}, 1 \text{ m} \leq h_{\text{UT}} \leq 2.5 \text{ m}$	

Optional Model I	Optional Model II
LOS	LOS
$f_c = 28\text{GHz}$ $PL_{\text{InH-LOS}} = 14.0 \log_{10}(d_{2D}) + 61.9, \sigma_{SF} = 1.7\text{ dB}$	$1\text{GHz} \leq f_c \leq 100\text{GHz},$ $PL_{\text{InH-LOS}} = 32.4 + 17.1 \log_{10}(d_{3D}) + 20 \log_{10}(f_c), \sigma_{SF} = 3\text{ dB}, 1\text{m} \leq d_{3D} \leq 150\text{m},$ $h_{BS} = 2.5 - 6\text{m}, h_{UT} = 1 - 2.5\text{m}$
NLOS	NLOS
$f_c = 28\text{GHz}$ $PL_{\text{InH-NLOS}} = 22 \log_{10}(d_{2D}) + 61.2, \sigma_{SF} = 3.3\text{ dB}$	$1\text{GHz} \leq f_c \leq 100\text{GHz},$ $PL_{\text{InH-NLOS}} = \max(PL_{\text{InH-LOS}}, PL'_{\text{InH-NLOS}}), \sigma_{SF} = 3.2 + 3.2 \log_{10}(f_c)\text{ dB}$ $PL'_{\text{InH-NLOS}} = 32.1 + 26.3 \log_{10}(f_c) + [23.6 + 1.0 \log_{10}(f_c)] \log_{10}(d_{3D})$

3.1.2 UMa_x

TABLE A1-3

Path loss and shadow fading for UMa_x

UMa_A	UMa_B
LOS	LOS
$0.5\text{GHz} \leq f_c \leq 6\text{GHz}$ and $6\text{GHz} < f_c \leq 100\text{GHz}$ $PL_{\text{UMa-LOS}} = \begin{cases} PL_1 & 10\text{m} \leq d_{2D} \leq d'_{BP}, \text{ see Note 3} \\ PL_2 & d'_{BP} \leq d_{2D} \leq 5\text{km} \end{cases}$ $PL_1 = 28.0 + 22\log_{10}(d_{3D}) + 20\log_{10}(f_c), \sigma_{SF} = 4\text{ dB}$ $PL_2 = 40\log_{10}(d_{3D}) + 28.0 + 20\log_{10}(f_c) - 9\log_{10}((d'_{BP})^2 + (h_{BS} - h_{UT})^2),$ $\sigma_{SF} = 4\text{ dB}$	$0.5\text{GHz} \leq f_c \leq 100\text{GHz}$ $PL_{\text{UMa-LOS}} = \begin{cases} PL_1 & 10\text{m} \leq d_{2D} \leq d'_{BP}, \text{ see Note 3} \\ PL_2 & d'_{BP} \leq d_{2D} \leq 5\text{km} \end{cases}$ $PL_1 = 28.0 + 22\log_{10}(d_{3D}) + 20\log_{10}(f_c), \sigma_{SF} = 4\text{ dB}$ $PL_2 = 40\log_{10}(d_{3D}) + 28.0 + 20\log_{10}(f_c) - 9\log_{10}((d'_{BP})^2 + (h_{BS} - h_{UT})^2),$ $\sigma_{SF} = 4\text{ dB}$
NLOS	NLOS
$0.5\text{GHz} \leq f_c \leq 6\text{GHz}$ $PL_{\text{UMa-NLOS}} = \max(PL_{\text{UMa-LOS}}, PL'_{\text{UMa-NLOS}})$ $PL'_{\text{UMa-NLOS}} = 161.04 - 7.1\log_{10}(W) + 7.5\log_{10}(h) - (24.37 - 3.7(h/h_{BS})^2)\log_{10}(h_{BS})$ $+ (43.42 - 3.1\log_{10}(h_{BS}))(\log_{10}(d_{3D}) - 3) + 20\log_{10}(f_c) - (3.2(\log_{10}(17.625))^2 - 4.97)$ $- 0.6(h_{UT} - 1.5)$ $, \sigma_{SF} = 6\text{ dB}, 10\text{m} < d_{2D} < 5000\text{m}, W = 20\text{m}, h = 20\text{m}$	$0.5\text{GHz} \leq f_c \leq 100\text{GHz}$ $PL_{\text{UMa-NLOS}} = \max(PL_{\text{UMa-LOS}}, PL'_{\text{UMa-NLOS}}), \text{ for } 10\text{m} \leq d_{2D} \leq 5\text{km}$ $PL'_{\text{UMa-NLOS}} = 13.54 + 39.08\log_{10}(d_{3D}) + 20\log_{10}(f_c) - 0.6(h_{UT} - 1.5), \sigma_{SF} = 6\text{ dB}$ Optional $PL = 32.4 + 20\log_{10}(f_c) + 30\log_{10}(d_{3D}) \sigma_{SF} = 7.8\text{ dB}$
$6\text{GHz} < f_c \leq 100\text{GHz}$ $PL_{\text{UMa-NLOS}} = \max(PL_{\text{UMa-LOS}}, PL'_{\text{UMa-NLOS}}), \text{ for } 10\text{m} \leq d_{2D} \leq 5\text{km}$ $PL'_{\text{UMa-NLOS}} = 13.54 + 39.08\log_{10}(d_{3D}) + 20\log_{10}(f_c) - 0.6(h_{UT} - 1.5), \sigma_{SF} = 6\text{ dB}$ Optional $PL = 32.4 + 20\log_{10}(f_c) + 30\log_{10}(d_{3D}) \sigma_{SF} = 7.8\text{ dB}$	
$h_{BS} = 25\text{m}, 1.5\text{m} \leq h_{UT} \leq 22.5\text{m}$	

3.1.3 UMi_x

TABLE A1-4
Path loss and shadow fading for UMi_x

UMi_A	UMi_B
LOS	LOS
$0.5 \text{ GHz} \leq f_c \leq 6 \text{ GHz}$ $PL = 22.0 \log_{10}(d_{3D}) + 28.0 + 20 \log_{10}(f_c), \sigma_{SF} = 3 \text{ dB}, 10 \text{ m} < d_{2D} < d'_{BP} \text{ }^{(3)}$ $PL = 40 \log_{10}(d_{3D}) + 28.0 + 20 \log_{10}(f_c) - 9 \log_{10}((d'_{BP})^2 + (h_{BS} - h_{UT})^2), \sigma_{SF} = 3 \text{ dB},$ $d'_{BP} < d_{2D} < 5000 \text{ m} \text{ }^{(3)}$ $6 \text{ GHz} < f_c \leq 100 \text{ GHz}$ $PL_{UMi-LOS} = \begin{cases} PL_1 & 10 \text{ m} \leq d_{2D} \leq d'_{BP} \\ PL_2 & d'_{BP} \leq d_{2D} \leq 5 \text{ km} \end{cases}, \text{ see Note 3}$ $PL_1 = 32.4 + 21 \log_{10}(d_{3D}) + 20 \log_{10}(f_c), \sigma_{SF} = 4 \text{ dB}$ $PL_2 = 32.4 + 40 \log_{10}(d_{3D}) + 20 \log_{10}(f_c) - 9.5 \log_{10}((d'_{BP})^2 + (h_{BS} - h_{UT})^2), \sigma_{SF} = 4$ dB	$0.5 \text{ GHz} \leq f_c \leq 100 \text{ GHz}$ $PL_{UMi-LOS} = \begin{cases} PL_1 & 10 \text{ m} \leq d_{2D} \leq d'_{BP} \\ PL_2 & d'_{BP} \leq d_{2D} \leq 5 \text{ km} \end{cases}, \text{ see Note 3}$ $PL_1 = 32.4 + 21 \log_{10}(d_{3D}) + 20 \log_{10}(f_c), \sigma_{SF} = 4 \text{ dB}$ $PL_2 = 32.4 + 40 \log_{10}(d_{3D}) + 20 \log_{10}(f_c) - 9.5 \log_{10}((d'_{BP})^2 + (h_{BS} - h_{UT})^2), \sigma_{SF} = 4$ dB
NLOS	NLOS
$0.5 \text{ GHz} \leq f_c \leq 6 \text{ GHz}$ $PL_{UMi-NLOS} = \max(PL_{UMi-LOS}, PL'_{UMi-NLOS}),$ $PL'_{UMi-NLOS} = 36.7 \log_{10}(d_{3D}) + 22.7 + 26 \log_{10}(f_c) - 0.3(h_{UT} - 1.5), \sigma_{SF} = 4 \text{ dB},$ $10 \text{ m} < d_{2D} < 2000 \text{ m}$	$0.5 \text{ GHz} \leq f_c \leq 100 \text{ GHz}$ $PL_{UMi-NLOS} = \max(PL_{UMi-LOS}, PL'_{UMi-NLOS}), \sigma_{SF} = 7.82 \text{ dB}, 10 \text{ m} \leq d_{2D} \leq 5 \text{ km},$ $PL'_{UMi-NLOS} = 35.3 \log_{10}(d_{3D}) + 22.4 + 21.3 \log_{10}(f_c) - 0.3(h_{UT} - 1.5)$ $\text{Optional PL} = 32.4 + 20 \log_{10}(f_c) + 31.9 \log_{10}(d_{3D}), \sigma_{SF} = 8.2 \text{ dB}$
$6 \text{ GHz} < f_c \leq 100 \text{ GHz}$ $PL_{UMi-NLOS} = \max(PL_{UMi-LOS}, PL'_{UMi-NLOS}), \sigma_{SF} = 7.82, 10 \text{ m} \leq d_{2D} \leq 5 \text{ km}$ $PL'_{UMi-NLOS} = 35.3 \log_{10}(d_{3D}) + 22.4 + 21.3 \log_{10}(f_c) - 0.3(h_{UT} - 1.5)$ $6 \text{ GHz} < f_c \leq 100 \text{ GHz optional PL} = 32.4 + 20 \log_{10}(f_c) + 31.9 \log_{10}(d_{3D}), \sigma_{SF} = 8.2 \text{ dB}$	
$h_{BS} = 10 \text{ m}, 1.5 \text{ m} \leq h_{UT} \leq 22.5 \text{ m}$	

3.1.4 RMa_x

TABLE A1-5
Path loss and shadow fading for RMa_x

RMa_A	RMa_B
LOS	LOS
$0.5 \text{ GHz} \leq f_c \leq 6 \text{ GHz},$ $PL_{\text{RMa-LOS}} = \begin{cases} PL_1 & 10\text{m} \leq d_{2D} \leq d_{\text{BP}}, \text{ see Note 4} \\ PL_2 & d_{\text{BP}} \leq d_{2D} \leq 21\text{km} \end{cases}$ $PL_1 = 20 \log_{10}(40\pi d_{3D} f_c / 3) + \min(0.03h^{1.72}, 10) \log_{10}(d_{3D}) - \min(0.044h^{1.72}, 14.77) + 0.002 \log_{10}(h) d_{3D}$ $, \sigma_{SF} = 4 \text{ dB}$ $PL_2 = PL_1(d_{\text{BP}}) + 40 \log_{10}(d_{3D} / d_{\text{BP}}), \sigma_{SF} = 6 \text{ dB}$	$0.5 \text{ GHz} \leq f_c \leq 30 \text{ GHz}$ $PL_{\text{RMa-LOS}} = \begin{cases} PL_1 & 10\text{m} \leq d_{2D} \leq d_{\text{BP}}, \text{ see Note 4} \\ PL_2 & d_{\text{BP}} \leq d_{2D} \leq 21\text{km} \end{cases}$ $PL_1 = 20 \log_{10}(40\pi d_{3D} f_c / 3) + \min(0.03h^{1.72}, 10) \log_{10}(d_{3D}) - \min(0.044h^{1.72}, 14.77) + 0.002 \log_{10}(h) d_{3D}$ $, \sigma_{SF} = 4 \text{ dB}$ $PL_2 = PL_1(d_{\text{BP}}) + 40 \log_{10}(d_{3D} / d_{\text{BP}}), \sigma_{SF} = 6 \text{ dB}$
NLOS	NLOS
$0.5 \text{ GHz} \leq f_c \leq 6 \text{ GHz},$ $PL_{\text{RMa-NLOS}} = 161.04 - 7.1 \log_{10}(W) + 7.5 \log_{10}(h) - (24.37 - 3.7(h/h_{\text{BS}})^2) \log_{10}(h_{\text{BS}}) + (43.42 - 3.1 \log_{10}(h_{\text{BS}})) (\log_{10}(d_{3D}) - 3) + 20 \log_{10}(f_c) - (3.2 (\log_{10}(11.75 h_{\text{UT}}))^2 - 4.97), \sigma_{SF} = 8 \text{ dB for } 10 \text{ m} < d_{2D} < 21 \text{ km.}$ $\text{For LMLC } PL_{\text{RMa-NLOS}} = \max(PL_{\text{RMa-LOS}}, PL'_{\text{RMa-NLOS}} - 12)$	$0.5 \text{ GHz} \leq f_c \leq 30 \text{ GHz},$ $PL_{\text{RMa-NLOS}} = \max(PL_{\text{RMa-LOS}}, PL'_{\text{RMa-NLOS}}), \text{ for } 10 \text{ m} < d_{2D} < 21 \text{ km}$ $PL'_{\text{RMa-NLOS}} = 161.04 - 7.1 \log_{10}(W) + 7.5 \log_{10}(h) - (24.37 - 3.7(h/h_{\text{BS}})^2) \log_{10}(h_{\text{BS}}) + (43.42 - 3.1 \log_{10}(h_{\text{BS}})) (\log_{10}(d_{3D}) - 3) + 20 \log_{10}(f_c) - (3.2 (\log_{10}(11.75 h_{\text{UT}}))^2 - 4.97), \sigma_{SF} = 8$ dB $\text{For LMLC } PL_{\text{RMa-NLOS}} = \max(PL_{\text{RMa-LOS}}, PL'_{\text{RMa-NLOS}} - 12)$
$h_{\text{BS}} = 35\text{m}, h_{\text{UT}} = 1.5\text{m}, W = 20\text{m}, h = 5\text{m}$ <p style="text-align: center;">The applicability ranges:</p> $5\text{m} \leq h \leq 50\text{m}, 5\text{m} \leq W \leq 50\text{m}, 10\text{m} \leq h_{\text{BS}} \leq 150\text{m}, 1\text{m} \leq h_{\text{UT}} \leq 10\text{m}$	$h_{\text{BS}} = 35\text{m}, h_{\text{UT}} = 1.5\text{m}, W = 20\text{m}, h = 5\text{m}$ <p style="text-align: center;">The applicability ranges:</p> $5\text{m} \leq h \leq 50\text{m}, 5\text{m} \leq W \leq 50\text{m}, 10\text{m} \leq h_{\text{BS}} \leq 150\text{m}, 1\text{m} \leq h_{\text{UT}} \leq 10\text{m}$ <p style="text-align: center;">NOTE – the RMa pathloss model for >7 GHz is validated based on a single measurement campaign conducted at 24 GHz.</p>

3.2 Outdoor to indoor (O-to-I) building penetration loss

The pathloss incorporating O-to-I building penetration loss is modelled as in the following:

$$PL = PL_b + PL_{tw} + PL_{in} + N(0, \sigma_P^2) \quad (2)$$

where PL_b is the basic outdoor pathloss given in § 3.1. PL_{tw} is the building penetration loss through the external wall, PL_{in} is the inside loss dependent on the depth into the building, and σ_P is the standard deviation for the penetration loss.

For model B, at all frequencies, and for model A, above 6 GHz, PL_{tw} is characterized as:

$$PL_{tw} = PL_{npi} - 10 \log_{10} \sum_{i=1}^N \left(p_i \times 10^{-\frac{L_{material_i}}{10}} \right) \quad (3)$$

PL_{npi} is an additional loss is added to the external wall loss to account for non-perpendicular incidence;

$L_{material_i} = a_{material_i} + b_{material_i} \cdot f$, is the penetration loss of material i, example values of which can be found in Table A1-6.

p_i is proportion of i-th materials, where $\sum_{i=1}^N p_i = 1$; and N is the number of materials.

TABLE A1-6

Material penetration losses

Material	Penetration loss [dB] (f is in GHz)
Standard multi-pane glass	$L_{glass} = 2 + 0.2 \cdot f$
Infrared Reflective (IRR) glass	$L_{IRRglass} = 23 + 0.3 \cdot f$
Concrete	$L_{concrete} = 5 + 4 \cdot f$
Wood	$L_{wood} = 4.85 + 0.12 \cdot f$

Tables A1-7 and A1-8 gives PL_{tw} , PL_{in} and σ_P for the O-to-I penetration loss models in model A and model B. The O-to-I penetration is UT-specifically generated, and is added to the shadow fading realization in the log domain.

TABLE A1-7

O-to-I penetration loss model for model A

	Path loss through external wall: PL_{tw} [dB]	Indoor loss: PL_{in} [dB]	Standard deviation: σ_P [dB]
Low-loss model (> 6 GHz)	$5 - 10\log_{10}(0.3 \cdot 10^{-L_{glass}/10} + 0.7 \cdot 10^{-L_{concrete}/10})$	$0.5d_{2D-in}$	4.4
High-loss model (> 6 GHz)	$5 - 10\log_{10}(0.7 \cdot 10^{-L_{IRRglass}/10} + 0.3 \cdot 10^{-L_{concrete}/10})$	$0.5d_{2D-in}$	6.5
≤ 6 GHz	20 (for UMa_A and UMi_A) 10 (for RMa_A)	$0.5d_{2D-in}$	0

NOTE 1 – For model A and frequencies equal and below 6 GHz, d_{2D-in} is assumed uniformly distributed between 0 and 25 m for UMa_A and UMi_A, and between 0 and 10 m for RMa_A.

NOTE 2 – For model A and frequencies equal and above 6 GHz, d_{2D-in} is minimum of two independently generated uniformly distributed variables between 0 and 25 m for UMa_A and UMi_A, and between 0 and 10 m for RMa_A. d_{2D-in} shall be UT-specifically generated.

TABLE A1-8

O-to-I penetration loss model for model B

	Path loss through external wall: PL_{tw} (dB)	Indoor loss: PL_{in} (dB)	Standard deviation: σ_P (dB)
Low-loss model	$5 - 10\log_{10}(0.3 \cdot 10^{-L_{glass}/10} + 0.7 \cdot 10^{-L_{concrete}/10})$	$0.5d_{2D-in}$	4.4
High-loss model	$5 - 10\log_{10}(0.7 \cdot 10^{-L_{IRRglass}/10} + 0.3 \cdot 10^{-L_{concrete}/10})$	$0.5d_{2D-in}$	6.5

NOTE – For model B, d_{2D-in} is minimum of two independently generated uniformly distributed variables between 0 and 25 m for UMa_B and UMi_B, and between 0 and 10 m for RMa_B. d_{2D-in} shall be UT-specifically generated.

Both low-loss and high-loss models are applicable to UMa_x and UMi_x. Only the low-loss model is applicable to RMa_x.

The composition of low and high loss is a simulation parameter that should be determined by the user of the channel models, and is dependent on the use of metal-coated glass in buildings and the deployment scenarios. Such use is expected to differ in different markets and regions of the world and also may increase over years to new regulations and energy saving initiatives. Furthermore, the use of such high-loss glass currently appears to be more predominant in commercial buildings than in residential buildings in some regions of the world.

3.3 Car penetration loss

The pathloss incorporating O-to-I car penetration loss is modelled as in the following:

$$PL = PL_b + N(\mu, \sigma_P^2) \quad (4)$$

where PL_b is the basic outdoor path loss given in § 3.1. $\mu = 9$, and $\sigma_P = 5$. Optionally, for metallized car windows, $\mu = 20$ can be used. The O-to-I car penetration loss models are applicable for at least 0.6-60 GHz.

3.4 LOS probability

The LOS probabilities are given in Table A1-9.

TABLE A1-9
LOS probability

Channel model	LOS probability
InH_x	$P_{LOS} = \begin{cases} 1 & , d_{2D} \leq 5\text{m} \\ \exp\left(-\frac{d_{2D}-5}{70.8}\right) & , 5\text{m} < d_{2D} \leq 49\text{m} \\ \exp\left(-\frac{d_{2D}-49}{211.7}\right) \cdot 0.54 & , 49\text{m} < d_{2D} \end{cases}$
UMa_x	<p>Outdoor users:</p> $P_{LOS} = \begin{cases} 1 & , d_{2D} \leq 18\text{m} \\ \left[\frac{18}{d_{2D}} + \exp\left(-\frac{d_{2D}}{63}\right) \left(1 - \frac{18}{d_{2D}}\right) \right] \left[1 + C'(h_{UT}) \frac{5}{4} \left(\frac{d_{2D}}{100}\right)^3 \exp\left(-\frac{d_{2D}}{150}\right) \right] & , 18\text{m} < d_{2D} \end{cases}$ <p>where</p> $C'(h_{UT}) = \begin{cases} 0 & , h_{UT} \leq 13\text{m} \\ \left(\frac{h_{UT}-13}{10}\right)^{1.5} & , 13\text{m} < h_{UT} \leq 23\text{m} \end{cases}$ <p>Indoor users: Use d_{2D-out} in the formula above instead of d_{2D}</p>
UMi_x	<p>Outdoor users:</p> $P_{LOS} = \begin{cases} 1 & , d_{2D} \leq 18\text{m} \\ \left[\frac{18}{d_{2D}} + \exp\left(-\frac{d_{2D}}{36}\right) \left(1 - \frac{18}{d_{2D}}\right) \right] & , 18\text{m} < d_{2D} \end{cases}$ <p>Indoor users: Use d_{2D-out} in the formula above instead of d_{2D}</p>
RMa_x	<p>Outdoor users:</p> $P_{LOS} = \begin{cases} 1 & , d_{2D} \leq 10\text{m} \\ \exp\left(-\frac{d_{2D}-10}{1000}\right) & , 10\text{m} < d_{2D} \end{cases}$ <p>Indoor users: Use d_{2D-out} in the formula above instead of d_{2D}</p>

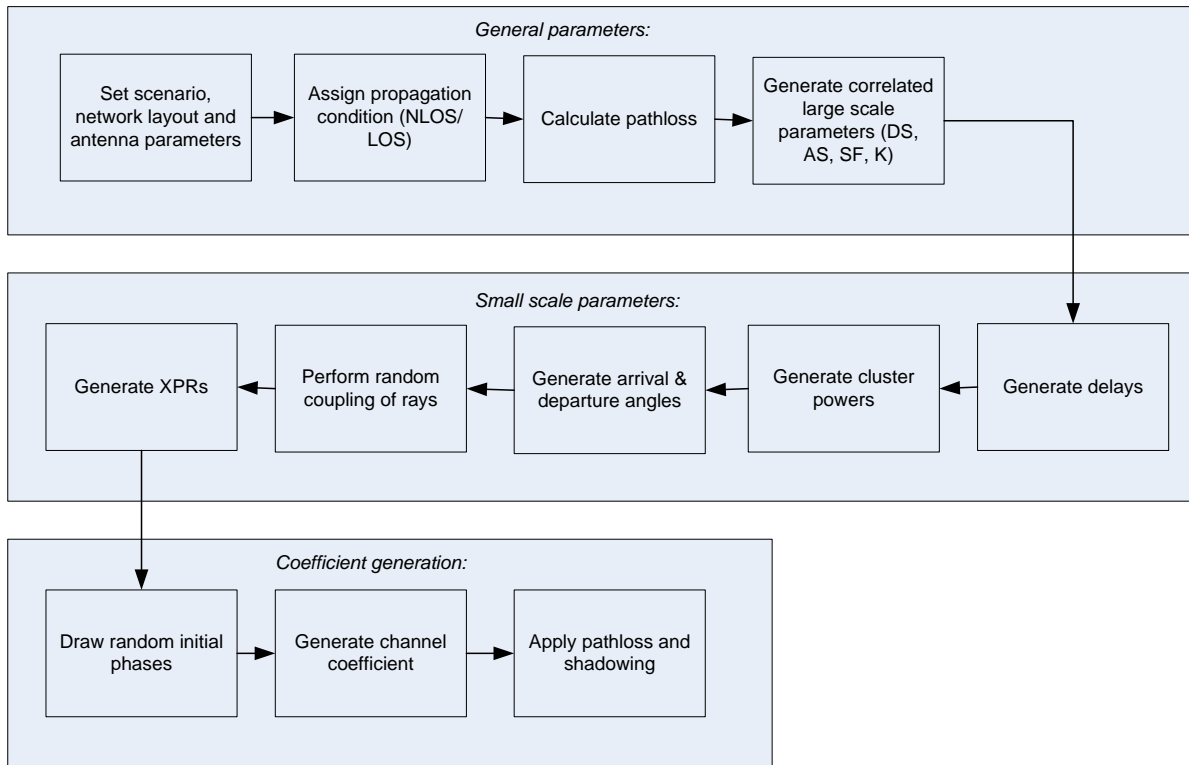
4 Fast fading model

The radio channels are created using the parameters listed in Tables A1-16 to A1-23. The main channel realizations are obtained by a step-wise procedure illustrated in Fig. A1-2 and described below. It has to be noted that the geometric description covers arrival angles from the last bounce scatterers and respectively departure angles to the first scatterers interacted from the transmitting side. The propagation between the first and the last interaction is not defined. Thus, this approach can model also multiple interactions with the scattering media. This indicates also that e.g. the delay of a

multipath component cannot be determined by the geometry. In the following steps, downlink is assumed. For uplink, arrival and departure parameters have to be swapped. Note that channel coefficient generation (steps 4 to 11) for LOS O-to-I case follow the same method as the NLOS case.

The main procedure of channel coefficient generation in this section is adequate in most cases. However, in certain simulations, the proponents may use one or more advanced modeling components. Such advanced modeling components and their recommended conditions are described in § 5.

FIGURE A1-2

Channel coefficient generation main procedure

A coordinate system is defined by the x, y, z axes, the spherical angles and the spherical unit vectors as shown in Fig. A1-3.

Figure A1-3 defines the zenith angle θ and the azimuth angle ϕ in a Cartesian coordinate system. Note that $\theta=0^\circ$ points to the zenith and $\theta=90^\circ$ points to the horizon. $\phi=0^\circ$ points to the x-axis direction with a positive value of counter-clockwise rotation.

The field component in the direction of $\hat{\theta}$ is given by F_θ and the field component in the direction of $\hat{\phi}$ is given by F_ϕ . The spherical basis vectors $\hat{\theta}$ and $\hat{\phi}$ shown above are defined based on the direction of propagation \hat{n} .

FIGURE A1-3

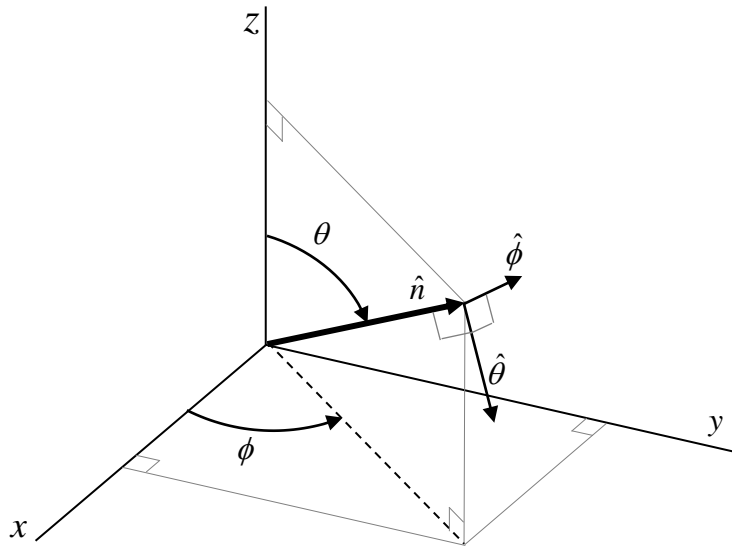
Definition of a global coordinate system showing the zenith angle θ and the azimuth angle ϕ 

TABLE A1-10

Notations in the global coordinate system (GCS)

Parameter	Notation	Comments
LOS AOD	$\phi_{LOS,AOD}$	defined by ϕ
LOS AOA	$\phi_{LOS,AOA}$	defined by ϕ
LOS ZOD	$\theta_{LOS,ZOD}$	defined by θ
LOS ZOA	$\theta_{LOS,ZOA}$	defined by θ
AOA for cluster n	$\phi_{n,AOA}$	defined by ϕ
AOD for cluster n	$\phi_{n,AOD}$	defined by ϕ
AOA for ray m in cluster n	$\phi_{n,m,AOA}$	defined by ϕ
AOD for ray m in cluster n	$\phi_{n,m,AOD}$	defined by ϕ
ZOA for cluster n	$\theta_{n,ZOA}$	defined by θ
ZOD for cluster n	$\theta_{n,ZOD}$	defined by θ
ZOA for ray m in cluster n	$\theta_{n,m,ZOA}$	defined by θ
ZOD for ray m in cluster n	$\theta_{n,m,ZOD}$	defined by θ
Receive antenna element u field pattern in the direction of the spherical basis vector $\hat{\theta}$	$F_{rx,u,\theta}$	
Receive antenna element u field pattern in the direction of the spherical basis vector $\hat{\phi}$	$F_{rx,u,\phi}$	
Transmit antenna element s field pattern in the direction of the spherical basis vector $\hat{\theta}$	$F_{tx,s,\theta}$	
Transmit antenna element s field pattern in the direction of the spherical basis vector $\hat{\phi}$	$F_{tx,s,\phi}$	

4.1 General parameter generation

In the following, the procedure for generating general parameters is described.

Step 1: Set environment, network layout, and antenna array parameters

- a) Choose one of the scenarios. Choose a global coordinate system and define zenith angle θ , azimuth angle ϕ , and spherical basis vectors $\hat{\theta}$, $\hat{\phi}$ as shown in Fig. A1-3.
- b) Give number of BS and UT.
- c) Give 3D locations of BS and UT, and determine LOS AOD ($\phi_{LOS,AOD}$), LOS ZOD ($\theta_{LOS,ZOD}$), and LOS AOA ($\phi_{LOS,AOA}$), LOS ZOA ($\theta_{LOS,ZOA}$) of each BS and UT in the global coordinate system.
- d) Give BS and UT antenna field patterns F_{rx} and F_{tx} in the global coordinate system and array geometries.
- e) Give BS and UT array orientations with respect to the global coordinate system. BS array orientation is defined by three angles $\Omega_{BS,\alpha}$ (BS bearing angle), $\Omega_{BS,\beta}$ (BS downtilt angle) and $\Omega_{BS,\gamma}$ (BS slant angle). UT array orientation is defined by three angles $\Omega_{UT,\alpha}$ (UT bearing angle), $\Omega_{UT,\beta}$ (UT downtilt angle) and $\Omega_{UT,\gamma}$ (UT slant angle).
- f) Give speed and direction of motion of UT in the global coordinate system.
- g) Give system centre frequency f_c and bandwidth B .

NOTE – In case wrapping is used, each wrapping copy of a BS or site should be treated as a separate BS/site considering channel generation.

4.2 Large scale parameter generation

In the following, the procedure for generating large scale parameters is described.

Step 2: Assign propagation condition (LOS/NLOS) according to Table A1-9. The propagation conditions for different BS-UT links are uncorrelated. Also assign an indoor/outdoor state for each UT. It is noted that all the links from a UT have the same indoor/outdoor state.

Step 3: Calculate pathloss with formulas in Tables A1-2 to A1-5 for each BS-UT link to be modelled.

Step 4: Generate large scale parameters e.g. root-mean-square delay spread (DS), root-mean-square angular spreads (ASA, ASD, ZSA, ZSD), Ricean K-factor (K) and shadow fading (SF) taking into account cross correlation according to Tables A4-7 to A4-14 and using the procedure described in § 3.3.1 of WINNER II Channel Models [15] with the square root matrix $\sqrt{C_{M \times M}(0)}$ being generated using the Cholesky decomposition and the following order of the large scale parameter vector: $\mathbf{s}_M = [SSF, SK, SDS, SASD, SASA, SZSD, SZSA]^T$.

These LSPs for different BS-UT links are uncorrelated, but the LSPs for links from co-sited TRxPs to a UT are the same. In addition, these LSPs for the links of UTs on different floors are uncorrelated.

Limit random RMS azimuth arrival and azimuth departure spread values to 104 degrees, i.e. $\sigma_{ASA} = \min(\sigma_{ASA}, 104)$, $\sigma_{ASD} = \min(\sigma_{ASD}, 104)$. Limit random RMS zenith arrival and zenith departure spread values to 52 degrees, i.e. $\sigma_{ZSA} = \min(\sigma_{ZSA}, 52)$, $\sigma_{ZSD} = \min(\sigma_{ZSD}, 52)$.

4.3 Small scale parameter generation

In the following, the procedure for generating small scale parameters is described.

Step 5: Generate delays τ_n .

Delays are drawn randomly from the delay distribution defined in Tables A1-16 to A1-23. With exponential delay distribution calculate:

$$\tau_n' = -r_\tau DS \ln(X_n), \quad (5)$$

where r_τ is the delay distribution proportionality factor, $X_n \sim \text{uniform}(0,1)$, and cluster index $n=1, \dots, N$. With uniform delay distribution the delay values τ_n' are drawn from the corresponding range. Normalise the delays by subtracting the minimum delay and sort the normalised delays to ascending order:

$$\tau_n = \text{sort}(\tau_n' - \min(\tau_n')). \quad (6)$$

In the case of LOS condition, additional scaling of delays is required to compensate for the effect of LOS peak addition to the delay spread. The heuristically determined Ricean K-factor dependent scaling constant is:

$$C_\tau = 0.7705 - 0.0433K + 0.0002K^2 + 0.000017K^3 \quad (7)$$

where K [dB] is the Ricean K-factor as generated in Step 4. The scaled delays:

$$\tau_n^{LOS} = \tau_n / C_\tau \quad (8)$$

are **not** to be used in cluster power generation.

Step 6: Generate cluster powers P_n .

Cluster powers are calculated assuming a single slope exponential power delay profile. Power assignment depends on the delay distribution defined in Tables A1-16 to A1-23. With exponential delay distribution the cluster powers are determined by

$$P_n' = \exp\left(-\tau_n \frac{r_\tau - 1}{r_\tau DS}\right) \cdot 10^{\frac{-Z_n}{10}} \quad (9)$$

where $Z_n \sim N(0, \zeta^2)$ is the per cluster shadowing term in [dB]. Normalise the cluster powers so that the sum power of all cluster powers is equal to one, i.e.:

$$P_n = \frac{P_n'}{\sum_{n=1}^N P_n'} \quad (10)$$

In the case of LOS condition an additional specular component is added to the first cluster. Power of the single LOS ray is:

$$P_{1,LOS} = \frac{K_R}{K_R + 1} \quad (11)$$

and the cluster powers are not as in equation (10), but:

$$P_n = \frac{1}{K_R + 1} \frac{P_n'}{\sum_{n=1}^N P_n'} + \delta(n-1) P_{1,LOS} \quad (12)$$

where $\delta(\cdot)$ is Dirac's delta function and K_R is the Ricean K-factor as generated in Step 4 converted to linear scale. These power values are used only in equations (13) and (18), but not in equation (27).

Assign the power of each ray within a cluster as P_n/M , where M is the number of rays per cluster.

Remove clusters with less than -25 dB power compared to the maximum cluster power. The scaling factors need not be changed after cluster elimination.

Step 7: Generate arrival angles and departure angles for both azimuth and elevation.

The composite PAS in azimuth of all clusters can be modelled as wrapped Gaussian or Laplacian (see Tables A1-16 to A1-23). The AOAs are determined by applying the inverse Gaussian function equation (13a) or the inverse Laplacian function equation (13b) with input parameters P_n and RMS angle spread ASA, respectively.

$$\text{Gaussian: } \phi_{n,AOA}' = \frac{2(ASA/1.4)\sqrt{-\ln(P_n/\max(P_n))}}{C_\phi} \quad (13a)$$

$$\text{Laplacian: } \phi_{n,AOA}' = -\frac{ASA \ln(P_n/\max(P_n))}{C_\phi} \quad (13b)$$

with C_ϕ defined as:

$$\text{Gaussian: } C_\phi = \begin{cases} C_\phi^{\text{NLOS}} \cdot (1.1035 - 0.028K - 0.002K^2 + 0.0001K^3) & , \text{for LOS} \\ C_\phi^{\text{NLOS}} & , \text{for NLOS} \end{cases} \quad (14a)$$

$$\text{Laplacian: } C_\phi = \begin{cases} C_\phi^{\text{NLOS}} \cdot (0.9275 + 0.0439K - 0.0071K^2 + 0.0002K^3) & , \text{for LOS} \\ C_\phi^{\text{NLOS}} & , \text{for NLOS} \end{cases} \quad (14b)$$

where C_ϕ^{NLOS} is defined as a scaling factor related to the total number of clusters and is given in Table A1-11.

TABLE A1-11

Scaling factors for AOA, AOD generation

# clusters	4	5	8	10	11	12	14	15	16	19	20
C_ϕ^{NLOS} Gaussian	0.779	0.860	1.018	1.090	1.123	1.146	1.190	1.211	1.226	1.273	1.289
C_ϕ^{NLOS} Laplacian								1.434		1.501	

In the LOS case, constant C_ϕ also depends on the Ricean K-factor in [dB], as generated in Step 4. Additional scaling of the angles is required to compensate for the effect of LOS peak addition to the angle spread.

Assign positive or negative sign to the angles by multiplying with a random variable X_n with uniform distribution to the discrete set of $\{1, -1\}$, and add component $Y_n \sim N(0, (ASA/7)^2)$ to introduce random variation

$$\phi_{n,AOA} = X_n \phi'_{n,AOA} + Y_n + \phi_{LOS,AOA}, \quad (15)$$

where $\phi_{LOS,AOA}$ is the LOS direction defined in the network layout description, see Step1c.

In the LOS case, substitute equation (15) by equation (16) to enforce the first cluster to the LOS direction $\phi_{LOS,AOA}$:

$$\phi_{n,AOA} = (X_n \phi'_{n,AOA} + Y_n) - (X_1 \phi'_{1,AOA} + Y_1 - \phi_{LOS,AOA}). \quad (16)$$

Finally add offset angles α_m from Table A1-12 to the cluster angles

$$\phi_{n,m,AOA} = \phi_{n,AOA} + c_{ASA} \alpha_m, \quad (17)$$

where c_{ASA} is the cluster-wise rms azimuth spread of arrival angles (cluster ASA) in Tables A1-16 to A1-23.

TABLE A1-12

Ray offset angles within a cluster, given for rms angle spread normalized to 1

Ray number m	Basis vector of offset angles α_m
1,2	± 0.0447
3,4	± 0.1413
5,6	± 0.2492
7,8	± 0.3715
9,10	± 0.5129
11,12	± 0.6797
13,14	± 0.8844
15,16	± 1.1481
17,18	± 1.5195
19,20	± 2.1551

The generation of AOD ($\phi_{n,m,AOD}$) follows a procedure similar to AOA as described above.

The generation of ZOA assumes that the composite PAS in the zenith dimension of all clusters is Laplacian (see Tables A1-16 to A1-23). The ZOAs are determined by applying the inverse Laplacian function equation (18) with input parameters P_n and RMS angle spread ZSA:

$$\theta'_{n,ZOA} = -\frac{ZSA \ln(P_n / \max(P_n))}{C_\theta} \quad (18)$$

For model A: with C_θ defined as:

$$C_\theta = \begin{cases} C_\theta^{\text{NLOS}} \cdot (1.35 + 0.0202K - 0.0077K^2 + 0.0002K^3) & , \text{ for LOS} \\ C_\theta^{\text{NLOS}} & , \text{ for NLOS} \end{cases} \quad (19)$$

where C_θ^{NLOS} is a scaling factor related to the total number of clusters and is given in Table A1-13.

TABLE A1-13
Scaling factors for ZOA, ZOD generation

# clusters	10	11	12	15	19	20
C_{θ}^{NLOS}	0.9854	1.013	1.04	1.1088	1.1764	1.1918

For model B: with C_{θ} defined as:

$$C_{\theta} = \begin{cases} C_{\theta}^{\text{NLOS}} \cdot (1.3086 + 0.0339K - 0.0077K^2 + 0.0002K^3) & , \text{ for LOS} \\ C_{\theta}^{\text{NLOS}} & , \text{ for NLOS} \end{cases} \quad (20)$$

where C_{θ}^{NLOS} is a scaling factor related to the total number of clusters and is given in Table A1-14.

TABLE A1-14
Scaling factors for ZOA, ZOD generation

# clusters	8	10	11	12	15	19	20
C_{θ}^{NLOS}	0.889	0.957	1.031	1.104	1.1088	1.184	1.178

In the LOS case, constant, C_{θ} also depends on the Ricean K-factor in [dB], as generated in Step 4. Additional scaling of the angles is required to compensate for the effect of LOS peak addition to the angle spread.

Assign positive or negative sign to the angles by multiplying with a random variable X_n with uniform distribution to the discrete set of $\{1, -1\}$, and add component $Y_n \sim \mathcal{N}(0, (ZSA/7)^2)$ to introduce random variation

$$\theta_{n,ZOA} = X_n \theta'_{n,ZOA} + Y_n + \bar{\theta}_{ZOA}, \quad (21)$$

where $\bar{\theta}_{ZOA} = 90^0$ if the BS-UT link is O2I and $\bar{\theta}_{ZOA} = \theta_{LOS,ZOA}$ otherwise. The LOS direction is defined in the network layout description, see Step 1c.

In the LOS case, substitute equation (21) by equation (22) to enforce the first cluster to the LOS direction $\theta_{LOS,ZOA}$

$$\theta_{n,ZOA} = (X_n \theta'_{n,ZOA} + Y_n) - (X_1 \theta'_{1,ZOA} + Y_1 - \theta_{LOS,ZOA}). \quad (22)$$

Finally add offset angles α_m from Table A1-12 to the cluster angles

$$\theta_{n,m,ZOA} = \theta_{n,ZOA} + c_{ZSA} \alpha_m, \quad (23)$$

where c_{ZSA} is the cluster-wise rms spread of ZOA (cluster ZSA) in Tables A1-16 to A1-23. Assuming that $\theta_{n,m,ZOA}$ is wrapped within $[0, 360^0]$, if $\theta_{n,m,ZOA} \in [180^0, 360^0]$, then $\theta_{n,m,ZOA}$ is set to $(360^0 - \theta_{n,m,ZOA})$

The generation of ZOD follows the same procedure as ZOA described above except equation (21) is replaced by equation (24):

$$\theta_{n,ZOD} = X_n \theta'_{n,ZOD} + Y_n + \theta_{LOS,ZOD} + \mu_{\text{offset,ZOD}}, \quad (24)$$

where variable X_n is with uniform distribution to the discrete set of $\{1,-1\}$, $Y_n \sim N(0, (ZSD/7)^2)$, $\mu_{offset,ZOD}$ is given in Tables A1-16 to A1-23 and equation (23) is replaced by equation (25).

$$\theta_{n,m,ZOD} = \theta_{n,ZOD} + (3/8)(10^{\mu_{1gZSD}}) \alpha_m \quad (25)$$

where μ_{1gZSD} is the mean of the ZSD log-normal distribution.

In the LOS case, the generation of ZOD follows the same procedure as ZOA described above using equation (22).

Step 8: Coupling of rays within a cluster for both azimuth and elevation

Couple randomly AOD angles $\phi_{n,m,AOD}$ to AOA angles $\phi_{n,m,AOA}$ within a cluster n , or within a sub-cluster in the case of two strongest clusters (see Step 11 and Table A1-12). Couple randomly ZOD angles $\theta_{n,m,ZOD}$ with ZOA angles $\theta_{n,m,ZOA}$ using the same procedure. Couple randomly AOD angles $\phi_{n,m,AOD}$ with ZOD angles $\theta_{n,m,ZOD}$ within a cluster n or within a sub-cluster in the case of two strongest clusters.

Step 9: Generate the cross polarization power ratios

Generate the cross polarization power ratios (XPR) κ for each ray m of each cluster n . XPR is log-Normal distributed. Draw XPR values as

$$\kappa_{n,m} = 10^{X/10} \quad (26)$$

where $X \sim N(\mu_{XPR}, \sigma_{XPR}^2)$ is Gaussian distributed with σ_{XPR} and μ_{XPR} from Tables A1-16 to A1-23.

The outcome of Steps 1-9 shall be identical for all the links from co-sited TRxPs to a UT.

4.4 Channel coefficient generation

In the following, the procedure for generating the channel coefficient is described.

Step 10: Draw initial random phases

Draw random initial phase $\{\Phi_{n,m}^{\theta\theta}, \Phi_{n,m}^{\theta\phi}, \Phi_{n,m}^{\phi\theta}, \Phi_{n,m}^{\phi\phi}\}$ for each ray m of each cluster n and for four different polarisation combinations $(\theta\theta, \theta\phi, \phi\theta, \phi\phi)$. The distribution for initial phases is uniform within $(-\pi, \pi)$.

In the LOS case, if ϕ_{LOS} is chosen as a random variable, then draw a random initial phase for both $\theta\theta$ and $\phi\phi$ polarisations, see equation (34).

Step 11: Generate channel coefficients for each cluster n and each receiver and transmitter element pair u, s .

For the $N-2$ weakest clusters, say $n = 3, 4, \dots, N$, the channel coefficients are given by:

$$H_{u,s,n}^{NLOS}(t) = \sqrt{\frac{P_n}{M}} \sum_{m=1}^M \begin{bmatrix} F_{rx,u,\theta}(\theta_{n,m,ZOA}, \varphi_{n,m,AOA}) \\ F_{rx,u,\phi}(\theta_{n,m,ZOA}, \varphi_{n,m,AOA}) \end{bmatrix}^T \begin{bmatrix} \exp(j\Phi_{n,m}^{\theta\theta}) & \sqrt{\kappa_{n,m}^{-1}} \exp(j\Phi_{n,m}^{\theta\phi}) \\ \sqrt{\kappa_{n,m}^{-1}} \exp(j\Phi_{n,m}^{\phi\theta}) & \exp(j\Phi_{n,m}^{\phi\phi}) \end{bmatrix} \\ \begin{bmatrix} F_{tx,s,\theta}(\theta_{n,m,ZOD}, \varphi_{n,m,AOD}) \\ F_{tx,s,\phi}(\theta_{n,m,ZOD}, \varphi_{n,m,AOD}) \end{bmatrix} \exp\left(j2\pi \frac{\hat{r}_{rx,n,m}^T \bar{d}_{rx,u}}{\lambda_0}\right) \exp\left(j2\pi \frac{\hat{r}_{tx,n,m}^T \bar{d}_{tx,s}}{\lambda_0}\right) \exp\left(j2\pi \frac{\hat{r}_{tx,n,m}^T \bar{v}}{\lambda_0} t\right) \quad (27)$$

where $F_{rx,u,\theta}$ and $F_{rx,u,\phi}$ are the field patterns of receive antenna element u in the direction of the spherical basis vectors, $\hat{\theta}$ and $\hat{\phi}$ respectively, $F_{tx,s,\theta}$ and $F_{tx,s,\phi}$ are the field patterns of transmit antenna element s in the direction of the spherical basis vectors, $\hat{\theta}$ and $\hat{\phi}$ respectively. $\hat{r}_{rx,n,m}$ is the spherical unit vector with azimuth arrival angle $\phi_{n,m,AOA}$ and elevation arrival angle $\theta_{n,m,ZOA}$, given by:

$$\hat{r}_{rx,n,m} = \begin{bmatrix} \sin \theta_{n,m,ZOA} \cos \phi_{n,m,AOA} \\ \sin \theta_{n,m,ZOA} \sin \phi_{n,m,AOA} \\ \cos \theta_{n,m,ZOA} \end{bmatrix}, \quad (28)$$

where n denotes a cluster and m denotes a ray within cluster n . $\hat{r}_{tx,n,m}$ is the spherical unit vector with azimuth departure angle $\phi_{n,m,AOD}$ and elevation departure angle $\theta_{n,m,ZOD}$, given by:

$$\hat{r}_{tx,n,m} = \begin{bmatrix} \sin \theta_{n,m,ZOD} \cos \phi_{n,m,AOD} \\ \sin \theta_{n,m,ZOD} \sin \phi_{n,m,AOD} \\ \cos \theta_{n,m,ZOD} \end{bmatrix}, \quad (29)$$

where n denotes a cluster and m denotes a ray within cluster n . Also, $\bar{d}_{rx,u}$ is the location vector of receive antenna element u and $\bar{d}_{tx,s}$ is the location vector of transmit antenna element s , $\kappa_{n,m}$ is the cross polarisation power ratio in linear scale, and λ_0 is the wavelength of the carrier frequency. If polarisation is not considered, the 2×2 polarisation matrix can be replaced by the scalar $\exp(j\Phi_{n,m})$ and only vertically polarised field patterns are applied.

The Doppler frequency component depends on the arrival angles (AOA, ZOA), and the UT velocity vector \bar{v} with speed v , travel azimuth angle ϕ_v , elevation angle θ_v and is given by

$$v_{n,m} = \frac{\hat{r}_{rx,n,m}^T \bar{v}}{\lambda_0}, \text{ where } \bar{v} = v \cdot [\sin \theta_v \cos \phi_v \quad \sin \theta_v \sin \phi_v \quad \cos \theta_v]^T. \quad (30)$$

For the two strongest clusters, say $n = 1$ and 2, rays are spread in delay to three sub-clusters (per cluster), with fixed delay offset.

The delays of the sub-clusters are

$$\begin{aligned} \tau_{n,1} &= \tau_n \\ \tau_{n,2} &= \tau_n + 1.28 c_{DS} \\ \tau_{n,3} &= \tau_n + 2.56 c_{DS} \end{aligned} \quad (31)$$

where c_{DS} is cluster delay spread specified in Tables A1-16 to A1-23. When intra-cluster delay spread is unspecified (i.e. N/A) the value 3.91 ns is used; it is noted that this value results in the legacy behaviour with 5 and 10 ns sub-cluster delays.

Twenty rays of a cluster are mapped to sub-clusters as presented in Table A1-15 below. The corresponding offset angles are taken from Table A1-12 with the mapping of Table A1-15.

TABLE A1-15

Sub-cluster information for intra cluster delay spread clusters

sub-cluster # i	mapping to rays R_i	Power $ R_i /M$	delay offset $\tau_{n,i} - \tau_n$
$i = 1$	$R_1 = \{1,2,3,4,5,6,7,8,19,20\}$	10/20	0
$i = 2$	$R_2 = \{9,10,11,12,17,18\}$	6/20	$1.28 c_{DS}$
$i = 3$	$R_3 = \{13,14,15,16\}$	4/20	$2.56 c_{DS}$

Then, the channel impulse response is given by:

$$H_{u,s}^{\text{NLOS}}(\tau, t) = \sum_{n=1}^2 \sum_{i=1}^3 \sum_{m \in R_i} H_{u,s,n,m}^{\text{NLOS}}(t) \delta(\tau - \tau_{n,i}) + \sum_{n=3}^N H_{u,s,n}^{\text{NLOS}}(t) \delta(\tau - \tau_n) \quad (32)$$

where $H_{u,s,n,m}^{\text{NLOS}}(t)$ defined as:

$$H_{u,s,n,m}^{\text{NLOS}}(t) = \sqrt{\frac{P_n}{M}} \begin{bmatrix} F_{rx,u,\theta}(\theta_{n,m,ZOA}, \varphi_{n,m,AOA}) \\ F_{rx,u,\varphi}(\theta_{n,m,ZOA}, \varphi_{n,m,AOA}) \end{bmatrix}^T \begin{bmatrix} \exp(j\Phi_{n,m}^{\theta\theta}) & \sqrt{\kappa_{n,m}^{-1}} \exp(j\Phi_{n,m}^{\theta\varphi}) \\ \sqrt{\kappa_{n,m}^{-1}} \exp(j\Phi_{n,m}^{\varphi\theta}) & \exp(j\Phi_{n,m}^{\varphi\varphi}) \end{bmatrix} \begin{bmatrix} F_{tx,s,\theta}(\theta_{n,m,ZOD}, \varphi_{n,m,AOD}) \\ F_{tx,s,\varphi}(\theta_{n,m,ZOD}, \varphi_{n,m,AOD}) \end{bmatrix} \exp\left(j2\pi \frac{\hat{r}_{rx,n,m}^T \bar{d}_{rx,u}}{\lambda_0} t\right) \exp\left(j2\pi \frac{\hat{r}_{tx,n,m}^T \bar{d}_{tx,s}}{\lambda_0} t\right) \exp\left(j2\pi \frac{\hat{r}_{rx,n,m}^T \bar{v}}{\lambda_0} t\right) \quad (33)$$

In the LOS case, determine the channel coefficient:

$$H_{u,s,1}^{\text{LOS}}(t) = \begin{bmatrix} F_{rx,u,\theta}(\theta_{LOS,ZOA}, \varphi_{LOS,AOA}) \\ F_{rx,u,\varphi}(\theta_{LOS,ZOA}, \varphi_{LOS,AOA}) \end{bmatrix}^T \begin{bmatrix} 1 & 0 \\ 0 & -1 \end{bmatrix} \begin{bmatrix} F_{tx,s,\theta}(\theta_{LOS,ZOD}, \varphi_{LOS,AOD}) \\ F_{tx,s,\varphi}(\theta_{LOS,ZOD}, \varphi_{LOS,AOD}) \end{bmatrix} \cdot \exp(j\Phi_{LOS}) \exp\left(j2\pi \frac{\hat{r}_{rx,LOS}^T \bar{d}_{rx,u}}{\lambda_0} t\right) \exp\left(j2\pi \frac{\hat{r}_{tx,LOS}^T \bar{d}_{tx,s}}{\lambda_0} t\right) \exp\left(j2\pi \frac{\hat{r}_{rx,LOS}^T \bar{v}}{\lambda_0} t\right) \quad (34)$$

where $\delta(\cdot)$ is the Dirac's delta function, K_R is the Ricean K-factor as generated in Step 4 converted to linear scale, and Φ_{LOS} is the initial phase of LOS path. It can be either random or calculated from the distance according to $\Phi_{LOS} = -2\pi \frac{d_{3D}}{\lambda_0}$. In model B, $\Phi_{LOS} = -2\pi \frac{d_{3D}}{\lambda_0}$. Then, the channel impulse response is given by adding the LOS channel coefficient to the NLOS channel impulse response and scaling both terms according to the desired K-factor K_R as

$$H_{u,s}^{\text{LOS}}(\tau, t) = \sqrt{\frac{1}{K_R + 1}} H_{u,s}^{\text{NLOS}}(\tau, t) + \sqrt{\frac{K_R}{K_R + 1}} H_{u,s,1}^{\text{LOS}}(t) \delta(\tau - \tau_1) \quad (35)$$

When antenna arrays are used, the vector channel impulse response can be generated according to the example in Attachment 3 to this Annex.

Step 12: Apply pathloss and shadowing for the channel coefficients.

4.5 Fast fading parameters

The fast fading parameters, including LSP and small scale parameters, which shall be employed in the channel model generation procedure, are provided in the following subsections, for the four channel model types that will be used in related test environments as given by Tables A1-16 to A1-23.

In the Tables A1-16 to A1-23, the following applies⁷:

- f_c is carrier frequency in GHz; d_{2D} is BS-UT distance in km.
- DS = rms delay spread, ASD = rms azimuth spread of departure angles, ASA = rms azimuth spread of arrival angles, ZSD = rms zenith spread of departure angles, ZSA = rms zenith spread of arrival angles, SF = shadow fading, and K = Ricean K-factor.
- The sign of the shadow fading is defined so that positive SF means more received power at UT than predicted by the path loss model.
- The following notation for mean ($\mu_{\lg X} = \text{mean}\{\log_{10}(X)\}$) and standard deviation ($\sigma_{\lg X} = \text{std}\{\log_{10}(X)\}$) is used for logarithmized parameters X.
- h_{BS} and h_{UT} are antenna heights in m for BS and UT respectively.
- The ZSD parameters for O2I links in UMa_x and UMi_x are the same parameters that are used for outdoor links, depending on the LOS condition of the outdoor link part.

⁷ The parameter values in the Tables have been obtained from different measurement and ray-tracing campaigns. The reliability of the estimated frequency-dependent trends is enhanced when using comparable multi-frequency measurements and confidence interval analysis method [16]. When comparable multi-frequency data was not available, trends were estimated using multiple single-frequency data sets, resulting in less reliable estimates which may have some impact on the simulated capacity.

4.5.1 InH_x

TABLE A1-16
Fast fading parameters for InH_x

Parameters		InH_A				InH_B		Optional Model I	
		0.5 GHz ≤ f _c ≤ 6 GHz		6GHz < f _c ≤ 100 GHz		0.5 GHz ≤ f _c ≤ 100 GHz NOTE – For InH and frequencies below 6 GHz, use f _c = 6 when determining the values of the frequency-dependent LSP values		28 GHz	
		LOS	NLOS	LOS	NLOS	LOS	NLOS	LOS	NLOS
Delay spread (DS) lgDS=log10(DS/1s)	μ _{lgDS}	-7.70	-7.41	-0.01 log ₁₀ (1+f _c)-7.692	-0.28 log ₁₀ (1+f _c)-7.173	-0.01 log ₁₀ (1+f _c)-7.692	-0.28 log ₁₀ (1+f _c)-7.173	-7.9	-7.8
	σ _{lgDS}	0.18	0.14	0.18	0.10 log ₁₀ (1+f _c)+0.055	0.18	0.10 log ₁₀ (1+f _c)+0.055	0.12	0.73
AOD spread (ASD) lgASD=log10 (ASD/1°)	μ _{lgASD}	1.60	1.62	1.60	1.62	1.60	1.62	0.88	1.07
	σ _{lgASD}	0.18	0.25	0.18	0.25	0.18	0.25	0.28	0.22
AOA spread (ASA) lgASA=log10 (ASA/1°)	μ _{lgASA}	1.62	1.77	-0.19 log ₁₀ (1+f _c)+1.781	-0.11 log ₁₀ (1+f _c)+1.863	-0.19 log ₁₀ (1+f _c)+1.781	-0.11 log ₁₀ (1+f _c)+1.863	1.15	1.24
	σ _{lgASA}	0.22	0.16	0.12 log ₁₀ (1+f _c)+0.119	0.12 log ₁₀ (1+f _c)+0.059	0.12 log ₁₀ (1+f _c)+0.119	0.12 log ₁₀ (1+f _c)+0.059	0.29	0.28
ZOA spread (ZSA) lgZSA=log10(ZSA/1°)	μ _{lgZSA}	1.22	1.26	-0.26 log ₁₀ (1+f _c)+1.44	-0.15 log ₁₀ (1+f _c)+1.387	-0.26 log ₁₀ (1+f _c)+1.44	-0.15 log ₁₀ (1+f _c)+1.387	0.12	0.02
	σ _{lgZSA}	0.23	0.67	-0.04 log ₁₀ (1+f _c)+0.264	-0.09 log ₁₀ (1+f _c)+0.746	-0.04 log ₁₀ (1+f _c)+0.264	-0.09 log ₁₀ (1+f _c)+0.746	0.19	0.15
Shadow fading (SF) [dB]	σ _{SF}	3	4	See Table A1-2	See Table A1-2	See Table A1-2	See Table A1-2	1.7	3.3

TABLE A1-16 (continued)

Parameters		InH_A				InH_B		Optional Model I	
		0.5 GHz ≤ f_c ≤ 6 GHz		6GHz < f_c ≤ 100 GHz		0.5 GHz ≤ f_c ≤ 100 GHz NOTE – For InH and frequencies below 6 GHz, use $f_c = 6$ when determining the values of the frequency-dependent LSP values		28 GHz	
		LOS	NLOS	LOS	NLOS	LOS	NLOS	LOS	NLOS
K-factor (K) [dB]	μ_K	7	N/A	7	N/A	7	N/A	6	N/A
	σ_K	4	N/A	4	N/A	4	N/A	3.5	N/A
Cross-Correlations	<i>ASD vs DS</i>	0.6	0.4	0.6	0.4	0.6	0.4	-0.1	0.3
	<i>ASA vs DS</i>	0.8	0	0.8	0	0.8	0	-0.1	0.2
	<i>ASA vs SF</i>	-0.5	-0.4	-0.5	-0.4	-0.5	-0.4	0	0
	<i>ASD vs SF</i>	-0.4	0	-0.4	0	-0.4	0	0	0
	<i>DS vs SF</i>	-0.8	-0.5	-0.8	-0.5	-0.8	-0.5	0.5	0.6
	<i>ASD vs ASA</i>	0.4	0	0.4	0	0.4	0	0.1	0.1
	<i>ASD vs K</i>	0	N/A	0	N/A	0	N/A	-0.2	N/A
	<i>ASA vs K</i>	0	N/A	0	N/A	0	N/A	0.4	N/A
	<i>DS vs K</i>	-0.5	N/A	-0.5	N/A	-0.5	N/A	-0.3	N/A
	<i>SF vs K</i>	0.5	N/A	0.5	N/A	0.5	N/A	-0.2	N/A
Cross-Correlations 1)	<i>ZSD vs SF</i>	0.2	0	0.2	0	0.2	0	0	0
	<i>ZSA vs SF</i>	0.3	0	0.3	0	0.3	0	0	0
	<i>ZSD vs K</i>	0	N/A	0	N/A	0	N/A	0	N/A
	<i>ZSA vs K</i>	0.1	N/A	0.1	N/A	0.1	N/A	0	N/A
	<i>ZSD vs DS</i>	0.1	-0.27	0.1	-0.27	0.1	-0.27	0.2	0.2
	<i>ZSA vs DS</i>	0.2	-0.06	0.2	-0.06	0.2	-0.06	0.3	0.1
	<i>ZSD vs ASD</i>	0.5	0.35	0.5	0.35	0.5	0.35	0.2	0.1

TABLE A1-16 (continued)

Parameters		InH_A				InH_B		Optional Model I	
		0.5 GHz ≤ f _c ≤ 6 GHz		6 GHz < f _c ≤ 100 GHz		0.5 GHz ≤ f _c ≤ 100 GHz NOTE – For InH and frequencies below 6 GHz, use f _c = 6 when determining the values of the frequency-dependent LSP values		28 GHz	
		LOS	NLOS	LOS	NLOS	LOS	NLOS	LOS	NLOS
	ZSA vs ASD	0	0.23	0	0.23	0	0.23	0.1	0.3
	ZSD vs ASA	0	-0.08	0	-0.08	0	-0.08	-0.3	0
	ZSA vs ASA	0.5	0.43	0.5	0.43	0.5	0.43	0.1	0
	ZSD vs ZSA	0	0.42	0	0.42	0	0.42	0.2	-0.1
Delay distribution		Exp	Exp	Exp	Exp	Exp	Exp	Exp	Exp
AOD and AOA distribution		Laplacian	Laplacian	Wrapped Gaussian	Wrapped Gaussian	Wrapped Gaussian	Wrapped Gaussian	Wrapped Gaussian	Wrapped Gaussian
ZOD and ZOA distribution		Laplacian	Laplacian	Laplacian	Laplacian	Laplacian	Laplacian	Laplacian	Laplacian
Delay scaling parameter r _t		3.6	3	3.6	3	3.6	3	N/A	N/A
XPR [dB]	μ _{XPR}	11	10	11	10	11	10	N/A	N/A
	σ _{XPR}	4	4	4	4	4	4	N/A	N/A
Number of clusters		15	19	15	19	15	19	4	7
Number of rays per cluster		20	20	20	20	20	20	20	20
Cluster DS (C _{DS})		N/A	N/A	N/A	N/A	N/A	N/A	6	5
Cluster ASD (C _{ASD})		5	5	5	5	5	5	N/A	N/A
Cluster ASA (C _{ASA})		8	11	8	11	8	11	N/A	N/A
Cluster ZSA (C _{ZSA})		9	9	9	9	9	9	N/A	N/A

TABLE A1-17

ZSD and ZOD offset parameters in InH_x

	Frequency	Parameters		InH_x	
				LOS	NLOS
InH_A	$0.5 \text{ GHz} \leq f_c \leq 6 \text{ GHz}$	ZOD spread (ZSD) $\lg \text{ZSD} = \log_{10}(\text{ZSD}/1^\circ)$	$\mu_{\lg \text{ZSD}}$	1.02	1.08
			$\sigma_{\lg \text{ZSD}}$	0.41	0.36
		ZOD offset	$\mu_{\text{offset,ZOD}}$	0	0
	$6 \text{ GHz} < f_c \leq 100 \text{ GHz}$	ZOD spread (ZSD) $\lg \text{ZSD} = \log_{10}(\text{ZSD}/1^\circ)$	$\mu_{\lg \text{ZSD}}$	$-1.43 \log_{10}(1+f_c)+2.228$	1.08
			$\sigma_{\lg \text{ZSD}}$	$0.13 \log_{10}(1+f_c)+0.30$	0.36
		ZOD offset	$\mu_{\text{offset,ZOD}}$	0	0
InH_B	$0.5 \text{ GHz} \leq f_c \leq 100 \text{ GHz}$ NOTE – For InH and frequencies below 6 GHz, use $f_c = 6$ when determining the values of the ZSD parameter values	ZOD spread (ZSD) $\lg \text{ZSD} = \log_{10}(\text{ZSD}/1^\circ)$	$\mu_{\lg \text{ZSD}}$	$-1.43 \log_{10}(1+f_c)+2.228$	1.08
			$\sigma_{\lg \text{ZSD}}$	$0.13 \log_{10}(1+f_c)+0.30$	0.36
		ZOD offset	$\mu_{\text{offset,ZOD}}$	0	0
Optional Model I	28 GHz	ZOD spread (ZSD) $\lg \text{ZSD} = \log_{10}(\text{ZSD}/1^\circ)$	$\mu_{\lg \text{ZSD}}$	0.16	0.06
			$\sigma_{\lg \text{ZSD}}$	0.18	0.17

4.5.2 UMa_x

TABLE A1-18
Fast fading parameters for UMa_x

Parameters		UMa_A						UMa_B		
		0.5 GHz ≤ f _c ≤ 6 GHz			6 GHz < f _c ≤ 100 GHz			0.5 GHz ≤ f _c ≤ 100 GHz NOTE : For UMa and frequencies below 6 GHz, use f _c = 6 when determining the values of the frequency-dependent LSP values		
		LOS	NLOS	O-to-I	LOS	NLOS	O-to-I	LOS	NLOS	O-to-I
Delay spread (DS) lgDS=log10(DS/1s)	μ _{gDS}	-7.03	-6.44	-6.62	-6.955 - 0.0963 log ₁₀ (f _c)	-6.28 - 0.204 log ₁₀ (f _c)	-6.63	-6.955 - 0.0963 log ₁₀ (f _c)	-6.28 - 0.204 log ₁₀ (f _c)	-6.62
	σ _{gDS}	0.66	0.39	0.32	0.66	0.39	0.32	0.66	0.39	0.32
AOD spread (ASD) lgASD=log10(ASD/1°)	μ _{gASD}	1.15	1.41	1.25	1.06 + 0.1114 log ₁₀ (f _c)	1.5 - 0.1144 log ₁₀ (f _c)	1.25	1.06 + 0.1114 log ₁₀ (f _c)	1.5 - 0.1144 log ₁₀ (f _c)	1.25
	σ _{gASD}	0.28	0.28	0.42	0.28	0.28	0.42	0.28	0.28	0.42
AOA spread (ASA) lgASA=log10(ASA/1°)	μ _{gASA}	1.81	1.87	1.76	1.81	2.08 - 0.27 log ₁₀ (f _c)	1.76	1.81	2.08 - 0.27 log ₁₀ (f _c)	1.76
	σ _{gASA}	0.20	0.11	0.16	0.20	0.11	0.16	0.20	0.11	0.16
ZOA spread (ZSA) lgZSA=log10(ZSA/1°)	μ _{gZSA}	0.95	1.26	1.01	0.95	-0.3236 log ₁₀ (f _c) + 1.512	1.01	0.95	-0.3236 log ₁₀ (f _c) + 1.512	1.01
	σ _{gZSA}	0.16	0.16	0.43	0.16	0.16	0.43	0.16	0.16	0.43
Shadow fading (SF) [dB]	σ _{SF}	4	6	7	See Table A1-3	See Table A1-3	7	See Table A1-3	See Table A1-3	7
K-factor (K) [dB]	μ _K	9	N/A	N/A	9	N/A	N/A	9	N/A	N/A
	σ _K	3.5	N/A	N/A	3.5	N/A	N/A	3.5	N/A	N/A

TABLE A1-18 (end)

Parameters		UMa_A						UMa_B		
		0.5 GHz ≤ f_c ≤ 6 GHz			6GHz < f_c ≤ 100 GHz			0.5 GHz ≤ f_c ≤ 100 GHz		
		LOS	NLOS	O-to-I	LOS	NLOS	O-to-I	NOTE : For UMa and frequencies below 6 GHz, use $f_c = 6$ when determining the values of the frequency-dependent LSP values		
	LOS	NLOS	O-to-I	LOS	NLOS	O-to-I	LOS	NLOS	O-to-I	
AOD and AOA distribution		Wrapped Gaussian	Wrapped Gaussian	Wrapped Gaussian	Wrapped Gaussian	Wrapped Gaussian	Wrapped Gaussian	Wrapped Gaussian	Wrapped Gaussian	Wrapped Gaussian
ZOD and ZOA distribution		Laplacian	Laplacian	Laplacian	Laplacian	Laplacian	Laplacian	Laplacian	Laplacian	Laplacian
Delay scaling parameter r_τ		2.5	2.3	2.2	2.5	2.3	2.2	2.5	2.3	2.2
XPR [dB]	μ_{XPR}	8	7	9	8	7	9	8	7	9
	σ_{XPR}	4	3	5	4	3	5	4	3	5
Number of clusters		12	20	12	12	20	12	12	20	12
Number of rays per cluster		20	20	20	20	20	20	20	20	20
Cluster DS (C_{DS})		NA	NA	NA	$\max(0.25, -3.4084 \log_{10}(f_c) + 6.5622)$	$\max(0.25, -3.4084 \log_{10}(f_c) + 6.5622)$	11	$\max(0.25, -3.4084 \log_{10}(f_c) + 6.5622)$	$\max(0.25, -3.4084 \log_{10}(f_c) + 6.5622)$	11
Cluster ASD (C_{ASD})		5	2	5	5	2	5	5	2	5
Cluster ASA (C_{ASA})		11	15	8	11	15	8	11	15	8
Cluster ZSA (C_{ZSA})		7	7	3	7	7	3	7	7	3
Per cluster shadowing std ζ [dB]		3	3	4	3	3	4	3	3	4
Correlation distance in the horizontal plane [m]	DS	30	40	10	30	40	10	30	40	10
	ASD	18	50	11	18	50	11	18	50	11
	ASA	15	50	17	15	50	17	15	50	17
	SF	37	50	7	37	50	7	37	50	7
	K	12	N/A	N/A	12	N/A	N/A	12	N/A	N/A
	ZSA	15	50	25	15	50	25	15	50	25
	ZSD	15	50	25	15	50	25	15	50	25

TABLE A1-19

ZSD and ZOD offset parameters in UMa_x

	Frequency	Parameters		UMa_x	
				LOS LOS O-to-I	NLOS NLOS O-to-I
UMa_A	$0.5 \text{ GHz} \leq f_c \leq 6 \text{ GHz}$	ZOD spread (ZSD) $\lg\text{ZSD}=\log_{10}(\text{ZSD}/1^\circ)$	$\mu_{\lg\text{ZSD}}$	$\max[-0.5, -2.1(d_{2D}/1000) - 0.01 (h_{UT} - 1.5)+0.75]$	$\max[-0.5, -2.1(d_{2D}/1000) - 0.01(h_{UT} - 1.5)+0.9]$
			$\sigma_{\lg\text{ZSD}}$	0.40	0.49
		ZOD offset	$\mu_{\text{offset,ZOD}}$	0	$-10^{\{-0.62\log_{10}(\max(10, d_{2D}))+1.93-0.07(h_{UT}-1.5)\}}$
	$6 \text{ GHz} < f_c \leq 100 \text{ GHz}$	ZOD spread (ZSD) $\lg\text{ZSD}=\log_{10}(\text{ZSD}/1^\circ)$	$\mu_{\lg\text{ZSD}}$	$\max[-0.5, -2.1(d_{2D}/1000) - 0.01 (h_{UT} - 1.5)+0.75]$	$\max[-0.5, -2.1(d_{2D}/1000)-0.01(h_{UT} - 1.5)+0.9]$
			$\sigma_{\lg\text{ZSD}}$	0.40	0.49
		ZOD offset	$\mu_{\text{offset,ZOD}}$	0	$e(f_c)-10^{\{a(f_c) \log_{10}(\max(b(f_c), d_{2D}))+c(f_c)\}}$
NOTE – For NLOS ZOD offset: $a(f_c) = 0.208\log_{10}(f_c) - 0.782$; $b(f_c) = 25$; $c(f_c) = -0.13\log_{10}(f_c)+2.03$; $e(f_c) = 7.66\log_{10}(f_c)-5.96$.					
UMa_B	$0.5 \text{ GHz} \leq f_c \leq 100 \text{ GHz}$ NOTE – For UMa and frequencies below 6 GHz, use $f_c = 6$ when determining the values of the frequency-dependent ZOD offset values	ZOD spread (ZSD) $\lg\text{ZSD}=\log_{10}(\text{ZSD}/1^\circ)$	$\mu_{\lg\text{ZSD}}$	$\max[-0.5, -2.1(d_{2D}/1000)- 0.01 (h_{UT}-1.5)+0.75]$	$\max[-0.5, -2.1(d_{2D}/1000)-0.01(h_{UT} - 1.5)+0.9]$
			$\sigma_{\lg\text{ZSD}}$	0.40	0.49
		ZOD offset	$\mu_{\text{offset,ZOD}}$	0	$e(f_c)-10^{\{a(f_c) \log_{10}(\max(b(f_c), d_{2D}))+c(f_c) - 0.07(h_{UT}-1.5)\}}$
		NOTE – For NLOS ZOD offset: $a(f_c) = 0.208\log_{10}(f_c) - 0.782$; $b(f_c) = 25$; $c(f_c) = -0.13\log_{10}(f_c)+2.03$; $e(f_c) = 7.66\log_{10}(f_c)-5.96$.			

4.5.3 UMi_x

TABLE A1-20
Fast fading parameters for UMi_x

Parameters		UMi_A						UMi_B		
		0.5 GHz ≤ f _c ≤ 6 GHz			6GHz < f _c ≤ 100 GHz			0.5 GHz ≤ f _c ≤ 100 GHz NOTE – For UMi and frequencies below 2 GHz, use f _c = 2 when determining the values of the frequency-dependent LSP values		
		LOS	NLOS	O-to-I	LOS	NLOS	O-to-I	LOS	NLOS	O-to-I
Delay spread (DS) lgDS=log10(DS/1s)	μ _{lgDS}	-7.19	-6.89	-6.62	$-0.24 \log_{10}(1+f_c) - 7.14$	$-0.24 \log_{10}(1+f_c) - 6.83$	-6.62	$-0.24 \log_{10}(1+f_c) - 7.14$	$-0.24 \log_{10}(1+f_c) - 6.83$	-6.62
	σ _{lgDS}	0.40	0.54	0.32	0.38	$0.16 \log_{10}(1+f_c) + 0.28$	0.32	0.38	$0.16 \log_{10}(1+f_c) + 0.28$	0.32
AOD spread (ASD) lgASD=log10(ASD/1°)	μ _{lgASD}	1.20	1.41	1.25	$-0.05 \log_{10}(1+f_c) + 1.21$	$-0.23 \log_{10}(1+f_c) + 1.53$	1.25	$-0.05 \log_{10}(1+f_c) + 1.21$	$-0.23 \log_{10}(1+f_c) + 1.53$	1.25
	σ _{lgASD}	0.43	0.17	0.42	0.41	$0.11 \log_{10}(1+f_c) + 0.33$	0.42	0.41	$0.11 \log_{10}(1+f_c) + 0.33$	0.42
AOA spread (ASA) lgASA=log10(ASA/1°)	μ _{lgASA}	1.75	1.84	1.76	$-0.08 \log_{10}(1+f_c) + 1.73$	$-0.08 \log_{10}(1+f_c) + 1.81$	1.76	$-0.08 \log_{10}(1+f_c) + 1.73$	$-0.08 \log_{10}(1+f_c) + 1.81$	1.76
	σ _{lgASA}	0.19	0.15	0.16	$0.014 \log_{10}(1+f_c) + 0.28$	$0.05 \log_{10}(1+f_c) + 0.3$	0.16	$0.014 \log_{10}(1+f_c) + 0.28$	$0.05 \log_{10}(1+f_c) + 0.3$	0.16

TABLE A1-20 (continued)

Parameters		UMi_A						UMi_B		
		0.5 GHz ≤ f _c ≤ 6 GHz			6 GHz < f _c ≤ 100 GHz			0.5 GHz ≤ f _c ≤ 100 GHz		
		LOS	NLOS	O-to-I	LOS	NLOS	O-to-I	LOS	NLOS	O-to-I
ZOA spread (ZSA) lgZSA=log10(ZSA/1°)	μ _{lgZSA}	0.60	0.88	1.01	-0.1 log ₁₀ (1+f _c) + 0.73	-0.04 log ₁₀ (1+f _c) + 0.92	1.01	-0.1 log ₁₀ (1+f _c) + 0.73	-0.04 log ₁₀ (1+f _c) + 0.92	1.01
	σ _{lgZSA}	0.16	0.16	0.43	-0.04 log ₁₀ (1+f _c) + 0.34	-0.07 log ₁₀ (1+f _c) + 0.41	0.43	-0.04 log ₁₀ (1+f _c) + 0.34	-0.07 log ₁₀ (1+f _c) + 0.41	0.43
Shadow fading (SF) [dB]	σ _{SF}	3	4	7	See Table A1-4	See Table A1-4	7	See Table A1-4	See Table A1-4	7
K-factor (K) [dB]	μ _K	9	N/A	N/A	9	N/A	N/A	9	N/A	N/A
	σ _K	5	N/A	N/A	5	N/A	N/A	5	N/A	N/A
Cross-Correlations	ASD vs DS	0.5	0	0.4	0.5	0	0.4	0.5	0	0.4
	ASA vs DS	0.8	0.4	0.4	0.8	0.4	0.4	0.8	0.4	0.4
	ASA vs SF	-0.4	-0.4	0	-0.4	-0.4	0	-0.4	-0.4	0
	ASD vs SF	-0.5	0	0.2	-0.5	0	0.2	-0.5	0	0.2
	DS vs SF	-0.4	-0.7	-0.5	-0.4	-0.7	-0.5	-0.4	-0.7	-0.5
	ASD vs ASA	0.4	0	0	0.4	0	0	0.4	0	0
	ASD vs K	-0.2	N/A	N/A	-0.2	N/A	N/A	-0.2	N/A	N/A
	ASA vs K	-0.3	N/A	N/A	-0.3	N/A	N/A	-0.3	N/A	N/A
	DS vs K	-0.7	N/A	N/A	-0.7	N/A	N/A	-0.7	N/A	N/A
SF vs K	0.5	N/A	N/A	0.5	N/A	N/A	0.5	N/A	N/A	

TABLE A1-20 (continued)

Parameters		UMi_A						UMi_B		
		0.5 GHz ≤ f _c ≤ 6 GHz			6GHz < f _c ≤ 100 GHz			0.5 GHz ≤ f _c ≤ 100 GHz NOTE – For UMi and frequencies below 2 GHz, use f _c = 2 when determining the values of the frequency-dependent LSP values		
		LOS	NLOS	O-to-I	LOS	NLOS	O-to-I	LOS	NLOS	O-to-I
Cross-Correlations 1)	ZSD vs SF	0	0	0	0	0	0	0	0	0
	ZSA vs SF	0	0	0	0	0	0	0	0	0
	ZSD vs K	0	N/A	N/A	0	N/A	N/A	0	N/A	N/A
	ZSA vs K	0	N/A	N/A	0	N/A	N/A	0	N/A	N/A
	ZSD vs DS	0	-0.5	-0.6	0	-0.5	-0.6	0	-0.5	-0.6
	ZSA vs DS	0.2	0	-0.2	0.2	0	-0.2	0.2	0	-0.2
	ZSD vs ASD	0.5	0.5	-0.2	0.5	0.5	-0.2	0.5	0.5	-0.2
	ZSA vs ASD	0.3	0.5	0	0.3	0.5	0	0.3	0.5	0
	ZSD vs ASA	0	0	0	0	0	0	0	0	0
	ZSA vs ASA	0	0.2	0.5	0	0.2	0.5	0	0.2	0.5
ZSD vs ZSA	0	0	0.5	0	0	0.5	0	0	0.5	
Delay distribution		Exp	Exp	Exp	Exp	Exp	Exp	Exp	Exp	Exp
AOD and AOA distribution		Wrapped Gaussian	Wrapped Gaussian	Wrapped Gaussian	Wrapped Gaussian	Wrapped Gaussian	Wrapped Gaussian	Wrapped Gaussian	Wrapped Gaussian	Wrapped Gaussian
ZOD and ZOA distribution		Laplacian	Laplacian	Laplacian	Laplacian	Laplacian	Laplacian	Laplacian	Laplacian	Laplacian
Delay scaling parameter r _τ		3.2	3	2.2	3	2.1	2.2	3	2.1	2.2
XPR [dB]	μ _{XPR}	9	8.0	9	9	8.0	9	9	8.0	9
	σ _{XPR}	3	3	11	3	3	5	3	3	5
Number of clusters		12	19	12	12	19	12	12	19	12
Number of rays per cluster		20	20	20	20	20	20	20	20	20
Cluster DS (c _{DS})		NA	NA	NA	5	11	11	5	11	11
Cluster ASD (c _{ASD})		3	10	5	3	10	5	3	10	5

TABLE A1-20 (end)

Parameters		UMi_A						UMi_B		
		0.5 GHz ≤ f _c ≤ 6 GHz			6GHz < f _c ≤ 100 GHz			0.5 GHz ≤ f _c ≤ 100 GHz NOTE – For UMi and frequencies below 2 GHz, use f _c = 2 when determining the values of the frequency-dependent LSP values		
		LOS	NLOS	O-to-I	LOS	NLOS	O-to-I	LOS	NLOS	O-to-I
Cluster ASA (<i>c_{ASA}</i>)		17	22	8	17	22	20	17	22	8
Cluster ZSA (<i>c_{ZSA}</i>)		7	7	3	7	7	6	7	7	3
Per cluster shadowing std ζ [dB]		3	3	4	3	3	4	3	3	4
Correlation distance in the horizontal plane [m]	DS	7	10	10	7	10	10	7	10	10
	ASD	8	10	11	8	10	11	8	10	11
	ASA	8	9	17	8	9	17	8	9	17
	SF	10	13	7	10	13	7	10	13	7
	K	15	N/A	N/A	15	N/A	N/A	15	N/A	N/A
	ZSA	12	10	25	12	10	25	12	10	25
	ZSD	12	10	25	12	10	25	12	10	25

TABLE A1-21

ZSD and ZOD offset parameters in UMi_x

	Frequency	Parameters		UMi_x	
				LOS/ LOS O-to-I	NLOS/ NLOS O-to-I
UMi_A	$0.5 \text{ GHz} \leq f_c \leq 6 \text{ GHz}$	ZOD spread (ZSD) $\lg\text{ZSD}=\log_{10}(\text{ZSD}/1^\circ)$	$\mu_{\lg\text{ZSD}}$	$\max[-0.5, -2.1(d_{2D}/1000)+0.01 h_{UT}-h_{BS} +0.75]$	$\max[-0.5, -2.1(d_{2D}/1000)+0.01\max(h_{UT}-h_{BS},0)+0.9]$
			$\sigma_{\lg\text{ZSD}}$	0.4	0.6
		ZOD offset	$\mu_{\text{offset,ZOD}}$	0	$-10^{\{-0.55\log_{10}(\max(10, d_{2D}))+1.6\}}$
	$6\text{GHz} < f_c \leq 100 \text{ GHz}$	ZOD spread (ZSD) $\lg\text{ZSD}=\log_{10}(\text{ZSD}/1^\circ)$	$\mu_{\lg\text{ZSD}}$	$\max[-0.21, -14.8(d_{2D}/1000) + 0.01 h_{UT}-h_{BS} + 0.83]$	$\max[-0.5, -3.1(d_{2D}/1000) + 0.01 \max(h_{UT}-h_{BS},0) + 0.2]$
			$\sigma_{\lg\text{ZSD}}$	0.35	0.35
		ZOD offset	$\mu_{\text{offset,ZOD}}$	0	$-10^{\{-1.5\log_{10}(\max(10, d_{2D}))+3.3\}}$
UMi_B	$0.5 \text{ GHz} \leq f_c \leq 100 \text{ GHz}$	ZOD spread (ZSD) $\lg\text{ZSD}=\log_{10}(\text{ZSD}/1^\circ)$	$\mu_{\lg\text{ZSD}}$	$\max[-0.21, -14.8(d_{2D}/1000) + 0.01 h_{UT}-h_{BS} + 0.83]$	$\max[-0.5, -3.1(d_{2D}/1000) + 0.01 \max(h_{UT}-h_{BS},0) + 0.2]$
			$\sigma_{\lg\text{ZSD}}$	0.35	0.35
		ZOD offset	$\mu_{\text{offset,ZOD}}$	0	$-10^{\{-1.5\log_{10}(\max(10, d_{2D}))+3.3\}}$

4.5.4 RMa_x

TABLE A1-22

Fast fading parameters for RMa_x

Parameters		RMa_A: $0.5 \text{ GHz} \leq f_c \leq 6 \text{ GHz}$		
		RMa_B: $0.5 \text{ GHz} \leq f_c \leq 7 \text{ GHz}$		
		LOS	NLOS	O2I
Delay spread (DS) $\lg DS = \log_{10}(DS/1s)$	$\mu_{\lg DS}$	-7.49	-7.43	-7.47
	$\sigma_{\lg DS}$	0.55	0.48	0.24
AOD spread (ASD) $\lg ASD = \log_{10}(ASD/1^\circ)$	$\mu_{\lg ASD}$	0.90	0.95	0.67
	$\sigma_{\lg ASD}$	0.38	0.45	0.18
AOA spread (ASA) $\lg ASA = \log_{10}(ASA/1^\circ)$	$\mu_{\lg ASA}$	1.52	1.52	1.66
	$\sigma_{\lg ASA}$	0.24	0.13	0.21
ZOA spread (ZSA) $\lg ZSA = \log_{10}(ZSA/1^\circ)$	$\mu_{\lg ZSA}$	0.47	0.58	0.93
	$\sigma_{\lg ZSA}$	0.40	0.37	0.22
Shadow fading (SF) [dB]	σ_{SF}	See Table A1-7		8
K-factor (K) [dB]	μ_K	7	N/A	N/A
	σ_K	4	N/A	N/A
Cross-Correlations	ASD vs DS	0	-0.4	0
	ASA vs DS	0	0	0
	ASA vs SF	0	0	0
	ASD vs SF	0	0.6	0
	DS vs SF	-0.5	-0.5	0
	ASD vs ASA	0	0	-0.7
	ASD vs K	0	N/A	N/A
	ASA vs K	0	N/A	N/A
	DS vs K	0	N/A	N/A
	SF vs K	0	N/A	N/A
Cross-Correlations	ZSD vs SF	0.01	-0.04	0
	ZSA vs SF	-0.17	-0.25	0
	ZSD vs K	0	N/A	N/A
	ZSA vs K	-0.02	N/A	N/A
	ZSD vs DS	-0.05	-0.10	0
	ZSA vs DS	0.27	-0.40	0
	ZSD vs ASD	0.73	0.42	0.66
	ZSA vs ASD	-0.14	-0.27	0.47
	ZSD vs ASA	-0.20	-0.18	-0.55
	ZSA vs ASA	0.24	0.26	-0.22
	ZSD vs ZSA	-0.07	-0.27	0
Delay scaling parameter r_τ		3.8	1.7	1.7
XPR [dB]	μ_{XPR}	12	7	7
	σ_{XPR}	4	3	3
Number of clusters N		11	10	10
Number of rays per cluster M		20	20	20

TABLE A1-22 (end)

Parameters		RMA_A: $0.5 \text{ GHz} \leq f_c \leq 6 \text{ GHz}$ RMA_B: $0.5 \text{ GHz} \leq f_c \leq 7 \text{ GHz}$		
		LOS	NLOS	O2I
Cluster DS (C_{DS}) in [ns]		N/A	N/A	N/A
Cluster ASD (C_{ASD}) in [deg]		2	2	2
Cluster ASA (C_{ASA}) in [deg]		3	3	3
Cluster ZSA (C_{ZSA}) in [deg]		3	3	3
Per cluster shadowing std ζ [dB]		3	3	3
Correlation distance in the horizontal plane [m]	DS	50	36	36
	ASD	25	30	30
	ASA	35	40	40
	SF	37	120	120
	K	40	N/A	N/A
	ZSA	15	50	50
	ZSD	15	50	50

TABLE A1-23

ZSD and ZOD offset parameters for RMA
(RMA_A: $0.5 \text{ GHz} \leq f_c \leq 6 \text{ GHz}$, RMA_B: $0.5 \text{ GHz} \leq f_c \leq 7 \text{ GHz}$)

Parameters		LOS	NLOS	O2I
ZOD spread (ZSD) $\lg ZSD = \log_{10}(ZSD/1^\circ)$	$\mu_{\lg ZSD}$	$\max(-1, -0.17 * (d_{2D} / 1000) - 0.01 * (h_{UT} - 1.5) + 0.22)$	$\max(-1, -0.19 * (d_{2D} / 1000) - 0.01 * (h_{UT} - 1.5) + 0.28)$	$\max(-1, -0.19 * (d_{2D} / 1000) - 0.01 * (h_{UT} - 1.5) + 0.28)$
	$\sigma_{\lg ZSD}$	0.34	0.30	0.30
ZOD offset	$\mu_{\text{offset,ZOD}}$	0	$\arctan((35-3.5)/d_{2D}) - \arctan((35-1.5)/d_{2D})$	$\arctan((35-3.5)/d_{2D}) - \arctan((35-1.5)/d_{2D})$

5 Advanced Modelling Components for IMT-2020 Channel Model

This section describes the detailed realization of advanced features given in § 2 of this Annex. The procedure of each advanced modeling components is added after each step of main procedure as sub-steps. Since each advanced modelling component is related to several steps of the main procedure, the correspondence main steps modified for each of the advanced modelling components are listed in Table A1-24. The use of the following advanced modeling components is optional and up to the proponents to decide.

TABLE A1-24

A summary of advanced modelling components

Subsection Number	Advanced modelling component	Corresponding steps in main procedure	Recommended condition
5.1	Oxygen absorption	Step 11	From 52 to 68 GHz
5.2.1	Large bandwidth and large antenna array – Modelling of propagation delay	Step 11	When the bandwidth B is greater than c/D Hz, where <ul style="list-style-type: none"> • D is the maximum antenna aperture in either azimuth or elevation (m) • c is the speed of light (m/s)
5.2.2	Large bandwidth and large antenna array- Modeling of intra-cluster angular and delay spread	Step 7	When inverse of bandwidth is smaller than the per-cluster delay spread or angular resolution of the antenna array is better than per-cluster angular spread.
5.3.1	Spatial consistency procedure	Steps 5-11	To ensure that the channel evolves smoothly without discontinuities which can be important when evaluating the system performance, including beam tracking or Multi-user MIMO (MU-MIMO) performance etc.
5.3.2	Spatial consistent UT mobility modeling	Steps 5, 6, 7	
5.3.3	Spatial consistent LOS/NLOS, indoor states and O-I parameters	Steps 2-12	
5.4	Blockage	Step between 9 and 10	When the transmitter and receiver are blocked by the stationary or moving objects, especially for the higher frequency bands.
5.5	Modeling of inter-frequency correlation of large scale parameters	Step 1, 2, 4, 5, 6, 7, 8-11	For simulations in multiple frequency band simultaneously.
5.6	Time-varying Doppler frequencies	Step 11	For nonlinear UT movement or when direction of arrival is time-varying, such as when using the feature in 5.3.
5.7	UT rotation	Step 1	For simulation that UT rotation is considered.
5.8	Ground reflection	Step 11	To increase the model accuracy in LOS conditions, especially in higher frequency band.
5.9	Random cluster number	Steps 5, 7	To better capture the cluster characteristics of the channel.

5.1 Oxygen absorption

Oxygen absorption loss is applied to the cluster responses generated in Step 11 in § 4.4. The additional loss, $OL_n(f_c)$ for cluster n at centre frequency f_c is modelled as:

$$OL_n(f_c) = \frac{\alpha(f_c)}{1000} \cdot (d_{3D} + c \cdot (\tau_n + \tau_\Delta)) \quad [\text{dB}] \quad (36)$$

where:

- $\alpha(f_c)$ is frequency dependent oxygen loss (dB/km) characterized in Table A1-25
- c is the speed of light (m/s) and d_{3D} is the 3D distance (m) between Rx antenna and Tx antenna
- τ_n is the n -th cluster delay (s) in Step 11 in § 4.4
- τ_Δ is 0 in the LOS case and $\min(\tau_n')$ otherwise, where $\min(\tau_n')$ is the minimum delay in Step 5.

For centre frequencies not specified in this table, the frequency dependent oxygen loss $\alpha(f_c)$ is obtained from a linear interpolation between two loss values corresponding to the two adjacent centre frequencies of the centre frequency f_c .

TABLE A1-25

Frequency dependent oxygen loss $\alpha(f)$ [dB/km]

Frequency f (GHz)	0-52	53	54	55	56	57	58	59	60	61	62	63	64	65	66	67	68-100
$\alpha(f)$ [dB/km]	0	1	2.2	4	6.6	9.7	12.6	14.6	15	14.6	14.3	10.5	6.8	3.9	1.9	1	0

For large channel bandwidth, first transform the time-domain channel response of each cluster (all rays within one cluster share common oxygen absorption loss for simplicity) into frequency-domain channel response, and apply the oxygen absorption loss to the cluster's frequency-domain channel response for frequency($f_c + \Delta f$) within the considered bandwidth. The oxygen loss, $OL_n(f_c + \Delta f)$ for cluster n at frequency ($f_c + \Delta f$) is modelled as:

$$OL_n(f_c + \Delta f) = \frac{\alpha(f_c + \Delta f)}{1000} \cdot (d_{3D} + c \cdot (\tau_n + \tau_\Delta)) \quad [\text{dB}] \quad (37)$$

where:

- $\alpha(f_c + \Delta f)$ is the oxygen loss (dB/km) at frequency($f_c + \Delta f$) characterized in Table A1-25. Note that Δf is in $[-B/2, B/2]$, where B is the bandwidth. Linear interpolation is applied for frequencies not provided in Table A1-24.

The final frequency-domain channel response is obtained by the summation of frequency-domain channel responses of all clusters.

Time-domain channel response is obtained by the reverse transform from the obtained frequency-domain channel response.

5.2 Large bandwidth and large antenna array

5.2.1 Modelling of the propagation delay

The modelling in this section applies only when bandwidth B is greater than c/D Hz, where:

- D is the maximum antenna aperture in either azimuth or elevation (m);
- c is the speed of light (m/s).

Each ray within a cluster for a given u (Rx) and s (Tx) has unique time of arrival (TOA). The channel coefficient generation step (Step 11 in § 4.4) is updated to model individual rays. In this case, the channel response of ray m in cluster n for a link between Rx antenna u and Tx antenna s at delay τ at time t is given by:

$$H_{u,s,n,m}^{\text{NLOS}}(t; \tau) = \sqrt{P_{n,m}} \begin{bmatrix} F_{rx,u,\theta}(\theta_{n,m,ZOA}, \phi_{n,m,AOA}) \\ F_{rx,u,\phi}(\theta_{n,m,ZOA}, \phi_{n,m,AOA}) \end{bmatrix}^T \begin{bmatrix} \exp(j\Phi_{n,m}^{\theta\theta}) & \sqrt{\kappa_{n,m}^{-1}} \exp(j\Phi_{n,m}^{\theta\phi}) \\ \sqrt{\kappa_{n,m}^{-1}} \exp(j\Phi_{n,m}^{\phi\theta}) & \exp(j\Phi_{n,m}^{\phi\phi}) \end{bmatrix} \begin{bmatrix} F_{tx,s,\theta}(\theta_{n,m,ZOD}, \phi_{n,m,AOD}) \\ F_{tx,s,\phi}(\theta_{n,m,ZOD}, \phi_{n,m,AOD}) \end{bmatrix} \exp\left(\frac{j2\pi(\hat{r}_{rx,n,m}^T \cdot \bar{d}_{rx,u})}{\lambda(f)}\right) \exp\left(\frac{j2\pi(\hat{r}_{tx,n,m}^T \cdot \bar{d}_{tx,s})}{\lambda(f)}\right) \cdot \exp\left(j2\pi \frac{\hat{r}_{rx,n,m}^T \cdot \bar{v}}{\lambda_0} t\right) \delta(\tau - \tau_{n,m}) \quad (38)$$

with $\lambda(f)$ is the wavelength on frequency $f \in \left[f_c - \frac{B}{2}, f_c + \frac{B}{2}\right]$, which can be implemented by user's own method. The delay (TOA) for ray m in cluster n for a link between Rx antenna u and Tx antenna s is given by:

$$\tau_{u,s,n,m} = \tau_{n,m} - \frac{1}{c} \hat{r}_{rx,n,m}^T \cdot \bar{d}_{rx,u} - \frac{1}{c} \hat{r}_{tx,n,m}^T \cdot \bar{d}_{tx,s} \quad (39)$$

Note that equation (39) only considers the delays $\tau_{n,m}$ intentionally. If unequal ray powers are considered, $P_{n,m}$ are generated according to § 5.2.2. Otherwise, ray powers are equal within a cluster, i.e. $P_{n,m} = P_n/M$ for all m . NOTE – this model is developed assuming plane wave propagation.

5.2.2 Modelling of intra-cluster angular and delay spreads

With large antenna arrays or large bandwidths, the angle and/or delay resolution can be larger than what the fast fading model in § 4.4 is designed to support. To model this effect, the following modifications to Step 7 in § 4.4 can be optionally used.

- 1 The offset angles α_m in equations (17), (23), and (25) are generated independently per cluster and ray using:

$$\alpha_{n,m,\{AOA,AOD,ZOA,ZOD\}} \sim \text{unif}(-2,2) \quad (40)$$

where $\text{unif}(a,b)$ denotes the continuous uniform distribution in the interval $[a,b]$. These random variables may further be modelled as spatially consistent with correlation distance equal to the cluster-specific random variable correlation distance of Table A1-26.

- 2 The relative delay of m -th ray is given by $\tau'_{n,m} = \tau_{n,m} - \min\left(\{\tau_{n,i}''\}_{i=1}^M\right)$ where n is a cluster index, $\tau_{n,m}'' \sim \text{unif}(0, 2c_{\text{DS}})$, the cluster DS c_{DS} is given in Tables A1-16, A1-18, A1-20 and A1-22. These random variables may further be modelled as spatially consistent with

correlation distance equal to the cluster-specific random variable correlation distance of Table A1-26. In this case, the sub-cluster mapping according to equation (31) and Table A1-23 shall not be applied. The delays to be used in equation (38) are given by $\tau_{n,m} = \tau_n + \tau'_{n,m}$.

3 Ray powers are determined unequally by the following process:

The power of m -th ray in n -th cluster is given by $P_{n,m} = P_n \cdot \frac{P'_{n,m}}{\sum_{m=1}^M P'_{n,m}}$ for $m = 1, \dots, M$, where

$$P'_{n,m} = \exp\left(-\frac{\tau'_{n,m}}{c_{DS}}\right) \exp\left(-\frac{\sqrt{2}|\alpha_{n,m,AOA}|}{c_{ASA}}\right) \exp\left(-\frac{\sqrt{2}|\alpha_{n,m,AOD}|}{c_{ASD}}\right) \cdot \exp\left(-\frac{\sqrt{2}|\alpha_{n,m,ZOA}|}{c_{ZSA}}\right) \exp\left(-\frac{\sqrt{2}|\alpha_{n,m,ZOD}|}{c_{ZSD}}\right) \quad (41)$$

and c_{DS} , c_{ASA} , c_{ASD} , and c_{ZSA} are respectively the intra-cluster delay spread and the corresponding intra-cluster angular spread that are given in Tables A1-16, A1-18, A1-20 and A1-22. The cluster zenith spread of departure is given by

$$c_{ZSD} = \frac{3}{8} 10^{\mu_{lgZSD}} \quad (42)$$

with μ_{lgZSD} being defined in Tables A1-17, A1-19, A1-21 and A1-23.

The number of rays per cluster shall be calculated as follows:

$$M = \min\left\{\max\left(M_t M_{AOD} M_{ZOD}, 20\right), M_{\max}\right\} \quad (43)$$

where:

$$M_t = \lceil 4kc_{DS}BW \rceil, \quad M_{AOD} = \left\lceil 4kc_{ASD} \frac{\pi \cdot D_h}{180 \cdot \lambda} \right\rceil, \quad M_{ZOD} = \left\lceil 4kc_{ZSD} \frac{\pi \cdot D_v}{180 \cdot \lambda} \right\rceil$$

M_{\max} is the upper limit of M , and it should be selected by the user of channel model based on the trade-off between simulation complexity and accuracy

D_h and D_v are the array size in m in horizontal and vertical dimension, B is bandwidth in Hz, c_{ASD} and c_{ZSD} are the cluster spreads in degrees, and λ is the wavelength

k is a “sparseness” parameter with value 0.5.

It is noted that each MPC may have different AOD, ZOD, and delay.

5.3 Spatial consistency

5.3.1 Spatial consistency procedure

A new procedure, namely *a spatial consistency procedure*, can be used for both cluster-specific and ray-specific random variables to be generated in various channel generation steps in § 4.4, so that they are spatially consistent for drop-based simulations. Alternatively, this can be used together with SC-II model described in § 5.3.2 for spatially consistent mobility simulations.

The procedure can be considered as a 2D random process (in the horizontal plane) given the UT locations based on the parameter-specific correlation distance values for spatial consistency, specified in Table A1-26. The cluster specific random variables include:

- Cluster specific random delay in Step 5;
- Cluster specific shadowing in Step 6; and
- Cluster specific offset for AOD/AOA/ZOD/ZOA in Step 7.
- Cluster specific sign for AOD/AOA/ZOD/ZOA in Step 7.
- Optionally in case of large bandwidth as described in § 5.2.2 the procedure may apply as well for the parameters of rays within a cluster.

The procedure shall apply to each cluster before sorting the delay. Cluster specific sign for AOD/AOA/ZOD/ZOA in Step 7 shall be kept unchanged per simulation drop even if UT position changes during simulation. The ray specific random variables include:

- Random coupling of rays in Step 8;
- XPR in Step 9; and
- Random phase in Step 10.

The random coupling of rays in Step 8 and the intra-cluster delays in Step 11 shall be kept unchanged per simulation drop even if UT position changes during simulation.

TABLE A1-26
Correlation distance for spatial consistency

Correlation distance (m)	RMa_x			UMi_x			UMa_x			InH_x
	LOS	NLOS	O-to-I	LOS	NLOS	O-to-I	LOS	NLOS	O-to-I	
For cluster and ray specific random variables	50	60	15	12	15	15	40	50	15	10
For LOS/NLOS state	60			50			50			10
For indoor/outdoor state	50			50			50			N/A

5.3.2 Spatially-consistent UT mobility modelling

For mobility simulation enhancement, two alternative spatial consistency procedures –**Spatial Consistency Model I(SC-I)** and **Spatial Consistency Model II(SC-II)** – are described as follows. The procedures presented below consider the downlink direction same as in § 4.

Spatial Consistency Model I (SC-I)

For $t_0=0$ when a UT is dropped into the network, spatially consistent powers/delays/angles of clusters are generated according to § 5.3.1.

The updated distance of UT should be limited within 1 meter, i.e. when $v \cdot \Delta t < 1$ m, and the updated procedure in the following should take the closest realization instead of $t_0=0$.

At $t_k + \Delta t$, update channel cluster power/delay/angles based on UT channel cluster power/delay/angles, moving speed moving direction and UT position at t_{k-1} .

Cluster delay is updated as:

$$\tilde{\tau}_n(t_k) = \tilde{\tau}_n(t_{k-1} + \Delta t) = \tilde{\tau}_n(t_{k-1}) - \frac{\hat{r}_{rx,n}(t_{k-1})^T \bar{v}(t_{k-1})}{c} \cdot \Delta t \quad (44)$$

where:

c is the speed of light

$\bar{v}(t_{k-1}) = [V_X(t_{k-1}) \ V_Y(t_{k-1}) \ V_Z(t_{k-1})]^T$ is the UT velocity vector and $\|\bar{v}(t_{k-1})\|_2 = v$.

And $\tilde{\tau}_n(t_0) = (d_{3D}(t_0) + c \cdot (\tau_n(t_0) + \tau_\Delta(t_0))) / c$,

where:

c is the speed of light (m/s) and $d_{3D}(t_0)$ is the 3-Dimension distance (m) between Rx antenna and Tx antenna

$\tau_n(t_0)$ is the n -th cluster delay (s) in Step 11 in § 4

$\tau_\Delta(t_0)$ is 0 in the LOS case and $\min(\tau_n)$ otherwise, where $\min(\tau_n)$ is the minimum delay in Step 5 in § 4.

also,

$$\hat{r}_{rx,n}(t_{k-1}) = \begin{bmatrix} \sin(\theta_{n,ZOA}(t_{k-1})) \cos(\phi_{n,AOA}(t_{k-1})) \\ \sin(\theta_{n,ZOA}(t_{k-1})) \sin(\phi_{n,AOA}(t_{k-1})) \\ \cos(\theta_{n,ZOA}(t_{k-1})) \end{bmatrix} \quad (45)$$

where $\theta_{n,ZOA}$ and $\phi_{n,AOA}$ are cluster specific arrival and departure angles.

After updating the delays according to equation (44), the delays over the mobility range are normalized. Equation (6) of the fast fading model is replaced by:

$$\tau_n(t_k) = \tau_n(t_{k-1} + \Delta t) = \tilde{\tau}_n(t_k) - \min(\tilde{\tau}_n(t_k)) \quad (45a)$$

in which t_k covers the entire duration of the mobility model.

Cluster power is updated using Step 6 with cluster delay $\tau_n(t_{k-1} + \Delta t)$.

For the n^{th} cluster, define rotation matrix R to transfer $\bar{v}(t_{k-1})$ to $\bar{v}'(t_{k-1})$:

$$[V'_X(t_{k-1}) \ V'_Y(t_{k-1}) \ V'_Z(t_{k-1})]^T = R \cdot [V_X(t_{k-1}) \ V_Y(t_{k-1}) \ V_Z(t_{k-1})]^T$$

where:

$$R = R_{Z,AOA'} \cdot R_{Y,ZOA'} \cdot R_{X,Bern} \cdot R_{Y,-ZOA} \cdot R_{Z,-AOA} \text{ for NLOS cluster and } R = \begin{bmatrix} 1 & 0 & 0 \\ 0 & 1 & 0 \\ 0 & 0 & 1 \end{bmatrix} \text{ for LOS cluster,}$$

and

$$R_{Z,-AOA} = \begin{bmatrix} \cos(-\phi_{n,AOA}(t_{k-1})) & -\sin(-\phi_{n,AOA}(t_{k-1})) & 0 \\ \sin(-\phi_{n,AOA}(t_{k-1})) & \cos(-\phi_{n,AOA}(t_{k-1})) & 0 \\ 0 & 0 & 1 \end{bmatrix} \quad (45b)$$

$$R_{Y,-ZOA} = \begin{bmatrix} \cos\left(-\left(\theta_{n,ZOA}(t_{k-1}) - 90^\circ\right)\right) & 0 & \sin\left(-\left(\theta_{n,ZOA}(t_{k-1}) - 90^\circ\right)\right) \\ 0 & 1 & 0 \\ -\sin\left(-\left(\theta_{n,ZOA}(t_{k-1}) - 90^\circ\right)\right) & 0 & \cos\left(-\left(\theta_{n,ZOA}(t_{k-1}) - 90^\circ\right)\right) \end{bmatrix}, \quad (45c)$$

$$R_{Z,AOA} = \begin{bmatrix} \cos(\phi'_{n,AOA}(t_{k-1})) & -\sin(\phi'_{n,AOA}(t_{k-1})) & 0 \\ \sin(\phi'_{n,AOA}(t_{k-1})) & \cos(\phi'_{n,AOA}(t_{k-1})) & 0 \\ 0 & 0 & 1 \end{bmatrix} \quad (45d)$$

$$R_{Y,ZOA} = \begin{bmatrix} \cos(\theta'_{n,ZOA}(t_{k-1}) - 90^\circ) & 0 & \sin(\theta'_{n,ZOA}(t_{k-1}) - 90^\circ) \\ 0 & 1 & 0 \\ -\sin(\theta'_{n,ZOA}(t_{k-1}) - 90^\circ) & 0 & \cos(\theta'_{n,ZOA}(t_{k-1}) - 90^\circ) \end{bmatrix} \quad (45e)$$

$$\phi'_{n,AOA}(t_{k-1}) = \phi_{n,AOD}(t_{k-1}) + \pi \quad (45f)$$

$$\theta'_{n,ZOA}(t_{k-1}) = \pi - \theta_{n,ZOD}(t_{k-1}) \quad (45g)$$

$R_{X,Bern} = R_B$, $B \in [0,1]$ is the random number of Bernoulli distribution with possibility density function:

$$P(B) = \begin{cases} 0.5 & \text{for } B = 0 \\ 0.5 & \text{for } B = 1 \end{cases} \quad (45h)$$

and

$$R_0 = \begin{bmatrix} 1 & 0 & 0 \\ 0 & 1 & 0 \\ 0 & 0 & 1 \end{bmatrix}, \quad R_1 = \begin{bmatrix} 1 & 0 & 0 \\ 0 & -1 & 0 \\ 0 & 0 & 1 \end{bmatrix} \quad (45i)$$

Note that the variable B is initialized on a NLOS cluster basis and is not changed during the UT mobility within a drop. The cluster specific correlation distance for B is 60 m, 15 m, 50 m and 10 m for RMa_x, UMi_x, UMa_x and InH_x scenarios, respectively.

Cluster departure angles ($\theta_{n,ZOD}$ and $\phi_{n,AOD}$) and arrival angles ($\theta_{n,ZOA}$ and $\phi_{n,AOA}$) are updated as

$$\phi_{n,AOD}(t_{k-1} + \Delta t) = \phi_{n,AOD}(t_{k-1}) + \frac{\Delta t \cdot \left(V'_y(t_{k-1}) \cdot \cos(\phi_{n,AOD}(t_{k-1})) - V'_x(t_{k-1}) \cdot \sin(\phi_{n,AOD}(t_{k-1})) \right) 180}{r_{n,3D}(t_{k-1}) \cdot \sin(\theta_{n,ZOD}(t_{k-1})) \pi} \quad (46)$$

$$\theta_{n,ZOD}(t_{k-1} + \Delta t) = \theta_{n,ZOD}(t_{k-1}) + \frac{\Delta t \cdot \left(V'_x(t_{k-1}) \cdot \cos(\phi_{n,AOD}(t_{k-1})) \cdot \cos(\theta_{n,ZOD}(t_{k-1})) - V'_z(t_{k-1}) \cdot \sin(\theta_{n,ZOD}(t_{k-1})) + V'_y(t_{k-1}) \cdot \cos(\theta_{n,ZOD}(t_{k-1})) \cdot \sin(\phi_{n,AOD}(t_{k-1})) \right) 180}{r_{n,3D}(t_{k-1}) \pi} \quad (47)$$

and

$$\phi_{n,AOA}(t_{k-1} + \Delta t) = \phi_{n,AOA}(t_{k-1}) - \frac{\Delta t \cdot \left(V'_y(t_{k-1}) \cdot \cos(\phi_{n,AOA}(t_{k-1})) - V'_x(t_{k-1}) \cdot \sin(\phi_{n,AOA}(t_{k-1})) \right) 180}{r_{n,3D}(t_{k-1}) \cdot \sin(\theta_{n,ZOA}(t_{k-1})) \pi} \quad (48)$$

$$\theta_{n,ZOA}(t_{k-1} + \Delta t) = \theta_{n,ZOA}(t_{k-1}) - \frac{\Delta t \cdot (V_X(t_{k-1}) \cdot \cos(\phi_{n,AOA}(t_{k-1})) \cos(\theta_{n,ZOA}(t_{k-1})) - V_Z(t_{k-1}) \cdot \sin(\theta_{n,ZOA}(t_{k-1})) + V_Y(t_{k-1}) \cdot \cos(\theta_{n,ZOA}(t_{k-1})) \cdot \sin(\phi_{n,AOA}(t_{k-1})))}{r_{n,3D}(t_{k-1})} \frac{180}{\pi} \quad (49)$$

For the n^{th} cluster, $r_{n,3D}(t_{k-1}) = c \cdot \tilde{\tau}_n(t_{k-1})$.

Spatial Consistency Model II (SC-II)

In SC-II model, spatial or time evolution of the channel is obtained by generating channel realizations separately for all links to different Rx positions using Steps 1-12 of § 4 together with the spatially consistent procedure of § 5.3.1. In the case of mobility these positions may be a function of time along one or more Rx trajectories. Furthermore, to ensure that the spatial or time evolution of delays and angles are within reasonable limits, Steps 5, 6, and 7 in § 4 should be replaced by the below procedure.

NOTE – For implementation purposes, LSPs and SSPs may be interpolated within the coherence length or time of the respective parameter.

Step 5: Generate cluster delays τ_n , with $n \in [1, N]$.

N delays are drawn randomly from a uniform distribution.

$$\tau'_n \sim \text{unif}\left(0, 2 \cdot 10^{\mu_{\text{lgDS}} + \sigma_{\text{lgDS}}}\right) \quad (50)$$

Normalise the delays by subtracting the minimum delay: $\tau_n = \tau'_n - \min(\tau'_n)$. The autocorrelation distance for τ'_n is $2c \cdot 10^{\mu_{\text{lgDS}} + \sigma_{\text{lgDS}}}$.

In the case of LOS, set the delay of the first cluster τ_1 to 0.

Step 6: Generate N arrival angles and departure angles for both azimuth and elevation using (51) instead of (44) and (49).

$$\phi'_{n,AOA} \sim 2 \cdot 10^{\mu_{\text{lgASA}} + \sigma_{\text{lgASA}}} \text{unif}(-1,1) \quad (51)$$

with $n \in [1, N]$. This step is repeated independently for AOD, AOA, ZOD, and ZOA with corresponding maximum angles for the uniform distribution. In case of LOS, set the angles of the first cluster ($\phi'_{1,AOA}$, etc) to 0.

The autocorrelation distances are $2c \cdot 10^{\mu_{\text{lgDS}} + \sigma_{\text{lgDS}}}$ for AOD, and ZOD, while they are fixed to 50 m for AOA, and ZOA.

Offset angles etc are applied in the modified Step 7b below after cluster powers have been calculated.

Step 7: Generate cluster powers P_n

Cluster powers are calculated assuming a single slope exponential power profile and Laplacian angular power profiles. The cluster powers are determined by:

$$P'_n = \exp\left(\frac{-\tau'_n}{\text{DS}}\right) \exp\left(\frac{-\sqrt{2}|\phi'_{n,\text{AOA}}|}{\text{ASA}}\right) \exp\left(\frac{-\sqrt{2}|\phi'_{n,\text{AOD}}|}{\text{ASD}}\right) \cdot \exp\left(\frac{-\sqrt{2}|\theta'_{n,\text{ZOA}}|}{\text{ZSA}}\right) \exp\left(\frac{-\sqrt{2}|\theta'_{n,\text{ZOD}}|}{\text{ZSD}}\right) \cdot 10^{\frac{-Z_n}{10}} \quad (52)$$

where $Z_n \sim N(0, \zeta^2)$ (autocorrelation distance same as for shadow fading) is the per cluster shadowing term in [dB]. Delay spread DS and angular spreads ASA, ASD, ZSA, ZSD are generated in Step 4 of § 4. Normalize the cluster powers so that the sum of all cluster powers is equal to one, i.e.:

$$P_n = \frac{P'_n}{\sum_{n=1}^N P'_n} \quad (52a)$$

In the case of LOS condition, substitute DS with $\sqrt{1+K_R}/2 \cdot \text{DS}$ and { ASA, ASD, ZSA, ZSD } with { $\sqrt{1+K_R} \cdot \text{ASA}$, $\sqrt{1+K_R} \cdot \text{ASD}$, $\sqrt{1+K_R} \cdot \text{ZSA}$, $\sqrt{1+K_R} \cdot \text{ZSD}$ } respectively to preserve the delay and angular spreads. K_R is the Ricean K-factor as generated in Step 4 converted to linear scale. Furthermore, an additional specular component is added to the first cluster. Power of the single LOS ray is:

$$P_{1,\text{LOS}} = \frac{K_R}{K_R + 1} \quad (52b)$$

and the cluster powers are not normalized as in equation (5-17a), but:

$$P_n = \frac{1}{K_R + 1} \frac{P'_n}{\sum_{n=1}^N P'_n} + \delta(n-1)P_{1,\text{LOS}} \quad (52c)$$

where $\delta(\cdot)$ is Dirac's delta function.

Assign the power of each ray within a cluster as P_n/M , where M is the number of rays per cluster.

Step 7b: Apply offset angles

The ray AOA angles are determined by:

$$\phi_{n,m,\text{AOA}} = \phi'_{n,\text{AOA}} + \phi_{\text{LOS,AOA}} + c_{\text{ASA}}\alpha_m \quad (52d)$$

where $\phi_{\text{LOS,AOA}}$ is the LOS direction defined in the network layout description, see Step 1c.

The generation of AOD ($\phi_{n,m,\text{AOD}}$) follows a procedure similar to AOA as described above.

The ZOA angles are determined by:

$$\theta_{n,m,\text{ZOA}} = \phi'_{n,\text{ZOA}} + \bar{\theta}_{\text{ZOA}} + c_{\text{ZSA}}\alpha_m \quad (52e)$$

where $\bar{\theta}_{\text{ZOA}} = 90^\circ$ if the BS-UT link is O2I and $\bar{\theta}_{\text{ZOA}} = \theta_{\text{LOS,ZOA}}$ otherwise. The LOS direction is defined in the network layout description, see Step 1c.

The ZOA angles are determined by:

$$\theta_{n,m,\text{ZOD}} = \phi'_{n,\text{ZOD}} + \theta_{\text{LOS,ZOD}} + \mu_{\text{offset,ZOD}} + (3/8)(10^{\mu_{\text{1gZSD}}})\alpha_m \quad (52f)$$

where μ_{lgZSD} is the mean of the ZSD log-normal distribution.

Some of the delay and angle spreads and standard deviations used in equations (50) and (51) may be frequency-dependent. In the case of multi-frequency simulations according to § 5.5, the largest value among all the simulated frequencies should be used in equations (50) and (51) so that the cluster and ray delays and angles (but not the powers or the resulting delay or angular spreads) are the same for all frequencies.

5.3.3 LOS/NLOS, indoor states and O-I parameters

The LOS state can be determined according to the spatial consistency procedure for random variables as mentioned in § 5.3.1, by comparing a realization of a random variable generated with distance-dependent LOS probability. If the realization is less than the LOS probability, the state is LOS; otherwise NLOS. Decision of LOS and NLOS status should be used in Step 2 in § 4 if this advanced simulation is performed.

The same procedure can be applied for determining the indoor state, with the indoor probability instead of the LOS probability.

The correlation distance for LOS state and indoor/outdoor is as Table A1-26.

The indoor distance can be modeled as the minimum of two spatially consistent uniform random variables within (0, 25) meters with correlation distance 25 m.

Note in case the UT is in an indoor state, the pathloss model changes and a penetration loss is considered. For details on the model, see § 3.2. Here, the focus is on modeling aspects with respect to spatial consistency. As described in § 3.2, the penetration loss deviation σ_p represents variations within and between buildings of the same type. For spatial consistency this can be modeled as a spatially consistent random variable with correlation distance 10 m, see § 5.3.1. The “building type” is determined using a spatially consistent uniform random variable with correlation distance 50 m. The building type is determined by comparing the random variable with P_1 , where P_1 is the probability of the building type with low loss penetration. If the realization of the random variable is less than P_1 , the building type is low loss; otherwise the building type is high loss.

The cluster-specific and ray-specific random variables as defined in § 5.3.1 on the same floor are generated in the spatial consistency modeling; otherwise, these variables across different floors are uncorrelated.

In case there is a transition from LOS to NLOS due to UT mobility, there will be a hard transition in the channel response. This is because pathloss and Large Scale parameters are different for these states, leading automatically to very different channel realizations. To circumvent such hard transitions the optional soft LOS state can be considered to determine the PL and the channel impulse responses containing characteristics of both LOS and NLOS. Soft LOS state LOS_{soft} is generated by floating numbers between 0 (NLOS) and 1 (LOS) in the spatial consistency modeling. The value of LOS_{soft} is determined by:

$$LOS_{soft} = \frac{1}{2} + \frac{1}{\pi} \arctan \left(\sqrt{\frac{20}{\lambda}} (G + F(d)) \right) \quad (53)$$

where:

G is a spatially consistent Gaussian random variable with correlation distance according to Table A1-26

$$F(d) = \sqrt{2} \operatorname{erf}^{-1} (2P_{LOS}(d) - 1);$$

$P_{\text{LOS}}(d)$ is the distance dependent LOS probability function; and
 λ is the wavelength of the carrier frequency.

After LOS_{soft} is obtained, Steps 2~12 of the channel coefficient generation described in § 4 are performed twice, once with the propagation condition in Step 2 set as LOS and once with the propagation condition in Step 2 set as NLOS. The resulting channel coefficients are denoted as H^{LOS} and H^{NLOS} respectively, where H^{LOS} is generated with the LOS path loss formula and channel model parameters while H^{NLOS} is generated using the NLOS path loss formula and channel model parameters. The channel matrix H with soft LOS state is determined from a linear combination of H^{LOS} and H^{NLOS} as:

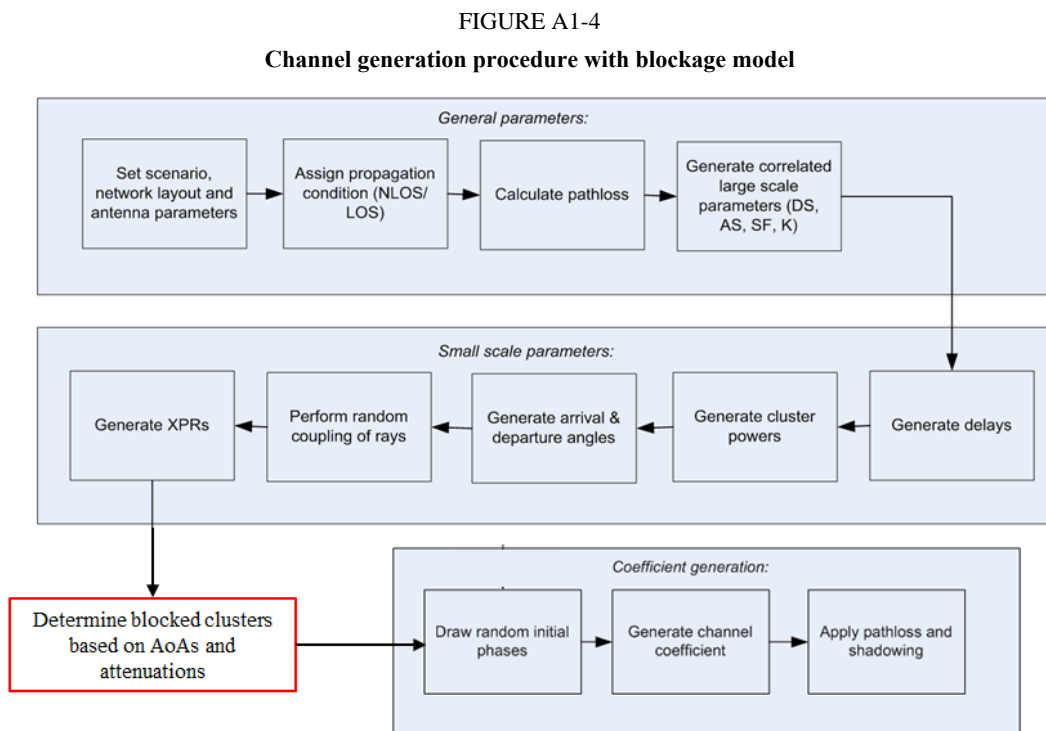
$$H(\text{LOS}_{\text{soft}}) = H^{\text{LOS}} \text{LOS}_{\text{soft}} + H^{\text{NLOS}} \sqrt{1 - \text{LOS}_{\text{soft}}^2} \quad (54)$$

It is noted that soft indoor/outdoor states are not modelled in this report. The model thus does not support move between indoor/outdoor states in mobility simulations.

5.4 Blockage

Blockage modelling is an advanced feature to the channel model. The method described in the following applies only when this feature is turned on. In addition, the temporal variability of the blockage modelling parameters is on-demand basis. It is also noted that the modeling of the blockage does not change LOS/NLOS state of each link.

When blockage model is applied, the channel generation in § 4.4 should have several additional steps between Step 9 and Step 10 as illustrated in Fig. A1-4.



Two alternative models (BL-I Model and BL-II Model) are provided for the blockage modelling. Both approaches have their own use cases. BL-I Model is applicable when a generic and

computationally efficient blockage modelling is desired. BL-II Model is applicable when a specific and more realistic blocking modelling is desired.

5.4.1 Blockage Model I (BL-I)

BL-I model adopts a stochastic method for capturing human and vehicular blocking.

Step 9-1: Determine the number of blockers

Multiple 2-dimensional (2D) angular blocking regions, in terms of center angle, azimuth and elevation angular span are generated around the UT. There is one self-blocking region, and $K = 4$ non-self-blocking regions, where K may be changed for certain scenarios (e.g. higher blocker density). Note that the self-blocking component of the model is important in capturing the effects of human body blocking.

Step 9-2: Generate the size and location of each blocker

For self-blocking, the blocking region in UT LCS is defined in terms of elevation and azimuth angles, $(\theta'_{sb}, \phi'_{sb})$ and azimuth and elevation angular span (x_{sb}, y_{sb}) .

$$\left\{ (\theta', \phi') \left(\theta'_{sb} - \frac{y_{sb}}{2} \leq \theta' \leq \theta'_{sb} + \frac{y_{sb}}{2}, \phi'_{sb} - \frac{x_{sb}}{2} \leq \phi' \leq \phi'_{sb} + \frac{x_{sb}}{2} \right) \right\} \quad (55)$$

where the parameters are described in Table A1-27.

TABLE A1-27

Self-blocking region parameters.

	ϕ'_{sb}	x_{sb}	θ'_{sb}	y_{sb}
Portrait mode	260°	120°	100°	80°
Landscape mode	40°	160°	110°	75°

For non-self-blocking $k = 1, \dots, 4$, the blocking region in GCS is defined by:

$$\left\{ (\theta, \phi) \left(\theta_k - \frac{y_k}{2} \leq \theta \leq \theta_k + \frac{y_k}{2}, \phi_k - \frac{x_k}{2} \leq \phi \leq \phi_k + \frac{x_k}{2} \right) \right\} \quad (56)$$

where the parameters are described in Table A1-28, as well as the distance r between the UT and the blocker.

TABLE A1-28

Blocking region parameters

Blocker index ($k = 1, \dots, 4$)	ϕ_k	x_k	θ_k	y_k	r
InH scenario	Uniform in [0°, 360°]	Uniform in [15°, 45°]	90°	Uniform in [5°, 15°]	2 m
UMi_x, Uma_x, RMa_x scenarios	Uniform in [0°, 360°]	Uniform in [5°, 15°]	90°	5°	10 m

Step 9-3: Determine the attenuation of each cluster due to blockers

The attenuation of each cluster due to self-blocking corresponding to the centre angle pair (θ'_{sb} , ϕ'_{sb}), is 30 dB provided that $|\phi'_{AOA} - \phi'_{sb}| < \frac{x_{sb}}{2}$ and $|\theta'_{ZOA} - \theta'_{sb}| < \frac{y_{sb}}{2}$. Otherwise, the attenuation is 0 dB.

The attenuation of each cluster due to the non-self-blocking regions ($k=1, \dots, 4$) is given by:

$$L_{dB} = -20 \log_{10} (1 - (F_{A_1} + F_{A_2})(F_{Z_1} + F_{Z_2})) \quad (57)$$

provided that $|\phi_{AOA} - \phi_k| < x_k$ and $|\theta_{ZOA} - \theta_k| < y_k$. Otherwise, the attenuation is 0 dB. The terms in the above equation are given as:

$$F_{A_1/A_2/Z_1/Z_2} = \frac{\tan^{-1} \left(\pm \frac{\pi}{2} \sqrt{\frac{\pi}{\lambda} r \left(\frac{1}{\cos(A_1/A_2/Z_1/Z_2)} - 1 \right)} \right)}{\pi} \quad (58)$$

where:

$$A_1 = \phi_{AOA} - \left(\phi_k + \frac{x_k}{2} \right), \quad (59)$$

$$A_2 = \phi_{AOA} - \left(\phi_k - \frac{x_k}{2} \right), \quad (60)$$

$$Z_1 = \theta_{ZOA} - \left(\theta_k + \frac{y_k}{2} \right), \quad (61)$$

$$Z_2 = \theta_{ZOA} - \left(\theta_k - \frac{y_k}{2} \right). \quad (62)$$

In the above formula for $F_{A_1/A_2/Z_1/Z_2}$, λ is the wavelength. The appropriate signs (\pm) within the \tan^{-1} term are described in Table A1-29.

TABLE A1-29

Description of signs

	$-y_k < \theta_{ZOA} - \theta_k \leq -\frac{y_k}{2}$	$-\frac{y_k}{2} < \theta_{ZOA} - \theta_k \leq \frac{y_k}{2}$	$\frac{y_k}{2} < \theta_{ZOA} - \theta_k \leq y_k$
$\frac{x_k}{2} < \phi_{AOA} - \phi_k \leq x_k$	(-, +) for (A_1, A_2) (+, -) for (Z_1, Z_2)	(-, +) for (A_1, A_2) (+, +) for (Z_1, Z_2)	(-, +) for (A_1, A_2) (-, +) for (Z_1, Z_2)
$-\frac{x_k}{2} < \phi_{AOA} - \phi_k \leq \frac{x_k}{2}$	(+, +) for (A_1, A_2) (+, -) for (Z_1, Z_2)	(+, +) for (A_1, A_2) (+, +) for (Z_1, Z_2)	(+, +) for (A_1, A_2) (-, +) for (Z_1, Z_2)
$-x_k < \phi_{AOA} - \phi_k \leq -\frac{x_k}{2}$	(+, -) for (A_1, A_2) (+, -) for (Z_1, Z_2)	(+, -) for (A_1, A_2) (+, +) for (Z_1, Z_2)	(+, -) for (A_1, A_2) (-, +) for (Z_1, Z_2)

Step 9-4: Spatial and temporal consistency of each blocker

The centre of the blocker is generated based on a uniformly distributed random variable, which is temporally and spatially consistent. The two-dimensional autocorrelation function $R(\Delta_x, \Delta_t)$ can be described with sufficient accuracy by the exponential function

$$R(\Delta_x, \Delta_t) = \exp\left(-\left(\frac{|\Delta_x|}{d_{\text{corr}}} + \frac{|\Delta_t|}{t_{\text{corr}}}\right)\right) \quad (63)$$

The spatial correlation distance d_{corr} for the random variable determining the centre of the blocker is given in Table A1-30 for different scenarios.

TABLE A1-30

Spatial correlation distance for different scenarios.

Spatial correlation distance d_{corr} (in m)	UMi_x			UMa_x			RMa_x			InH_x	
	LOS	NLOS	O-I	LOS	NLOS	O-I	LOS	NLOS	O-I	LOS	NLOS
for the random variable determining the centre of the blocker	10	10	5	10	10	5	10	10	5	5	5

The correlation time $t_{\text{corr}} = d_{\text{corr}}/v$, where v is the speed of moving blocker.

NOTE – The rectangular blocker description is chosen for self-blocking region with the specific choices of $(\theta'_{sb}, \phi'_{sb})$ assumed here. Generalization of this description to other choices should be done with care as the rectangular description may not be accurate.

5.4.2 Blockage Model II (BL-II)

BL-II Model adopts a geometric method for capturing e.g. human and vehicular blocking.

Step 9-1: Determine blockers

A number, K , of blockers are modelled as rectangular screens that are physically placed on the map. Each screen has the dimension by height (h_k) and width (w_k), with the screen centre at coordinate (x_k, y_k, z_k) .

NOTE –

- The number of blockers (K), their horizontal and vertical extensions (h_k and w_k), locations (x_k, y_k, z_k) , density, and movement pattern (if non-stationary) are all simulation assumptions, to allow different blocking scenarios to be constructed depending on the need of the particular simulation study.
- Recommended parameters for typical blockers are provided in Table A1-31.
- The blocking effect diminishes with increasing distance to the blocker. For implementation purposes it may be sufficient to consider only the K nearest blockers or the blockers closer than some distance from a specific UT.

TABLE A1-31

Recommended blocker parameters

	Typical set of blockers	Blocker dimensions	Mobility pattern
Indoor; Outdoor	Human	Cartesian: w=0.3 m; h=1.7 m	Stationary or up to 3 km/h
Outdoor	Vehicle	Cartesian: w=4.8 m; h=1.4 m	Stationary or up to 100 km/h

Step 9-b: Determine the blockage attenuation for each cluster

Attenuation caused by each blocker to each of clusters is modelled using a simple knife edge diffraction model and is given by:

$$L_{dB} = -20 \log_{10}(1 - (F_{h1} + F_{h2})(F_{w1} + F_{w2})) \quad (64)$$

where F_{h1}, F_{h2} and F_{w1}, F_{w2} account for knife edge diffraction at the four edges, and are given by

$$F_{h1|h2|w1|w2} = \begin{cases} \frac{\operatorname{atan}\left(\pm \frac{\pi}{2} \sqrt{\frac{\pi}{\lambda}} (D1_{h1|h2|w1|w2} + D2_{h1|h2|w1|w2} - r)\right)}{\pi} & \text{for direct path in LOS} \\ \frac{\operatorname{atan}\left(\pm \frac{\pi}{2} \sqrt{\frac{\pi}{\lambda}} (D1_{h1|h2|w1|w2} - r')\right)}{\pi} & \text{for all other paths} \end{cases} \quad (65)$$

where λ is the wavelength, as shown in Figs A1-5 and A1-6, $D1_{h1|h2|w1|w2}$ are the projected (onto the side and top view planes) distances between the receiver and four edges of the corresponding blocker, and $D2_{h1|h2|w1|w2}$ are the projected (onto the side and top view planes) distances between the transmitter and four edges of the corresponding blocker. The side view plane is perpendicular to the horizontal ground plane. The top view is perpendicular to the side view. For each cluster, the blocker screen is rotated around its centre such that the arrival direction of the corresponding path is always perpendicular to the screen. It should be noted that different rotations are required for each individual sub-path. Meanwhile, the base and top edges of the screens are always parallel to the horizontal plane. As the screen is perpendicular to each sub-path, r is the distance between the transmitter and receiver for direct path in LOS, and r' is the distance between the blocker screen and receiver, projected onto the incoming sub-path direction, for all the other (NLOS) paths. In the equation of $F_{h1|h2|w1|w2}$, the plus and minus signs are determined in such a way that, as shown in Figs A1-5 and A1-6:

- if the sub-path (terminated at the receiver or transmitter) does not intersect the screen in side view, minus sign is applied for the shortest path among $D1_{h1}$ and $D1_{h2}$ in the NLOS case ($D1_{h1} + D2_{h1}$ and $D1_{h2} + D2_{h2}$ in the LOS case) and plus sign is applied for the other edge;
- if the sub-path (terminated at the receiver or transmitter) does not intersect the screen in top view, minus sign is applied for the shortest path among $D1_{w1}$ and $D1_{w2}$ in the NLOS case ($D1_{w1} + D2_{w1}$ and $D1_{w2} + D2_{w2}$ for the LOS case) and plus sign is applied for the other edge;
- if the sub-path intersects the screen plus signs are applied for both edges.

For the case of multiple screens the total loss is given by summing the losses of each contributing screen in dB units.

The model according to option B is consistent in time, frequency and space, and is more appropriate to be used for simulations with arbitrarily designated blocker density.

FIGURE A1-5

Illustration of the geometric relation among blocker, receiver and transmitter for LOS path

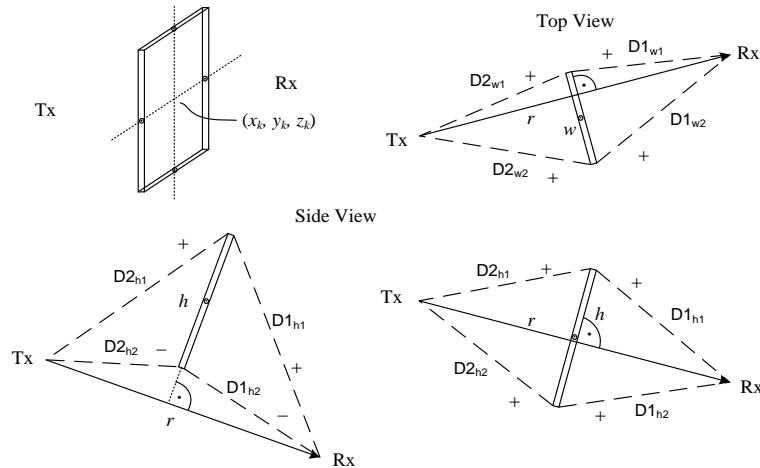
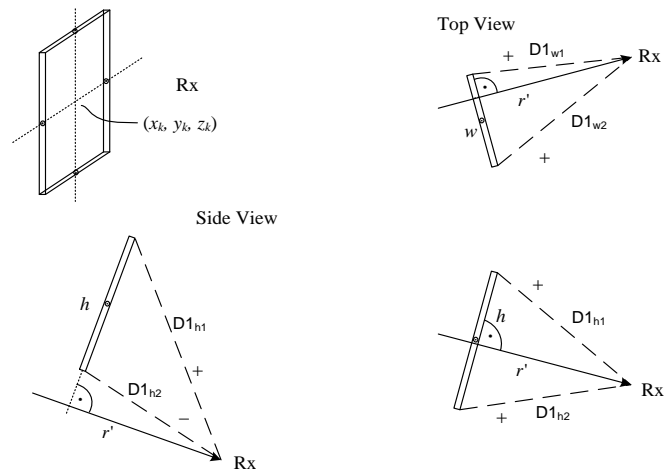


FIGURE A1-6

Illustration of the geometric relation between blocker and receiver for NLOS path



5.5 Modeling of inter-frequency correlation of large scale parameters

This section describes two approaches for modeling the inter-frequency correlation between specific large-scale parameters. The method in § 5.5.1 applies to all LSPs and can be used for all modeled environments, whereas the method in § 5.5.2 applies to the shadow fading and is parameterized for InH_x only. The techniques described in the two subsections are separate and mutually exclusive.

5.5.1 Correlation modelling for multi-frequency simulations

This section describes how to generate parameters to reflect correlation across different frequencies for a BS-UT link, for simulations involved with multiple frequencies.

For those simulations, the steps in § 4.4 should be revised according to the following:

- The parameters generated in Step 1 are the same for all the frequencies, except for antenna patterns, array geometries, system center frequency and bandwidth.
- Propagation conditions generated in Step 2 are the same for all the frequencies. It is noted that soft LOS states may be different due to frequency dependent function.
- The parameters generated in Step 4 are the same for all the frequencies, except for possibly frequency-dependent scaling of e.g. delay spread and angular spreads according to the LSP tables. i.e. let x be a random variable drawn from a Gaussian distribution: $x \sim N(0,1)$. Then the delay spread at frequency f is $DS(f) = 10^{(\mu \lg DS(f) + \sigma \lg DS(f) \cdot x)}$, where the same value of x is used for all frequencies. A corresponding procedure applies to each of the angular spreads.
- The cluster delays and angles resulting from Steps 5-7 are the same for all frequency bands.
- Per-cluster shadowing Z_n in Step 6 are independently generated for the frequency bands.
- Cluster powers in Step 6 may be frequency-dependent.
- Steps 8-11 are independently applied for the frequency bands.

In addition, when blockage is modeled according to § 5.4, the positions of blockers are the same across all the frequencies.

NOTE – The requirements above may not be fully aligned with the behavior of the model according to § 4, since cluster delays and angles will be frequency-dependent in scenarios where the DS or AS is frequency-dependent. The procedure below may alternatively be used to ensure that cluster delays and angles are frequency-independently generated.

5.5.1.1 Alternative channel generation method

The alternative method replaces Steps 5-7 in § 4 with the below Steps 5'-7'. The inputs to the alternative method are the delay and angular spreads determined according to Step 4 at an anchor frequency, e.g. 2 GHz: DS_0 , ASD_0 , ASA_0 , ZSD_0 , ZSA_0 , the delay and angular spreads determined according to Step 4 at a frequency of interest: DS , ASD , ASA , ZSD , ZSA , and the number of clusters N from Tables A1-16, A1-18, A1-20 and A1-22.

Step 5': Generate nominal delays τ'_n and angles $\phi'_{AOD,n}$, $\phi'_{AOA,n}$, $\theta'_{ZOD,n}$, $\theta'_{ZOA,n}$.

Generate N delays from a single-sided exponential distribution with zero mean and standard deviation of $r DS_0$, according to $\tau'_n = -r DS_0 \ln(X_n)$ with $X_n \sim \text{unif}(0,1)$.

Generate N AODs from a wrapped Gaussian distribution with zero mean and standard deviation of $r ASD_0$, according to $\phi'_{AOD,n} = \arg(\exp(-j r ASD_0 Y_n))$ with $Y_n \sim N(0,1)$.

Generate N AOA from a wrapped Gaussian distribution with zero mean and standard deviation of $r ASA_0$, according to $\phi'_{AOA,n} = \arg(\exp(-j r ASA_0 Z_n))$ with $Z_n \sim N(0,1)$.

Generate N ZODs from a wrapped Laplacian distribution with zero mean and standard deviation of $r ZSD_0$, according to $\theta'_{ZOD,n} = \arg(\exp(-j r ZSD_0 \text{sgn}(V_n - 0.5) \ln(1 - 2|V_n - 0.5|/\sqrt{2})))$ with $V_n \sim \text{unif}(0,1)$.

Generate N ZOAs from a wrapped Laplacian distribution with zero mean and standard deviation of $r ZSA_0$, according to $\theta'_{ZOA,n} = \arg(\exp(-j r ZSA_0 \text{sgn}(W_n - 0.5) \ln(1 - 2|W_n - 0.5|/\sqrt{2})))$ with $W_n \sim \text{unif}(0,1)$.

r is a proportionality factor, $r=1.5$. The principal value of the arg function should be used, e.g. $(-180,180)$.

In case of LOS, set $\tau'_1 = 0$, $\phi'_{AOD,1} = 0$, $\phi'_{AOA,1} = 0$, $\theta'_{ZOD,1} = 0$, and $\theta'_{ZOA,1} = 0$.

Step 6': Generate cluster powers P_n .

Generate cluster powers as:

$$P'_n = \exp\left(-\tau'_n g_{DS} - \left(\frac{\phi'_{AOD,n} g_{ASD}}{\sqrt{2}}\right)^2 - \left(\frac{\phi'_{AOA,n} g_{ASA}}{\sqrt{2}}\right)^2 - \sqrt{2}|\theta'_{ZOD,n}|g_{ZSD} - \sqrt{2}|\theta'_{ZOA,n}|g_{ZSA}\right) \cdot 10^{-Q_n/10} \quad (66a)$$

where $Q_n \sim N(0, \zeta^2)$ is the per cluster shadowing term in [dB] and:

$$g_{DS} = \frac{\max(r \cdot DS_0 - DS, 0)}{DS \cdot r \cdot DS_0} \quad (66b)$$

$$g_{ASD} = \frac{\sqrt{\max((r \cdot ASD_0)^2 - ASD^2, 0)}}{ASD \cdot r \cdot ASD_0} \quad (66c)$$

$$g_{ASA} = \frac{\sqrt{\max((r \cdot ASA_0)^2 - ASA^2, 0)}}{ASA \cdot r \cdot ASA_0} \quad (66d)$$

$$g_{ZSD} = \frac{\max(r \cdot ZSD_0 - ZSD, 0)}{ZSD \cdot r \cdot ZSD_0} \quad (66e)$$

$$g_{ZSA} = \frac{\max(r \cdot ZSA_0 - ZSA, 0)}{ZSA \cdot r \cdot ZSA_0} \quad (66f)$$

Normalize the cluster powers so that the sum of all cluster powers is equal to one, i.e.:

$$P_n = \frac{P'_n}{\sum_{n=1}^N P'_n} \quad (66g)$$

or, in the case of LOS, so that:

$$P_n = \frac{1}{1 + K_R} \frac{P'_n}{\sum_{n=1}^N P'_n} + \frac{K_R}{1 + K_R} \delta(n-1) \quad (66h)$$

where K_R is the K-factor converted to linear scale.

Step 7': Generate delays τ_n and angles $\phi_{AOD,n}$, $\phi_{AOA,n}$, $\theta_{ZOD,n}$, $\theta_{ZOA,n}$.

$$\tau_n = \begin{cases} \tau'_n & , \text{for NLOS} \\ \sqrt{1 + \frac{K_R}{2}} \tau'_n & , \text{for LOS} \end{cases} \quad (66i)$$

$$\phi_{n,m,AOA} = \begin{cases} \phi'_{n,AOA} + \phi_{LOS,AOA} + c_{ASA} \alpha_m & , \text{for NLOS} \\ \sqrt{1 + K_R} \phi'_{n,AOA} + \phi_{LOS,AOA} + c_{ASA} \alpha_m & , \text{for LOS} \end{cases} \quad (66j)$$

$$\phi_{n,m,AOD} = \begin{cases} \phi'_{n,AOD} + \phi_{LOS,AOD} + c_{ASD} \alpha_m & , \text{for NLOS} \\ \sqrt{1 + K_R} \phi'_{n,AOD} + \phi_{LOS,AOD} + c_{ASD} \alpha_m & , \text{for LOS} \end{cases} \quad (66k)$$

$$\theta_{n,m,ZOA} = \begin{cases} \theta'_{n,ZOA} + \theta_{\text{LOS,ZOA}} + c_{\text{ZSA}} \alpha_m & , \text{ for NLOS} \\ \sqrt{1 + K_R} \theta'_{n,ZOA} + \theta_{\text{LOS,ZOA}} + c_{\text{ZSA}} \alpha_m & , \text{ for LOS} \end{cases} \quad (66l)$$

$$\theta_{n,m,ZOD} = \begin{cases} \theta'_{n,ZOD} + \theta_{\text{LOS,ZOD}} + c_{\text{ZSD}} \alpha_m & , \text{ for NLOS} \\ \sqrt{1 + K_R} \theta'_{n,ZOD} + \theta_{\text{LOS,ZOD}} + c_{\text{ZSD}} \alpha_m & , \text{ for LOS} \end{cases} \quad (66m)$$

Repeat Steps 6'-7' for each frequency of interest, reusing the delays and angles from Step 5' for all frequencies.

NOTE – The resulting delay and angular spreads of channels generated with this alternative method will be similar but not identical to when using Steps 5-7 in § 4.

5.5.2 Correlation model for shadow fading

The shadow fading term, which represents random variations about the distance-dependent mean path loss, has been observed to exhibit positive cross-correlation across different radio frequencies. This behaviour is intuitive as heavily (lightly) obstructed locations would be expected to experience above-(below-) average propagation loss for any radio frequency as long as the same fundamental propagation mechanisms are at work. This cross-correlation is modelled by the exponential function

$$R(\Delta F) = e^{-\frac{|\Delta F|}{\Delta F_{cor}}}$$

where ΔF denotes difference of log₁₀-frequency, and ΔF_{cor} is a frequency correlation parameter that depends on the environment.

TABLE A1-32

Shadow fading cross-correlation parameters for InH_x

Scenarios		InH_x	
		LOS	NLOS
Frequency cross-correlation parameter	ΔF_{cor}	N/A (uncorrelated)	5.1

5.6 Time-varying Doppler shift

The Doppler shift generally depends on the time evolution of the channel as it is defined as the derivative of the channels phase over time. It can be the result from Tx, Rx, or scatterer movement. The more general form of the exponential Doppler term as used in equation (27) is given by

$$\exp \left(j2\pi \int_{t_0}^t \frac{\hat{r}_{rx,n,m}^T(\tilde{t}) \cdot \vec{v}(\tilde{t})}{\lambda_0} d\tilde{t} \right). \quad (67)$$

Here, $\hat{r}_{rx,n,m}(t)$ is the normalized vector that points into the direction of the incoming wave as seen from the Rx at time t . $\vec{v}(t)$ denotes the velocity vector of the Rx at time t , while t_0 denotes a reference point in time that defines the initial phase, e.g. $t_0 = 0$.

Note that equation (27) only holds for time-invariant Doppler shift, i.e. $\hat{r}_{rx,n,m}^T(t) \cdot \vec{v}(t) = \hat{r}_{rx,n,m}^T \cdot \vec{v}$.

5.7 UT rotation

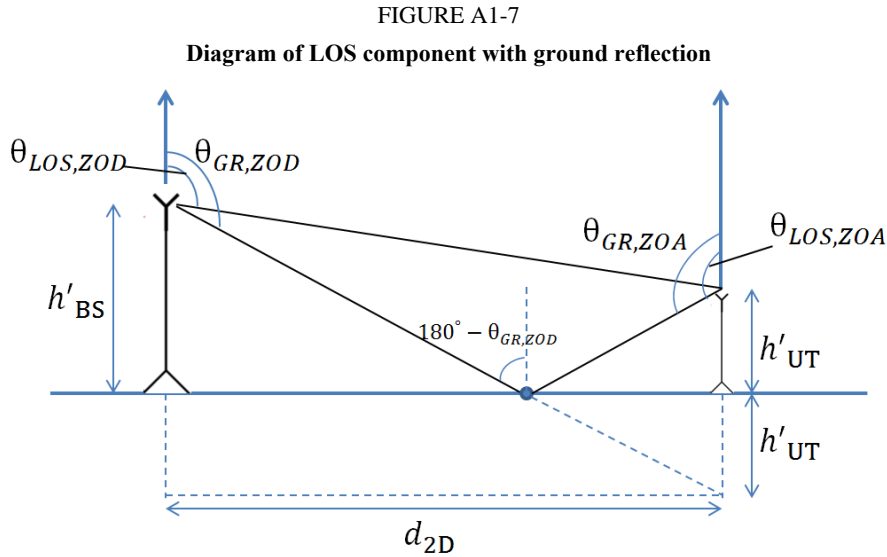
UT rotation modelling is an add-on feature. When modelled, Step 1 in § 4.4 shall consider UT rotational motion.

Step 1:

Add: h) Give rotational motion of UT in terms of its bearing angle, down tilt angle and slant angle.

5.8 Modelling of Ground Reflection⁸

Consider a base station (BS) and a user terminal (UT) with distance d_{2D} on the horizontal plane. The effective height of the BS is denoted by h'_{BS} and the effective height of the UT is denoted by h'_{UT} . The definition of effective height can be found in [5], where the effective height equals the actual height minus the effective environment height. Let c be the speed of light and λ_0 be the wavelength of the central carrier frequency. Figure A1-7 shows the diagram of the LOS component with ground reflection.



When ground reflection is considered, the randomly generated shadow fading is largely replaced by deterministic fluctuations in terms of distance. As a result, the standard deviation of shadow fading with ground reflection considered is set to 1 dB. The value of 1 dB was obtained via simulations in order to maintain a similar level of random channel fluctuations without ground reflection.

It can be observed from Fig. A1-7 that the ground reflection path has the same azimuth angle as the LOS path. However, the ground reflection path has different elevation angles, phase, and path gain. According to geometry, the ground reflection ZOD and ZOA can be computed as:

$$\theta_{GR,ZOA} = \theta_{GR,ZOD} = 180^\circ - \arctan\left(\frac{d_{2D}}{h'_{BS} + h'_{UT}}\right). \quad (68)$$

The phase Φ_{GR} and delay τ_{GR} of the ground reflection path can be computed as:

$$\Phi_{GR} = \frac{2\pi}{\lambda_0} \sqrt{(h'_{BS} + h'_{UT})^2 + d_{2D}^2}. \quad (69)$$

⁸ The additional feature of the ground reflection only can be implemented when the distance range before the breaking point of the LoS path loss model, to avoid the double-counting of the effects.

$$\tau_{GR} = \frac{d_{GR}}{c} = \frac{1}{c} \sqrt{(h'_{BS} + h'_{UT})^2 + d_{2D}^2}. \quad (70)$$

Then, the direction vector of the ground reflection component at the transmitter is expressed as:

$$\hat{r}_{tx,GR}^T = \begin{bmatrix} \sin \theta_{GR,ZOD} \cos \phi_{LOS,AOD} \\ \sin \theta_{GR,ZOD} \sin \phi_{LOS,AOD} \\ \cos \theta_{GR,ZOD} \end{bmatrix} \quad (71)$$

Also, the direction vector of the ground reflection component at the receiver is expressed as:

$$\hat{r}_{rx,GR}^T = \begin{bmatrix} \sin \theta_{GR,ZOA} \cos \phi_{LOS,AOA} \\ \sin \theta_{GR,ZOA} \sin \phi_{LOS,AOA} \\ \cos \theta_{GR,ZOA} \end{bmatrix} \quad (72)$$

The reflection coefficients $\rho_{\perp}(\theta_{GR,ZOD})$ and $\rho_{\parallel}(\theta_{GR,ZOD})$ for perpendicular and parallel polarizations can be computed as [8].

$$\rho_{\perp}(\theta_{GR,ZOD}) = \frac{\cos(180^\circ - \theta_{GR,ZOD}) - \sqrt{\varepsilon - \sin^2(180^\circ - \theta_{GR,ZOD})}}{\cos(180^\circ - \theta_{GR,ZOD}) + \sqrt{\varepsilon - \sin^2(180^\circ - \theta_{GR,ZOD})}} = \frac{\cos \theta_{GR,ZOD} + \sqrt{\varepsilon - \sin^2 \theta_{GR,ZOD}}}{\cos \theta_{GR,ZOD} - \sqrt{\varepsilon - \sin^2 \theta_{GR,ZOD}}} \quad (73)$$

$$\rho_{\parallel}(\theta_{GR,ZOD}) = \frac{\varepsilon \cos(180^\circ - \theta_{GR,ZOD}) - \sqrt{\varepsilon - \sin^2(180^\circ - \theta_{GR,ZOD})}}{\varepsilon \cos(180^\circ - \theta_{GR,ZOD}) + \sqrt{\varepsilon - \sin^2(180^\circ - \theta_{GR,ZOD})}} = \frac{\varepsilon \cos \theta_{GR,ZOD} + \sqrt{\varepsilon - \sin^2 \theta_{GR,ZOD}}}{\varepsilon \cos \theta_{GR,ZOD} - \sqrt{\varepsilon - \sin^2 \theta_{GR,ZOD}}} \quad (74)$$

where $\varepsilon = \varepsilon_r - j \frac{\sigma}{2\pi f_c \varepsilon_0}$ is the complex-valued relative permittivity of the ground, f_c is the carrier frequency, ε_0 is the permittivity of the vacuum, ε_r is the relative permittivity, and σ is the conductivity of the material. Frequency-dependent values of ε_r and σ for different materials can be found in [17].

After obtaining the elevation angles, phase, reflection coefficients, and path gain of the ground reflection path, the channel response of the ground reflection path can be presented as

$$H_{u,s}^{GR}(t) = \begin{bmatrix} F_{rx,u,\theta}(\theta_{GR,ZOA}, \phi_{LOS,AOA}) \\ F_{rx,u,\phi}(\theta_{GR,ZOA}, \phi_{LOS,AOA}) \end{bmatrix}^T \begin{bmatrix} \rho_{\parallel}(\theta_{GR,ZOD}) & 0 \\ 0 & -\rho_{\perp}(\theta_{GR,ZOD}) \end{bmatrix} \begin{bmatrix} F_{tx,s,\theta}(\theta_{GR,ZOD}, \phi_{LOS,AOD}) \\ F_{tx,s,\phi}(\theta_{GR,ZOD}, \phi_{LOS,AOD}) \end{bmatrix} \quad (75)$$

$$\cdot \exp(j\Phi_{GR}) \cdot \exp\left(\frac{j2\pi(\hat{r}_{rx,GR}^T \cdot \vec{d}_{rx,u})}{\lambda_0}\right) \cdot \exp\left(\frac{j2\pi(\hat{r}_{tx,GR}^T \cdot \vec{d}_{tx,s})}{\lambda_0}\right) \cdot \exp\left(j2\pi \frac{\hat{r}_{rx,GR}^T \cdot \vec{v}}{\lambda_0} t\right)$$

Then the channel impulse response with LOS and ground reflection can be expressed by

$$H_{u,s}^{LOS}(\tau, t) = \sqrt{\frac{1}{K_R + 1}} H_{u,s}^{NLOS}(\tau - \tau_{LOS}, t) + \sqrt{\frac{K_R}{K_R + 1}} \left(H_{u,s,1}^{LOS}(t) \delta(\tau - \tau_{LOS}) + \frac{d_{3D}}{d_{GR}} H_{u,s}^{GR}(t) \delta(\tau - \tau_{GR}) \right) \quad (76)$$

5.9 Random cluster number

Random Cluster Number is proposed to be a new advanced feature in § 2.2. The following modifications in Step 5 in § 4.3 can be optionally used to model this feature.

- 1 Random Cluster Number with Poisson distribution need to be determined before generating the cluster delays. The Poisson distribution is given as:

$$P(X = k) = \frac{\lambda^k}{k!} e^{-\lambda}, k = 0, 1, \dots$$

where λ is the Poisson distribution parameter. It indicates the mean value of the random cluster number. Based on some measurements reported in the literature, typical values for λ are in the range 3 to 10. Then the inverse transform sampling method is used to generate the random variable. The inverse transform sampling method is as follows:

- Generate a random number U according to the standard uniform distribution in the interval $[0,1]$.
- Find k such that $\sum_{k=0}^K P(X = k) \leq U < \sum_{k=0}^{K+1} P(X = k)$
- Take k to be the random number drawn according to the distribution described by $P(X=k)$.
- The cluster number generated need to be limited within the range of $[2, 20]$, i.e. the maximum cluster number is 20 and minimum cluster number is 2.

2 Once the cluster number is generated, the scaling factor corresponding to the total number of cluster in Step 7 need be updated as the following tables. Regarding LOS state, the corresponding formula in the Step 7 can be referred.

TABLE A1-33

Scaling factors for AOA, AOD generation (Wrapped Gaussian Distribution)

Number of Cluster	2	3	4	5	6	7	8	9	10	11
C_{ϕ}^{NLOS} Gaussian	0.471	0.664	0.777	0.882	0.945	1.007	1.031	1.062	1.110	1.129
Number of Cluster	12	13	14	15	16	17	18	19	20	
C_{ϕ}^{NLOS} Gaussian	1.155	1.172	1.195	1.234	1.241	1.262	1.267	1.282	1.300	

TABLE A1-34

Scaling factors for AOA, AOD generation (Laplacian Distribution)

Number of Cluster	2	3	4	5	6	7	8	9	10	11
C_{ϕ}^{NLOS} Laplacian	0.324	0.616	0.713	0.759	0.801	0.876	0.917	0.956	1.022	1.012
Number of Cluster	12	13	14	15	16	17	18	19	20	
C_{ϕ}^{NLOS} Gaussian	1.048	1.086	1.082	1.101	1.131	1.133	1.158	1.171	1.216	

TABLE A1-35
Scaling factors for ZOA, ZOD generation

Number of Cluster	2	3	4	5	6	7	8	9	10	11
C_{θ}^{NLOS} Gaussian	0.369	0.531	0.657	0.721	0.800	0.851	0.892	0.940	0.966	0.991
Number of Cluster	12	13	14	15	16	17	18	19	20	
C_{θ}^{NLOS} Gaussian	1.012	1.048	1.051	1.088	1.096	1.113	1.139	1.149	1.166	

6 Channel models for link-level evaluations

6.1 Clustered Delay Line (CDL) models

The CDL models are defined for the full frequency range from 0.5 GHz to 100 GHz with a maximum bandwidth of 2 GHz. CDL models can be implemented by e.g. coefficient generation Step 10 and Step 11 in § 4 or generating TDL model using spatial filter from § 6.4.

Three CDL models, namely CDL-i, CDL-ii and CDL-iii are constructed to represent three different channel profiles for NLOS while CDL-iv and CDL-v are constructed for LOS, the parameters of which can be found respectively in Tables A1-36, A1-37, A1-38, A1-39 and A1-40.

Each CDL model can be scaled in delay so that the model achieves a desired RMS delay spread, according to the procedure described in § 6.3. Each CDL model can also be scaled in angles so that the model achieves desired angle spreads, according to the procedure described in § 6.5.1.

For LOS channel models, the K-factor of CDL-iv and CDL-v can be set to a desired value following the procedure described in § 6.6.

For modelling effect of beamforming in a simplified way, a brick-wall window can be applied to a delay-scaled CDL model. The power shall be normalized after applying the window. A TDL model for simplified evaluations can be obtained from the CDL model, according to this method.

The following step by step procedure should be used to generate channel coefficients using the CDL models.

Step 1: Generate departure and arrival angles

Generate arrival angles of azimuth using the following equation:

$$\phi_{n,m,AOA} = \phi_{n,AOA} + c_{ASA} \alpha_m, \quad (77)$$

Where $\phi_{n,AOA}$ is the cluster AOA and c_{ASA} is the cluster-wise rms azimuth spread of arrival angles (cluster ASA) in Tables A1-36 to A1-40 below, and α_m is the ray offset angles within a cluster given by Table A1-12. If angular scaling according to § 6.5.1 is used, this is applied to the ray angles $\phi_{n,m,AOA}$. The generation of AOD ($\phi_{n,m,AOD}$), ZSA ($\theta_{n,m,ZOA}$), and ZSD ($\theta_{n,m,ZOD}$) follows a procedure similar to AOA as described above.

Step 2: Coupling of rays within a cluster for both azimuth and elevation:

Couple randomly AOD angles $\phi_{n,m,\text{AOD}}$ to AOA angles $\phi_{n,m,\text{AOA}}$ within a cluster n . Couple randomly ZOD angles $\theta_{n,m,\text{ZOD}}$ with ZOA angles $\theta_{n,m,\text{ZOA}}$ using the same procedure. Couple randomly AOD angles $\phi_{n,m,\text{AOD}}$ with ZOD angles $\theta_{n,m,\text{ZOD}}$ within a cluster n .

Step 3: Generate the cross polarization power ratios

Generate the cross polarization power ratios (XPR) κ for each ray m of each cluster n as:

$$\kappa_{n,m} = 10^{X/10} \quad (78)$$

where X is the per-cluster XPR in dB from Tables A1-36 to A1-40.

Step 4: Coefficient generation

Follow the same procedure as in Steps 10 and 11 in § 4, with the exception that all clusters are treated as “weaker cluster”, i.e. no further sub-clusters in delay should be generated. Additional clusters representing delay spread of the stronger clusters are already provided in Tables A1-36 to A1-40.

TABLE A1-36

CDL-i

Clusters						
Cluster	Normalized delay	Power	AOD	AOA	ZOD	ZOA
#		dB	°	°	°	°
1	0.0000	-13.4	-178.1	51.3	50.2	125.4
2	0.3819	0	-4.2	-152.7	93.2	91.3
3	0.4025	-2.2	-4.2	-152.7	93.2	91.3
4	0.5868	-4	-4.2	-152.7	93.2	91.3
5	0.4610	-6	90.2	76.6	122	94
6	0.5375	-8.2	90.2	76.6	122	94
7	0.6708	-9.9	90.2	76.6	122	94
8	0.5750	-10.5	121.5	-1.8	150.2	47.1
9	0.7618	-7.5	-81.7	-41.9	55.2	56
10	1.5375	-15.9	158.4	94.2	26.4	30.1
11	1.8978	-6.6	-83	51.9	126.4	58.8
12	2.2242	-16.7	134.8	-115.9	171.6	26
13	2.1718	-12.4	-153	26.6	151.4	49.2
14	2.4942	-15.2	-172	76.6	157.2	143.1
15	2.5119	-10.8	-129.9	-7	47.2	117.4
16	3.0582	-11.3	-136	-23	40.4	122.7
17	4.0810	-12.7	165.4	-47.2	43.3	123.2
18	4.4579	-16.2	148.4	110.4	161.8	32.6
19	4.5695	-18.3	132.7	144.5	10.8	27.2
20	4.7966	-18.9	-118.6	155.3	16.7	15.2
21	5.0066	-16.6	-154.1	102	171.7	146
22	5.3043	-19.9	126.5	-151.8	22.7	150.7
23	9.6586	-29.7	-56.2	55.2	144.9	156.1
Per-Cluster Parameters						
Parameter	C_{ASD}	C_{ASA}	C_{ZSD}	C_{ZSA}	XPR	
Unit	°	°	°	°	dB	
Value	5	11	3	3	10	

TABLE A1-37

CDL-ii

Clusters						
Cluster	Normalized delay	Power	AOD	AOA	ZOD	ZOA
#		dB	°	°	°	°
1	0.0000	0	9.3	-173.3	105.8	78.9
2	0.1072	-2.2	9.3	-173.3	105.8	78.9
3	0.2155	-4	9.3	-173.3	105.8	78.9
4	0.2095	-3.2	-34.1	125.5	115.3	63.3
5	0.2870	-9.8	-65.4	-88.0	119.3	59.9
6	0.2986	-1.2	-11.4	155.1	103.2	67.5
7	0.3752	-3.4	-11.4	155.1	103.2	67.5
8	0.5055	-5.2	-11.4	155.1	103.2	67.5
9	0.3681	-7.6	-67.2	-89.8	118.2	82.6
10	0.3697	-3	52.5	132.1	102.0	66.3
11	0.5700	-8.9	-72	-83.6	100.4	61.6
12	0.5283	-9	74.3	95.3	98.3	58.0
13	1.1021	-4.8	-52.2	103.7	103.4	78.2
14	1.2756	-5.7	-50.5	-87.8	102.5	82.0
15	1.5474	-7.5	61.4	-92.5	101.4	62.4
16	1.7842	-1.9	30.6	-139.1	103.0	78.0
17	2.0169	-7.6	-72.5	-90.6	100.0	60.9
18	2.8294	-12.2	-90.6	58.6	115.2	82.9
19	3.0219	-9.8	-77.6	-79.0	100.5	60.8
20	3.6187	-11.4	-82.6	65.8	119.6	57.3
21	4.1067	-14.9	-103.6	52.7	118.7	59.9
22	4.2790	-9.2	75.6	88.7	117.8	60.1
23	4.7834	-11.3	-77.6	-60.4	115.7	62.3
Per-Cluster Parameters						
Parameter	C_{ASD}	C_{ASA}	C_{ZSD}	C_{ZSA}	XPR	
Unit	°	°	°	°	dB	
Value	10	22	3	7	8	

TABLE A1-38

CDL-iii

Clusters						
Cluster	Normalized delay	Power	AOD	AOA	ZOD	ZOA
#		dB	°	°	°	°
1	0	-4.4	-46.6	-101	97.2	87.6
2	0.2099	-1.2	-22.8	120	98.6	72.1
3	0.2219	-3.5	-22.8	120	98.6	72.1
4	0.2329	-5.2	-22.8	120	98.6	72.1
5	0.2176	-2.5	-40.7	-127.5	100.6	70.1
6	0.6366	0	0.3	170.4	99.2	75.3
7	0.6448	-2.2	0.3	170.4	99.2	75.3
8	0.6560	-3.9	0.3	170.4	99.2	75.3
9	0.6584	-7.4	73.1	55.4	105.2	67.4
10	0.7935	-7.1	-64.5	66.5	95.3	63.8
11	0.8213	-10.7	80.2	-48.1	106.1	71.4
12	0.9336	-11.1	-97.1	46.9	93.5	60.5
13	1.2285	-5.1	-55.3	68.1	103.7	90.6
14	1.3083	-6.8	-64.3	-68.7	104.2	60.1
15	2.1704	-8.7	-78.5	81.5	93.0	61.0
16	2.7105	-13.2	102.7	30.7	104.2	100.7
17	4.2589	-13.9	99.2	-16.4	94.9	62.3
18	4.6003	-13.9	88.8	3.8	93.1	66.7
19	5.4902	-15.8	-101.9	-13.7	92.2	52.9
20	5.6077	-17.1	92.2	9.7	106.7	61.8
21	6.3065	-16	93.3	5.6	93.0	51.9
22	6.6374	-15.7	106.6	0.7	92.9	61.7
23	7.0427	-21.6	119.5	-21.9	105.2	58
24	8.6523	-22.8	-123.8	33.6	107.8	57
Per-Cluster Parameters						
Parameter	CASD	CASA	CZSD	CZSA	XPR	
Unit	°	°	°	°	dB	
Value	2	15	3	7	7	

TABLE A1-39

CDL-iv

Cluster	Cluster PAS	Normalized Delay	Power	AOD	AOA	ZOD	ZOA
#			dB	°	°	°	°
1	Specular(LOS path)	0	-0.2	0	-180	98.5	81.5
	Laplacian	0	-13.5	0	-180	98.5	81.5
2	Laplacian	0.035	-18.8	89.2	89.2	85.5	86.9
3	Laplacian	0.612	-21	89.2	89.2	85.5	86.9
4	Laplacian	1.363	-22.8	89.2	89.2	85.5	86.9
5	Laplacian	1.405	-17.9	13	163	97.5	79.4
6	Laplacian	1.804	-20.1	13	163	97.5	79.4
7	Laplacian	2.596	-21.9	13	163	97.5	79.4
8	Laplacian	1.775	-22.9	34.6	-137	98.5	78.2
9	Laplacian	4.042	-27.8	-64.5	74.5	88.4	73.6
10	Laplacian	7.937	-23.6	-32.9	127.7	91.3	78.3
11	Laplacian	9.424	-24.8	52.6	-119.6	103.8	87
12	Laplacian	9.708	-30.0	-132.1	-9.1	80.3	70.6
13	Laplacian	12.525	-27.7	77.2	-83.8	86.5	72.9
Per-Cluster Parameters							
Parameter		C_{ASD}	C_{ASA}	C_{ZSD}	C_{ZSA}	XPR	
Unit		°	°	°	°	dB	
Value		5	8	3	3	11	

TABLE A1-40

CDL-v

Cluster	Cluster	Normalized Delay	Power	AOD	AOA	ZOD	ZOA
#	PAS		dB	°	°	°	°
1	Specular (LOS path)	0.000	-0.03	0	-180	99.6	80.4
	Laplacian	0.000	-22.03	0	-180	99.6	80.4
2	Laplacian	0.5133	-15.8	57.5	18.2	104.2	80.4
3	Laplacian	0.5440	-18.1	57.5	18.2	104.2	80.4
4	Laplacian	0.5630	-19.8	57.5	18.2	104.2	80.4
5	Laplacian	0.5440	-22.9	-20.1	101.8	99.4	80.8
6	Laplacian	0.7112	-22.4	16.2	112.9	100.8	86.3
7	Laplacian	1.9092	-18.6	9.3	-155.5	98.8	82.7
8	Laplacian	1.9293	-20.8	9.3	-155.5	98.8	82.7
9	Laplacian	1.9589	-22.6	9.3	-155.5	98.8	82.7
10	Laplacian	2.6426	-22.3	19	-143.3	100.8	82.9
11	Laplacian	3.7136	-25.6	32.7	-94.7	96.4	88
12	Laplacian	5.4524	-20.2	0.5	147	98.9	81
13	Laplacian	12.0034	-29.8	55.9	-36.2	95.6	88.6
14	Laplacian	20.6419	-29.2	57.6	-26	104.6	78.3
Per-Cluster Parameters							
	Parameter	<i>C</i> _{ASD}	<i>C</i> _{ASA}	<i>C</i> _{ZSD}	<i>C</i> _{ZSA}	XPR	
	Unit	°	°	°	°	dB	
	Value	5	11	3	7	8	

6.2 Tapped Delay Line (TDL) models

The TDL models for simplified evaluations, e.g. for non-MIMO evaluations, are defined for the full frequency range from 0.5 GHz to 100 GHz with a maximum bandwidth of 2 GHz.

Three TDL models, namely TDL-i, TDL-ii and TDL-iii, are constructed to represent three different channel profiles for NLOS while TDL-iv and TDL-v are constructed for LOS, the parameters of which can be found respectively in Tables A1-41 and A1-42.

The Doppler spectrum for each tap is characterized by a classical (Jakes) spectrum shape and a maximum Doppler shift f_D where $f_D = |\bar{v}|/\lambda_0$. Due to the presence of a LOS path, the first tap in the LOS models (TDL-iv and TDL-v) follows a Ricean fading distribution. For those taps the Doppler spectrum additionally contains a peak at the Doppler shift $f_S = 0.7 f_D$ with an amplitude such that the resulting fading distribution has the specified K-factor.

Each TDL model can be scaled in delay so that the model achieves a desired RMS delay spread, according to the procedure described in § 6.3.

For LOS channel models, the K-factor of TDL-iv and TDL-v can be set to a desired value following the procedure described in § 6.6.

TABLE A1-41
NLOS models TDL-i, TDL-ii, and TDL-iii

Tap #	Fading distribution	TDL-i		TDL-ii		TDL-iii	
		Normalized delays	Power in [dB]	Normalized delays	Power in [dB]	Normalized delays	Power in [dB]
1	Rayleigh	0.0000	-13.4	0.0000	0	0.0000	-4.4
2	Rayleigh	0.3819	0	0.1072	-2.2	0.2099	-1.2
3	Rayleigh	0.4025	-2.2	0.2155	-4	0.2219	-3.5
4	Rayleigh	0.5868	-4	0.2095	-3.2	0.2329	-5.2
5	Rayleigh	0.4610	-6	0.2870	-9.8	0.2176	-2.5
6	Rayleigh	0.5375	-8.2	0.2986	-1.2	0.6366	0
7	Rayleigh	0.6708	-9.9	0.3752	-3.4	0.6448	-2.2
8	Rayleigh	0.5750	-10.5	0.5055	-5.2	0.6560	-3.9
9	Rayleigh	0.7618	-7.5	0.3681	-7.6	0.6584	-7.4
10	Rayleigh	1.5375	-15.9	0.3697	-3	0.7935	-7.1
11	Rayleigh	1.8978	-6.6	0.5700	-8.9	0.8213	-10.7
12	Rayleigh	2.2242	-16.7	0.5283	-9	0.9336	-11.1
13	Rayleigh	2.1718	-12.4	1.1021	-4.8	1.2285	-5.1
14	Rayleigh	2.4942	-15.2	1.2756	-5.7	1.3083	-6.8
15	Rayleigh	2.5119	-10.8	1.5474	-7.5	2.1704	-8.7
16	Rayleigh	3.0582	-11.3	1.7842	-1.9	2.7105	-13.2
17	Rayleigh	4.0810	-12.7	2.0169	-7.6	4.2589	-13.9
18	Rayleigh	4.4579	-16.2	2.8294	-12.2	4.6003	-13.9
19	Rayleigh	4.5695	-18.3	3.0219	-9.8	5.4902	-15.8
20	Rayleigh	4.7966	-18.9	3.6187	-11.4	5.6077	-17.1
21	Rayleigh	5.0066	-16.6	4.1067	-14.9	6.3065	-16
22	Rayleigh	5.3043	-19.9	4.2790	-9.2	6.6374	-15.7
23	Rayleigh	9.6586	-29.7	4.7834	-11.3	7.0427	-21.6
24	Rayleigh	N/A	N/A	N/A	N/A	8.6523	-22.8

TABLE A1-42
LOS models TDL-iv and TDL-v

Tap #	Fading distribution	TDL-iv		TDL-v	
		Normalized delay	Power in [dB]	Normalized delay	Power in [dB]
1	LOS path	0	-0.2	0	-0.03
	Rayleigh	0	-13.5	0	-22.03
2	Rayleigh	0.035	-18.8	0.5133	-15.8
3	Rayleigh	0.612	-21	0.5440	-18.1
4	Rayleigh	1.363	-22.8	0.5630	-19.8
5	Rayleigh	1.405	-17.9	0.5440	-22.9
6	Rayleigh	1.804	-20.1	0.7112	-22.4
7	Rayleigh	2.596	-21.9	1.9092	-18.6
8	Rayleigh	1.775	-22.9	1.9293	-20.8
9	Rayleigh	4.042	-27.8	1.9589	-22.6
10	Rayleigh	7.937	-23.6	2.6426	-22.3
11	Rayleigh	9.424	-24.8	3.7136	-25.6
12	Rayleigh	9.708	-30.0	5.4524	-20.2
13	Rayleigh	12.525	-27.7	12.0034	-29.8
14	Rayleigh			20.6519	-29.2
The first tap follows a Ricean distribution with a K-factor of K1 and a mean power of 0 dB		K1 = 13.3 dB		K1 = 22 dB	

6.3 Scaling of delays

The RMS delay spread values of both CDL and TDL models are normalized and they can be scaled in delay so that a desired RMS delay spread can be achieved. The scaled delays can be obtained according to the following equation:

$$\tau_{n,\text{scaled}} = \tau_{n,\text{model}} \cdot DS_{\text{desired}} \quad (79)$$

in which:

$\tau_{n,\text{model}}$ is the normalized delay value of the n th cluster in a CDL or a TDL model

$\tau_{n,\text{scaled}}$ is the new delay value (in [ns]) of the n th cluster

DS_{desired} is the wanted delay spread (in [ns]).

The example scaling parameters are selected according to Table A1-43 where the values have been chosen such that the RMS delay spreads span the range observed in measurements corresponding to the typical 5G evaluation scenarios. It can therefore be understood that a particular RMS delay spread in Table A1-43 may occur in any scenario; however certain values may be more likely in some scenarios than in others.

The example parameters given in Table A1-43 does not preclude the use of other scaling values if this is found appropriate, for instance if additional scenarios are introduced or if e.g. the effect of

beamforming needs to be captured in a TDL. Both of these examples can potentially result in an increased range of experienced RMS delay spreads.

TABLE A1-43

Example scaling parameters for CDL and TDL models.

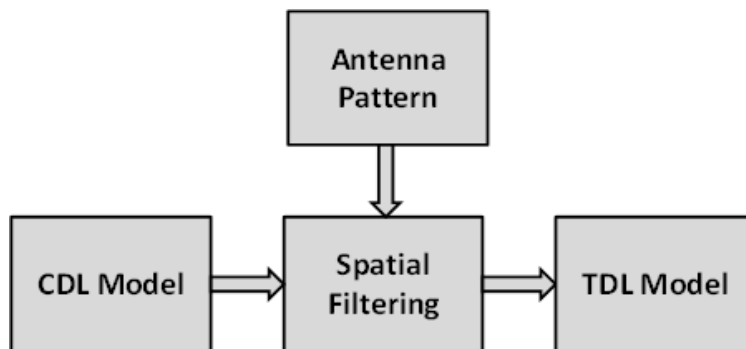
Model	DS_{desired}
Very short delay spread	10 ns
Short delay spread	30 ns
Nominal delay spread	100 ns
Long delay spread	300 ns
Very long delay spread	1 000 ns

6.4 Spatial filter for generating TDL channel model

The TDL models described in § 6.2 are generated from the CDL models assuming ideal isotropic antennas at both Tx and Rx. It is also possible to generate TDL models by assuming non-isotropic antennas like directive horn antennas or array antennas.

The basic idea to generate a TDL model based on a filtered CDL model is shown in Fig. A1-8 below.

FIGURE A1-8

The basic idea for filtering the CDL model to TDL model

6.4.1 Exemplary filters/antenna patterns

Note that any filter/pattern can be applied on a CDL to derive a TDL for evaluating directional algorithms.

Example 1: Isotropic pattern

$$A'_{f_{tx,rx}j}(\theta', \phi') = 1 \quad (80)$$

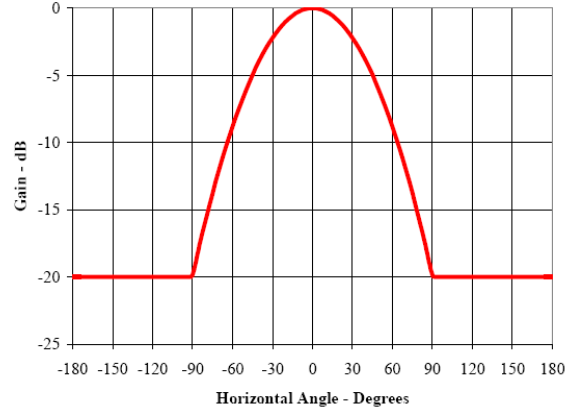
Example 2: Rectangular mask

$$A'_{f_{tx,rx}j}(\theta', \phi', BW) = \begin{cases} 1, & |\theta' - 90^\circ| \leq \frac{BW}{2} \ \& \ |\phi'| \leq \frac{BW}{2} \\ 0, & \text{otherwise.} \end{cases} \quad (81)$$

with BW denotes beamwidth.

Example 3: Simplified antenna pattern given in [5].

FIGURE A1-9
Simplified antenna pattern [5]



6.4.2 Generation procedure

1. The following steps are needed to generate tapped delay line (TDL) models: Choose a CDL model (e.g. CDL-i). Note that the models may be scaled according to § 6.5.1 prior to the filtering in order to represent different angular spreads.
2. Choose spatial filters A'_{tx} and A'_{rx} defined in LCS.
3. Transform the spatial filter into GCS to obtain A_{tx} and A_{rx} such that the pointing direction (θ_p, ϕ_p) is centered within the filter. The pointing direction may be defined:
 - a) by the dominant path $(\theta_p, \phi_p) = (\theta_i, \phi_i)$ with $i = \arg \max_n (P_n^{\text{CDL}})$, where P_n^{CDL} denotes the CDL cluster power values.
 - b) Or an arbitrary direction.
4. Calculate TDL cluster power values P_n^{TDL} given the following equation

$$P_n^{\text{TDL}} = P_n^{\text{CDL}} A_{rx}(\theta_{n,\text{ZOA}}, \phi_{n,\text{AOA}}) A_{tx}(\theta_{n,\text{ZOD}}, \phi_{n,\text{AOD}}) \quad (82)$$

6.5 Extension for MIMO simulations

Extended MIMO link-level channel models can be constructed according to two alternative methods described in the following subsections.

6.5.1 CDL extension: Scaling of angles

The angle values of CDL models are fixed, which is not very suitable for MIMO simulations for several reasons. The PMI statistics can become biased, and a fixed precoder may perform better than open-loop and on par with closed-loop or reciprocity beamforming. Furthermore, a CDL only represents a single channel realization. The predefined angle values in the CDL models can be generalized by introducing angular translation and scaling. By translation, mean angle can be changed to $\mu_{\phi,\text{desired}}$ and angular spread can be changed by scaling. The translated and scaled ray angles can be obtained according to the following equation:

$$\phi_{n,\text{scaled}} = \frac{AS_{\text{desired}}}{AS_{\text{model}}} (\phi_{n,\text{model}} - \mu_{\phi,\text{model}}) + \mu_{\phi,\text{desired}} \quad (83)$$

in which:

$\phi_{n,\text{model}}$ is the tabulated CDL ray angle

- AS_{model} is the rms angular spread of the tabulated CDL including the offset ray angles, calculated using the angular spread definition in § 6.5.3
- $\mu_{\phi,\text{model}}$ is the mean angle of the tabulated CDL
- $\mu_{\phi,\text{desired}}$ is the desired mean angle
- AS_{desired} is the desired rms angular spread
- $\phi_{n,\text{scaled}}$ is the resulting scaled ray angle.

The angular scaling is applied on the ray angles including offsets from the tabulated cluster angles. Typical angular spreads for different scenarios can be obtained from the system-level model.

Example scaling values are:

- AOD spread (ASD) for each CDL model: {5, 10, 15, 25} degrees.
- AOA spread (ASA) for each CDL model: {30, 45, 60} degrees.
- ZOA spread (ZSA) for each CDL model: {5, 10, 15} degrees.
- ZOD spread (ZSD) for each CDL model: {1, 3, 5} degrees.

The angular scaling and translation can be applied to some or all of the azimuth and zenith angles of departure and arrival.

NOTE – The azimuth angles may need to be wrapped around to be within [0, 360] degrees, while the zenith angles may need to be clipped to be within [0, 180] degrees.

6.5.2 TDL extension: Applying a correlation matrix

The TDLs and the spatial-filtered TDLs can be used with the correlation matrices for MIMO link-level simulations. Typical correlation parameters can be derived from 1) delay & angular scaled CDLs with antenna array assumptions, 2) system-level model with antenna array assumptions, or 3) by selecting extreme cases, e.g. uncorrelated, highly correlated etc. For example, these following options can be considered:

- 1) Zero correlation (IID channel coefficients) can be used for any number of antenna elements
- 2) The correlation matrix construction method from 3GPP TS36.101/104 [18][19] can be used for linear and planar (single- or dual-polarized) arrays.
 - Other correlation parameters α , β , γ than those specified in 3GPP TS36.101/104 [18][19] and extensions to larger antenna arrays can be considered. For typical scenarios, α and β will be in the range 0-1
 - A representative set of values is {0,0.7,0.9,0.99}.

NOTE – This approach can be applied to TDLs derived from spatially filtered CDLs to emulate hybrid BF system

NOTE – Other methodologies could also be developed, e.g.:

- extending the 3GPP TS36.101/104 [18][19] procedure to planar arrays or more elements;
- using CDLs in combination with array assumptions to derive per-tap correlation matrices as in [20];
- using the system-level model in combination with array assumptions to derive per-tap or per-channel correlation matrices.

6.5.3 Calculation of angular spread

Based on the circular standard deviation in directional statistics, the following expression for the angular spread AS in radians is proposed

$$AS = \sqrt{-2 \log \left(\frac{\sum_{n=1}^N \sum_{m=1}^M \exp(j\phi_{n,m}) P_{n,m}}{\sum_{n=1}^N \sum_{m=1}^M P_{n,m}} \right)} \quad (84)$$

where $P_{n,m}$ is the power for the m th subpath of the n th path and $\phi_{n,m}$ is the subpaths angle (either AOA, AOD, EOA, EOD) given in radians.

6.6 K-factor for LOS channel models

For the LOS channel models of CDL/TDL-iv and CDL/TDL-v, the K-factor values may be changed by the user. Mean and standard deviation of K-factor values can be found in Tables A1-16, A1-18, A1-20 and A1-22, although other values may also be used.

If the K-factor of a model shall be changed to K_{desired} [dB], the cluster powers for the Laplacian clusters (in case of CDL) or the tap powers for the Rayleigh fading taps (in case of TDL) are determined by

$$P_{n,\text{scaled}} = P_{n,\text{model}} - K_{\text{desired}} + K_{\text{model}}, \quad (85)$$

where $P_{n,\text{scaled}}$ and $P_{n,\text{model}}$ denote the scaled and the model path power (as given in the tables) of tap/cluster n . The model's K-factor K_{model} is defined as

$$K_{\text{model}} = P_{1,\text{model}}^{\text{LOS}} - 10 \log_{10} \left(\sum_{n=1}^N 10^{P_{n,\text{model}}/10} \right). \quad (86)$$

After scaling the powers, the delay spread needs to be re-normalized. This is done through the two steps below.

- 1) Calculate the actual RMS delay spread after the K-factor adjustment.
- 2) Divide the delays by that value to obtain $DS = 1$.

References

- [1] J. H. Zhang, C. Pan, F. Pei, G. Y. Liu, and X. Cheng, "Three-dimensional fading channel models: A survey of elevation angle research," *IEEE Communications Magazine*, vol. 52, no. 6, pp. 218-226, 2014.
- [2] X. Chen, L. Tian, P. Tang and J. H. Zhang, "Modelling of human body shadowing based on 28 GHz measurement results," in *Proc. 84th Veh. Tech. Conf (VTC2016-Fall)*, Montreal, Canada, Sep, 2016.
- [3] ICT-317669-METIS/D1.4: "METIS channel model, METIS 2020", Feb., 2015.
- [4] ITU-R Rec. P.676-8, "Attenuation by atmospheric gases," 2009. R2.
- [5] ITU-R, "Guidelines for evaluation of radio interface technologies for IMT-Advanced", Report ITU-R M.2135-1 (12/2009).
- [6] 3GPP TR 36.873, "Study on 3D channel model for LTE (Release 12)", Tech Report, 2014.
- [7] 3GPP TR 38.900, "Channel model for frequency spectrum above 6 GHz", Tech Report, June 2016.
- [8] 3GPP TR 38.901, "Study on channel model for frequencies from 0.5 to 100 GHz", V14.0.0.
- [9] J. H. Zhang, Y. X. Zhang, Y. W. Yu, R. J. Xu, Q. F. Zheng, and P. Zhang, "3D MIMO: How much does it meet our expectation observed from antenna channel measurements?", *IEEE Journal on Selected Areas in Communications*, vol. 35, no. 8, pp. 1887 – 1903, Aug. 2017.
- [10] J. H. Zhang, P. Tang, L. Tian, Z. X. Hu, T. Wang, and H. Wang, "6-100 GHz research progress and challenges from channel perspective for 5g and future communication," *SCIENCE CHINA Information Sciences*, vol. 60, no. 8, pp. 1 – 16, Aug. 2017.
- [11] Aalto University, BUPT, CMCC, Nokia, NTT DOCOMO, New York University, Ericsson, Qualcomm, Huawei, Samsung, Intel, University of Bristol, KT Corporation, University of Southern California, "5G channel model for bands up to 100 GHz", Tech. Rep. Oct. 2016, <http://www.5gworkshops.com/5GCM.html>.
- [12] K. Haneda, J.H. Zhang, L. Tian, G.Y. Liu, Y. Zheng, H. Asplund, and J. Li et. al. "5G 3GPP-like channel models for outdoor urban microcellular and macrocellular environments." In *Proc. IEEE 83rd Veh. Tech. Conf (VTC 2016-Spring)*, Nanjing, China, pp. 1-7. May. 2016.
- [13] P. Tang, J. H. Zhang, and L. Tian, "Analysis of the Millimeter Wave Channel Characteristics for Urban Micro-Cell Mobile Communication Scenario," 2017 IEEE 11th European Conference on Antennas and Propagation (EuCAP), Paris, Mar. 2017.
- [14] L. Tian, J.H. Zhang, Y. X. Zhang, and Y. Zheng, "Spatial characteristics of 3D MIMO wideband channel in indoor hotspot scenario at 3.5ghz," <http://www.zjhlab.net/publications/spatial-characteristics-of-3d-mimo-wideband-channel-in-indoor-hotspot-scenario-at-3-5-ghz/>.
- [15] IST-WINNER II Deliverable 1.1.2 v.1.2., "WINNER II channel models, IST-WINNER2, Tech. Rep., 2008.
- [16] H2020-ICT-671650-mmMAGIC D2.2, "Measurement results and final mmMAGIC channel models", Tech. Rep., 2017.
- [17] ITU-R P.527-3, "Electrical characteristics of the surface of the earth," Tech. Report, 1992.
- [18] 3GPP TR36.101: "User Equipment (UE) radio transmission and reception", V14.3.0, Mar. 2017.
- [19] 3GPP TR36.104: "Base Station (BS) radio transmission and reception", Tech. Report, V14.3.0, Mar. 2017.
- [20] H. Asplund, J. Medbo, B. Göransson, J. Karlsson and J. Sköld, "A Simplified Approach to Applying the 3GPP Spatial Channel Model," 2006 IEEE 17th International Symposium on Personal, Indoor and Mobile Radio Communications, Helsinki, 2006, pp. 1-5.
- [21] ITU-R P.1238-8 (07/2015), "Propagation data and prediction methods for the planning of indoor radiocommunication systems and radio local area networks in the frequency range 300 MHz to 100 GHz"

- [22] T. Kurner, D. J. Cichon, and W. Wiesbeck, "Concepts and results for 3D digital terrain-based wave propagation models: An overview", *IEEE J. Select. Areas Commun.*, vol. 11, pp. 1002–1012, 1993.
- [23] M. Born and E. Wolf, "Principles of optics: electromagnetic theory of propagation, interference and diffraction of light", CUP Archive, 2000.
- [24] ITU-R P.525-3, "Calculation of free-space attenuation", Sept. 2016.
- [25] ITU-R P.526-12, "Propagation by diffraction", Feb. 2012.
- [26] J. W. Dou, L. Tian, and N. Zhang, *et al.*, "45GHz propagation channel modeling for an indoor conference scenario", in *Proc. of IEEE 26th Annual International Symposium on Personal, Indoor, and Mobile Radio Communications (PIMRC)*, 2015.
- [27] Recommendation ITU-R P.1816-3 "The prediction of the time and the spatial profile for broadband land mobile services using UHF and SHF bands", July 2015.

Attachment 1 to Annex 1

Map-based hybrid channel model (alternative channel model methodology)

The alternative module is an optional module.

1 Coordinate system

The same coordinate system as defined in Annex 1 § 4 is applied.

2 Scenarios

The same scenarios as in Annex 1 § 1 can be applied.

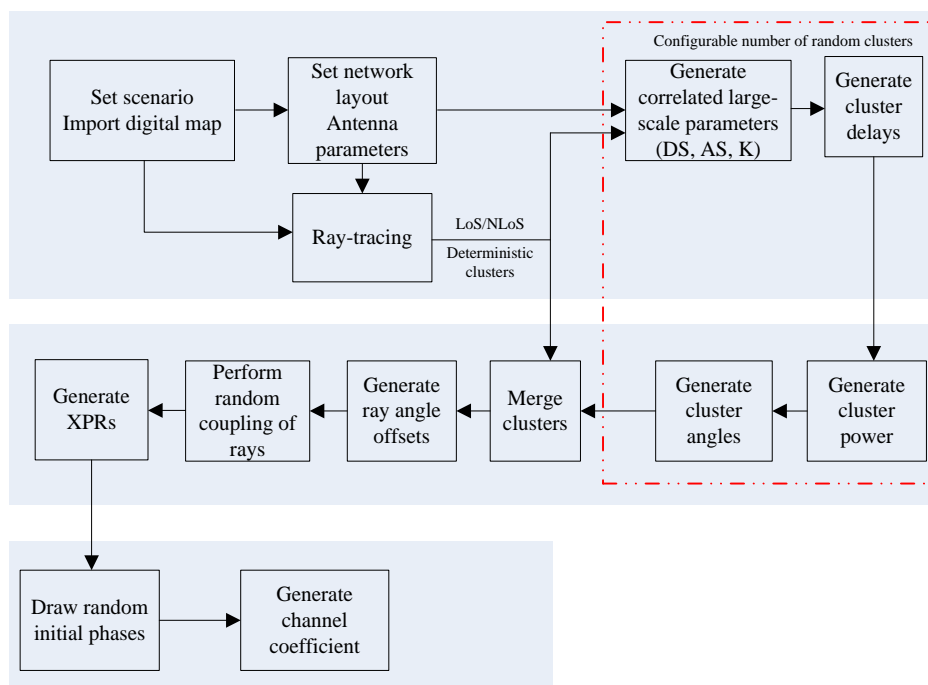
3 Antenna modelling

The same antenna modelling as defined in § 8.5 in main body text can be applied.

4 Channel generation

The radio channels are created using the deterministic ray-tracing upon a digitized map and emulating certain stochastic components according to the statistic parameters listed in Tables A1-16 to A1-23¹. The channel realizations are obtained by a step-wise procedure illustrated in Fig. A1-10 and described below. In the following steps, downlink is assumed. For uplink, arrival and departure parameters have to be swapped.

FIGURE A1-10
Channel coefficient generation procedure



Step-wise procedure

Step 1: Set environment and import digitized map accordingly

¹ Not all parameters listed in these Tables are used in Map-based hybrid channel model.

- a) Choose scenario. Choose a global coordinate system and define zenith angle θ , azimuth angle ϕ , and spherical basis vectors $\hat{\theta}$, $\hat{\phi}$ as shown in Fig. A1-3.
- b) Import digitized map according to the chosen scenario. The digitized map should at least contain the following information:
 - The 3D geometric information for each of major structures involving with buildings or rooms. The external building walls and internal room walls are represented by surfaces and identified by the coordinates of the vertices on each wall.
 - The material and thickness of each wall as well as the corresponding electromagnetic properties including permittivity and conductivity.
 - Random small objects in certain scenarios (e.g. UMi outdoor)

The format of digitized map, including additional information besides above-mentioned, is per implementation wise and out of scope of this description.

Step 2: Set network layout, and antenna array parameters

- a) Give number of BS and UT.
- b) Give 3D locations of BS and UT, and calculate LOS AOD ($\phi_{LOS,AOD}$), LOS ZOD ($\theta_{LOS,ZOD}$), LOS AOA ($\phi_{LOS,AOA}$), LOS ZOA ($\theta_{LOS,ZOA}$) of each BS and UT in the global coordinate system
- c) Give BS and UT antenna field patterns F_{rx} and F_{tx} in the global coordinate system and array geometries
- d) Give BS and UT array orientations with respect to the global coordinate system. BS array orientation is defined by three angles $\Omega_{BS,\alpha}$ (BS bearing angle), $\Omega_{BS,\beta}$ (BS downtilt angle) and $\Omega_{BS,\gamma}$ (BS slant angle). UT array orientation is defined by three angles $\Omega_{UT,\alpha}$ (UT bearing angle), $\Omega_{UT,\beta}$ (UT downtilt angle) and $\Omega_{UT,\gamma}$ (UT slant angle). Give rotational motion of UT in terms of its bearing angle, downtilt angle and slant angle if UT rotation is modelled.
- e) Give speed and direction of motion of UT in the global coordinate system for virtual motion.
- f) Give system centre frequency/frequencies and bandwidth(s) for each of BS-UT links.

If the bandwidth (denoted as B) is greater than c/D Hz, where c is the speed of light and D is the maximum antenna aperture in either azimuth or elevation, the whole bandwidth is split into K_B

equal-sized frequency bins, where $K_B \geq \left\lceil \frac{B}{c/D} \right\rceil$ is a per-implementation parameter taking into account

the channel constancy as well as other potential evaluation needs, and the bandwidth of each

frequency bin is $\Delta B = \frac{B}{K_B}$. Within k -th frequency bin, the channel power attenuation, phase rotation,

Doppler shift are assumed constant, whose corresponding values are calculated based on the centre

frequency of k -th frequency bin $f_k = f_c - \frac{K_B - 2k + 1}{2} \Delta B$ for $1 \leq k \leq K_B$, where f_c is the centre

frequency of the corresponding BS-UT link.

Step 3: Apply ray-tracing to each pair of link ends (i.e. end-to-end propagation between pair of Tx/Rx arrays).

- a) Perform geometric calculations in ray-tracing to identify propagation interaction types, including LOS, reflections, diffractions, penetrations and scattering (in case the digitized map contains random small objects), for each propagation path. In general, some maximum orders of different interaction types can be set.

The theoretical principles and procedures of geometric tracing calculations can be found in [3], [21]-[23], and [25]. This description does not intend to mandate new concepts and/or procedures to the conventional ray-tracing algorithms; on the other hand, the implementation-based variations aiming to reduce computation complexity are allowed within limits of acceptable calibration tolerances.

The same geometric calculation is shared among all K_B frequency bins.

- b) Perform electric field calculations over propagation path, based on identified propagation interaction types (LOS, reflection, diffraction, penetration and scattering) and centre frequencies of frequency bins.

The details of electric field calculation can be found in [3], [15], and [21]-[26].

The modelling algorithms in geometry and electric field calculations for different propagation interactions are summarized in Table A1-44 below.

TABLE A1-44

Principles applied in ray-tracing

	Geometry calculation	Electric field calculation
LOS	Free space LOS	Friis equation [24]
Reflection	Snell's law with image-based method [21]	Fresnel equation [21]
Diffraction	Fermat's principle [25]	UTD [25]
Penetration	Snell's law for transmission through slab [21]	Fresnel equation [21]
Scattering (upon small objects)	Omni-directional scattering [3]	RCS-based scattering coefficient [3]

NOTE – For reasons of simplicity and simulation speed, the maximum order of reflection on a path without diffraction is configurable from {1,2,3}; the maximum order of diffraction on a path without reflection is configurable from {1,2}; the path containing both reflection and diffraction has 1-order reflection and 1-order diffraction, besides any potential penetrations; and the maximum order of penetration on a path is configurable, with the recommended value equal to 5.

The outputs from Step 3 should at least contain following for each pair of link ends:

- the LOS/NLOS flag to indicate whether a LOS propagation mechanism exists;
- the number of deterministic propagation paths L_{RT} (also referred as deterministic clusters in Step 8. To avoid the unnecessary computation complexity, these L_{RT} deterministic paths only include those paths whose powers are higher than 25dB below the maximum deterministic path power, where the path power is denoted as $P_{l_{RT}}^{RT,real}$ and defined below);
- for each deterministic path (l_{RT} -th path sorted in ascending order of path delay):
- the flag indicating whether the deterministic path is generated with scattering upon random small objects;
- the normalized path delay $\tau_{l_{RT}}^{RT} = \tau_{l_{RT}}' - \min_{l_{RT}}(\tau_{l_{RT}}')$ and the first arrival absolute delay $\min_{l_{RT}}(\tau_n')$ (with $\tau_{l_{RT}}'$ to be the real absolute propagation delay of the path);
- angles of arrival and departure $[\phi_{l_{RT},AOA}^{RT}, \theta_{l_{RT},ZOA}^{RT}, \phi_{l_{RT},AOD}^{RT}, \theta_{l_{RT},ZOD}^{RT}]$;

- the power $P_{l_{RT},k}^{RT,real}$ for k-th frequency bin, and the path power $P_{l_{RT}}^{RT,real} = \frac{1}{K_B} \sum_{k=1}^{K_B} P_{l_{RT},k}^{RT,real}$;
- the XPR $\kappa_{l_{RT}}^{RT}$ of the path, where $\kappa_{l_{RT}}^{RT} = \frac{1}{K_B} \sum_{k=1}^{K_B} \kappa_{l_{RT},k}^{RT}$ with $\kappa_{l_{RT},k}^{RT}$ being the XPR for k-th frequency bin.
- to support for true motion, i.e. the case when a trajectory is specified for UT, a path ID is associated for each deterministic path. The same ID is associated for a path across a number of UT locations as far as 1) it has same interaction types in the same order and 2) its interactions occur in same walls or other surfaces.

The L_{RT} deterministic paths are sorted by normalized path delay ($\tau_{l_{RT}}^{RT}$) in ascending order. That is to say, $\tau_1^{RT} = 0$.

If $L_{RT}=0$ for a pair of link ends, the channel gain for this pair of link ends is assumed to be zero and the remaining steps are skipped with none of random cluster.

Step 4: Generate large scale parameters e.g. delay spread, angular spreads and Ricean K factor for random clusters.

The generation of large scale parameters takes into account cross correlation according to Tables A1-16, A1-18, A1-20 and A1-22 and uses the procedure described in § 3.3.1 of WINNER II Channel Models[15] with the square root matrix $\sqrt{C_{M \times M}}(0)$ being generated using the Cholesky decomposition and the following order of the large scale parameter vector: $sM = [sK, sDS, sASD, sASA, sZSD, sZSA]^T$. Limit random RMS azimuth arrival and azimuth departure spread values to 104 degrees, i.e. $ASA = \min(ASA, 104^\circ)$, $ASD = \min(ASD, 104^\circ)$. Limit random RMS zenith arrival and zenith departure spread values to 52 degrees, i.e. $ZSA = \min(ZSA, 52^\circ)$, $ZSD = \min(ZSD, 52^\circ)$. For the parameters selection from Tables A1-16, A1-18, A1-20 and A1-22, the LOS/NLOS condition determined in Step 3 is applied. For the parameters selection from Tables A1-16, A1-18, A1-20 and A1-22, the LOS/NLOS condition determined in Step 3 is applied.

Step 5: Generate delays (denoted as $\{\tau^{RC}\}$) for random clusters

Delays are drawn randomly according to the exponential delay distribution

$$\tau_n' = -\mu_\tau^{RC} \ln(X_n) \quad (87)$$

where $\mu_\tau^{RC} = \max\left\{\mu_\tau, \frac{1}{L_{RT}} \sum_{l_{RT}=1}^{L_{RT}} \tau_{l_{RT}}^{RT}\right\}$, $X_n \sim \text{unif}(0,1)$, and cluster index $n = 0, \dots, L'_{RC}$ with L'_{RC} to be

configurable. A recommended value for L'_{RC} is the number of clusters given in Tables A1-16, A1-18, A1-20 and A1-22.

$\mu_\tau = r_\tau DS + \frac{L_{RT}}{L'_{RC} + 1} \left(r_\tau DS - \frac{1}{L_{RT}} \sum_{l_{RT}=1}^{L_{RT}} \tau_{l_{RT}}^{RT} \right)$, where r_τ is the delay distribution proportionality factor

given in Tables A1-16, A1-18, A1-20 and A1-22.

Normalise the delays by subtracting the minimum delay and sort the normalised delays to ascending order:

$$\tau_n = \text{sort}\left(\tau_n' - \min(\tau_n')\right) / C_\tau \quad (88)$$

where C_τ is the additional scaling of delays to compensate for the effect of LOS peak addition to the delay spread, and is depending on the heuristically determined Ricean K-factor [dB] as generated in Step 4:

$$C_\tau = \begin{cases} 0.7705 - 0.0433K + 0.0002K^2 + 0.000017K^3 & \text{LOS condition} \\ 1 & \text{NLOS condition} \end{cases} \quad (89)$$

For the delay used in cluster power generation in Step 6, the scaling factor C_τ is always 1.

The n -th random cluster is removed if $n=0$ or $|\tau_n - \tau_{l_{RT}}^{RT}| < \tau_{th}$ for any of $1 \leq l_{RT} \leq L_{RT}$, where τ_{th} is given by $\tau_{th} = \mu_\tau^{RC} \cdot \ln\left(\frac{1}{1-p_0}\right)$, and p_0 is the configurable probability for cluster inter-arrival interval to be less than τ_{th} . For example, set $p_0=0.2$ to obtain $\tau_{th}=0.223 \mu_\tau^{RC}$.

Denote τ_n^{RC} for $1 \leq n \leq L_{RC}$ as the delays of the L_{RC} random clusters that remain after the cluster removal.

Step 6: Generate powers (denoted as $P_i^{RC,real}$ for $1 \leq i \leq L_{RC}$) for random clusters.

Cluster powers for the random clusters are calculated assuming a single slope exponential power delay profile. First, the virtual powers (denoted as $P_i^{RC,virtual}$ for $1 \leq i \leq L_{RC}$) of random clusters and virtual powers (denoted as $P_j^{RT,virtual}$ for $1 \leq j \leq L_{RT}$) of deterministic clusters are calculated as following.

Denote:

$$V_i^{RC} = \exp\left(-\tau_i^{RC} \frac{r_\tau - 1}{r_\tau DS}\right) \cdot 10^{\frac{-Z_{i,RC}}{10}} \quad (90)$$

$$V_j^{RT} = \exp\left(-\tau_j^{RT} \frac{r_\tau - 1}{r_\tau DS}\right) \cdot 10^{\frac{-Z_{j,RT}}{10}} \quad (91)$$

where $Z_{i,RC}$ and $Z_{j,RT}$ are the per cluster shadowing terms in [dB] and meet distribution of $N(0, \zeta^2)$. Then,

$$P_i^{RC,virtual} = \frac{1}{A+1} \cdot \frac{V_i^{RC}}{\sum_{i=1}^{L_{RC}} V_i^{RC} + \sum_{j=1}^{L_{RT}} V_j^{RT}} \quad (92)$$

$$P_j^{RT,virtual} = \frac{1}{A+1} \cdot \frac{V_j^{RT}}{\sum_{i=1}^{L_{RC}} V_i^{RC} + \sum_{j=1}^{L_{RT}} V_j^{RT}} + \frac{A}{A+1} \cdot \delta(j-1) \quad (93)$$

In the case of LOS condition, $A=K_R$ with K_R being the Ricean K-factor obtained in Step 4 and converted to linear scale; otherwise, $A=0$. The real power (including effects of pathloss) per random cluster in k -th frequency bin is given by

$$P_{i,k}^{RC,real} = \frac{\sum_{j=1}^{L_{RT}} P_{j,k}^{RT,real}}{\sum_{j=1}^{L_{RT}} P_j^{RT,virtual}} \cdot P_i^{RC,virtual} \quad (94)$$

for $1 \leq i \leq L_{RC}$ and $1 \leq k \leq K_B$. Similar to path power of deterministic cluster, the path power of i -th random cluster is calculated as:

$$P_i^{RC,real} = \frac{1}{K_B} \sum_{k=1}^{K_B} P_{i,k}^{RC,real} \quad (95)$$

Step 7: Generate arrival angles and departure angles for both azimuth and elevation, for each random cluster.

For azimuth angles of the n -th random cluster:

The composite PAS in azimuth of all random clusters is modelled as wrapped Gaussian (see Tables A1-16, A1-18, A1-20 and A1-22). The AOA's are determined by applying the inverse Gaussian function with input parameters $P_n^{RC,real}$ and RMS angle spread ASA

$$\phi'_{n,AOA} = \frac{2(ASA/1.4) \sqrt{-\ln \left(P_n^{RC,real} / \max_{i,j} (P_i^{RC,real}, P_j^{RT,real}) \right)}}{C_\phi} \quad (96)$$

with constant C_ϕ defined as

$$C_\phi = \begin{cases} C_\phi^{NLOS} \cdot (1.1035 - 0.028K - 0.002K^2 + 0.0001K^3) & , \text{for LOS} \\ C_\phi^{NLOS} & , \text{for NLOS} \end{cases} \quad (97)$$

where C_ϕ^{NLOS} is defined as a scaling factor related to the total number of clusters and is given in Table A1-11.

In the LOS case, constant C_ϕ also depends on the Ricean K-factor K in [dB], as generated in Step 4. Additional scaling of the angles is required to compensate for the effect of LOS peak addition to the angle spread.

Assign positive or negative sign to the angles by multiplying with a random variable X_n with uniform distribution to the discrete set of $\{1, -1\}$, and add component $Y_n \sim N\left(0, (ASA/7)^2\right)$ to introduce random variation:

$$\phi_{n,AOA} = X_n \phi'_{n,AOA} + Y_n + \phi_{center,AOA} \quad (98)$$

where $\phi_{center,AOA}$ is calculated as

$$\phi_{center,AOA} = \arg \left(\sum_{l=1}^{L_{RT}} P_l^{RT,real} \cdot \exp(j\phi_{l,AOA}^{RT}) \right) \quad (99)$$

Note that $\phi_{l,AOA}^{RT}$ shall be given in radians here.

The generation of AOD ($\phi_{n,AOD}$) follows a procedure similar to AOA as described above.

For zenith angles of the n-th random cluster:

The generation of ZOA assumes that the composite PAS in the zenith dimension of all random clusters is Laplacian (see Tables A1-16, A1-18, A1-20 and A1-22). The ZOAs are determined by applying the inverse Laplacian function with input parameters $P_n^{RC,real}$ and RMS angle spread ZSA:

$$\theta'_{n,ZOA} = -\frac{ZSA \ln\left(P_n^{RC,real} / \max_{i,j} (P_i^{RC,real}, P_j^{RT,real})\right)}{C_\theta} \quad (100)$$

with C_θ defined as:

$$C_\theta = \begin{cases} C_\theta^{NLOS} \cdot (1.3086 + 0.0339K - 0.0077K^2 + 0.0002K^3) & , \text{ for LOS} \\ C_\theta^{NLOS} & , \text{ for NLOS} \end{cases} \quad (101)$$

where C_θ^{NLOS} is a scaling factor related to the total number of clusters and is given in Tables A1-13 and A1-14.

In the LOS case, constant C_θ also depends on the Ricean K-factor K in [dB], as generated in Step 4. Additional scaling of the angles is required to compensate for the effect of LOS peak addition to the angle spread.

Assign positive or negative sign to the angles by multiplying with a random variable X_n with uniform distribution to the discrete set of $\{1,-1\}$, and add component $Y_n \sim N\left(0, (ZSA/7)^2\right)$ to introduce random variation

$$\theta_{n,ZOA} = X_n \theta'_{n,ZOA} + Y_n + \bar{\theta}_{ZOA} \quad (102)$$

where $\bar{\theta}_{ZOA} = 90^\circ$ if the UT is located indoors and $\bar{\theta}_{ZOA} = \theta_{center,ZOA}$ if the UT is located outdoors, where $\theta_{center,ZOA}$ is calculated as

$$\theta_{center,ZOA} = \arg\left(\sum_{l=1}^{L_{RT}} P_l^{RT,real} \cdot \exp(j\theta_{l,ZOA}^{RT})\right) \quad (103)$$

Note that $\theta_{l,ZOA}^{RT}$ shall be given in radians here.

The generation of ZOD follows the same procedure as ZOA described above except equation (102) is replaced by:

$$\theta_{n,ZOD} = X_n \theta'_{n,ZOD} + Y_n + \theta_{center,ZOD} + \mu_{offset,ZOD} \quad (104)$$

where variable X_n is with uniform distribution to the discrete set of $\{1,-1\}$, $Y_n \sim N\left(0, (ZSD/7)^2\right)$, $\mu_{offset,ZOD}$ is given in Tables A1-17, A1-19, A1-21 and A1-23.

Step 8: Merge deterministic clusters and random clusters.

First, remove any deterministic or random cluster with less than -25 dB power compared to $\max\{P_j^{RT,real}, P_i^{RC,real}\}$ for all $1 \leq j \leq L_{RT}$ and $1 \leq i \leq L_{RC}$. Then, simply put the remaining deterministic

clusters and random clusters into single set of clusters, and meanwhile maintain an attribute for each cluster to indicate whether the cluster is a deterministic cluster or a random cluster.

Step 9: Generate ray delays and ray angle offsets inside each cluster, where the cluster can be either random or deterministic.

Denote M as the number of rays per cluster, where $M=1$ if the cluster corresponds to $n=1$ in the LOS case, otherwise the value of M is given in Tables A1-16, A1-18, A1-20 and A1-22.

When $K_B = 1$:

The relative delay of m -th ray within n -th cluster is given by $\tau'_{n,m} = 0$ for $m = 1, \dots, M$.

The azimuth angle of arrival (AOA) for the m -th ray in n -th cluster is given by:

$$\phi_{n,m,AOA} = \phi_{n,AOA} + c_{ASA} \alpha_m \quad (105)$$

where c_{ASA} is the cluster-wise rms azimuth spread of arrival angles (cluster ASA) in Tables A1-16, A1-18, A1-20 and A1-22, and offset angle α_m is given in Table A1-12. $\phi_{n,AOA}$ equals to the AOA angle output from Step 3 if n -th cluster is deterministic cluster, and equals to the AOA angle equation (A1-12) in Step 7 if n -th cluster is random cluster.

The generation of AOD ($\phi_{n,m,AOD}$) follows a procedure similar to AOA as described above.

The zenith angle of arrival (ZOA) for the m -th ray in n -th cluster is given by:

$$\theta_{n,m,ZOA} = \theta_{n,ZOA} + c_{ZSA} \alpha_m \quad (106)$$

where c_{ZSA} is the cluster-wise rms spread of ZOA (cluster ZOA) in Tables A1-16, A1-18, A1-20 and A1-22, and offset angle α_m is given in Table A1-12. Assuming that $\theta_{n,m,ZOA}$ is wrapped within $[0, 360^\circ]$, if $\theta_{n,m,ZOA} \in [180^\circ, 360^\circ]$, then $\theta_{n,m,ZOA}$ is set to $(360^\circ - \theta_{n,m,ZOA})$. $\theta_{n,ZOA}$ equals to the ZOA angle output from Step 3 if n -th cluster is deterministic cluster, and equals to the ZOA angle equation (102) in Step 7 if n -th cluster is random cluster.

The zenith angle of departure (ZOD) for the m -th ray in n -th cluster is given by:

$$\theta_{n,m,ZOD} = \theta_{n,ZOD} + (3/8)(10^{\mu_{\text{lgZSD}}}) \alpha_m \quad (107)$$

where μ_{lgZSD} is the mean of the ZSD log-normal distribution. $\theta_{n,ZOD}$ equals to the ZOD angle output from Step 3 if n -th cluster is deterministic cluster, and equals to the ZOD angle equation (A1-18) in Step 7 if n -th cluster is random cluster.

When $K_B > 1$:

The relative delay of m -th ray within n -th cluster is given by $\tau'_{n,m} = \text{sort} \left(\tau''_{n,m} - \min_{1 \leq m \leq M} \{ \tau''_{n,m} \} \right)$ that are sorted in ascending order, where $\tau''_{n,m} \sim \text{unif}(0, 2c_{DS})$ with the cluster delay spread that is given in Tables A1-16, A1-18, A1-20 and A1-22, $\text{unif}(a, b)$ denotes the continuous uniform distribution on the interval $[a, b]$. Note that $\tau''_{n,m}$ shall be independently generated.

The azimuth angles (AOA and AOD) and zenith angles (ZOA and ZOD) for the m -th ray in n -th cluster in each frequency bin is given by:

$$\begin{aligned}
 \phi_{n,m,AOA} &= \phi_{n,AOA} + \phi'_{n,m,AOA} \\
 \phi_{n,m,AOD} &= \phi_{n,AOD} + \phi'_{n,m,AOD} \\
 \theta_{n,m,ZOA} &= \theta_{n,ZOA} + \theta'_{n,m,ZOA} \\
 \theta_{n,m,ZOD} &= \theta_{n,ZOD} + \theta'_{n,m,ZOD}
 \end{aligned} \tag{108}$$

for $m = 1, \dots, M$, where $\phi_{n,\{AOA|AOD\}}$ and $\theta_{n,\{ZOA|ZOD\}}$ equal to the {AOA,AOD} and {ZOA, ZOD} angle outputs from Step 3 if n -th cluster is deterministic cluster, and equal to the {AOA,AOD} and {ZOA, ZOD} angle in Step 7 if n -th cluster is random cluster; and

$$\begin{aligned}
 \phi'_{n,m,AOA} &\sim 2c_{ASA} \text{unif}(-1,1) \\
 \phi'_{n,m,AOD} &\sim 2c_{ASD} \text{unif}(-1,1) \\
 \theta'_{n,m,ZOA} &\sim 2c_{ZSA} \text{unif}(-1,1) \\
 \theta'_{n,m,ZOD} &\sim 2c_{ZSD} \text{unif}(-1,1)
 \end{aligned} \tag{109}$$

with the respective cluster angular spreads as given in Tables A1-16 to A1-23.

Assuming that $\theta_{n,m,ZOA}$ is wrapped within $[0, 360^0]$, if $\theta_{n,m,ZOA} \in [180^0, 360^0]$, then $\theta_{n,m,ZOA}$ is set to $(360^0 - \theta_{n,m,ZOA})$.

Step 10: Generate power of rays in each cluster, where coupling of rays within a cluster for both azimuth and elevation could be needed.

Given $P_{n,k}$ as the real power in k -th frequency bin for the n -th cluster (either deterministic or random) obtained from Step 8,

When $K_B = 1$:

Couple randomly AOD angles $\phi_{n,m,AOD}$ to AOA angles $\phi_{n,m,AOA}$ within a cluster n . Couple randomly ZOD angles $\theta_{n,m,ZOD}$ with ZOA angles $\theta_{n,m,ZOA}$ using the same procedure. Couple randomly AOD angles $\phi_{n,m,AOD}$ with ZOD angles $\theta_{n,m,ZOD}$ within a cluster n .

The power of m -th ray in n -th cluster and in k -th frequency bin is given by $P_{n,m,k} = P_{n,k}/M$ for $m = 1, \dots, M$.

When $K_B > 1$:

The power of m -th ray in n -th cluster and in k -th frequency bin is given by $P_{n,m,k} = P_{n,k} \cdot \frac{P'_{n,m}}{\sum_{m=1}^M P'_{n,m}}$ for

$m = 1, \dots, M$, where:

$$P'_{n,m} = \exp\left(-\frac{\tau'_{n,m}}{c_{DS}}\right) \exp\left(-\frac{\sqrt{2}|\phi'_{n,m,AOA}|}{c_{ASA}}\right) \exp\left(-\frac{\sqrt{2}|\phi'_{n,m,AOD}|}{c_{ASD}}\right) \cdot \exp\left(-\frac{\sqrt{2}|\theta'_{n,m,ZOA}|}{c_{ZSA}}\right) \exp\left(-\frac{\sqrt{2}|\theta'_{n,m,ZOD}|}{c_{ZSD}}\right) \quad (110)$$

and c_{DS} , c_{ASA} , c_{ASD} and c_{ZSA} are respectively the intra-cluster delay spread and the corresponding intra-cluster angular spread that are given in Tables A1-16, A1-18, A1-20 and A1-22. The cluster zenith spread of departure is given by:

$$c_{ZSD} = \frac{3}{8} 10^{\mu_{lgZSD}} \quad (111)$$

with μ_{lgZSD} being defined in Tables A1-17, A1-19, A1-21 and A1-23.

Step 11: Generate XPRs

Generate the cross polarization power ratios (XPR) κ for each ray m of each cluster n . XPR is log-Normal distributed. Draw XPR values as:

$$\kappa_{n,m} = 10^{X/10} \quad (112)$$

where $X \sim N(\mu, \sigma_{XPR}^2)$ is Gaussian distributed with σ_{XPR} given from Tables A1-16, A1-18, A1-20 and A1-22. If n -th cluster is a deterministic cluster, $\mu = 10 \log_{10} \kappa_{l_{RT}}^{RT}$; otherwise, $\mu = \mu_{XPR}$ is given in Tables A1-16, A1-18, A1-20 and A1-22.

Step 12: Draw initial random phases

Draw random initial phase $\{\Phi_{n,m}^{\theta\theta}, \Phi_{n,m}^{\theta\phi}, \Phi_{n,m}^{\phi\theta}, \Phi_{n,m}^{\phi\phi}\}$ for each ray m of each cluster n and for four different polarisation combinations ($\theta\theta$, $\theta\phi$, $\phi\theta$, $\phi\phi$). The distribution for initial phases is uniform within $(-\pi, \pi)$.

In the LOS case, calculate an initial phase $\Phi_{LOS} = -2\pi d_{3D} / \lambda_0$ for both $\theta\theta$ and $\phi\phi$ polarisations, where d_{3D} is the 3D distance between transmitter and receiver and $\lambda_0 = c/f_c$ is the wavelength of the modelled propagation link.

Step 13: Generate channel coefficients for each cluster n and each receiver and transmitter element pair u, s .

In case of NLOS, the channel coefficients of ray m in cluster n for a link between Rx antenna u and Tx antenna s at time t in k -th frequency bin can be calculated as:

$$\begin{aligned}
 H_{u,s,n,m,k}(t) = & \begin{bmatrix} F_{rx,u,\theta}(\theta_{n,m,ZOA}, \phi_{n,m,AOA}) \\ F_{rx,u,\phi}(\theta_{n,m,ZOA}, \phi_{n,m,AOA}) \end{bmatrix}^T \begin{bmatrix} \exp(j\Phi_{n,m}^{\theta\theta}) & \sqrt{\kappa_{n,m}^{-1}} \exp(j\Phi_{n,m}^{\theta\phi}) \\ \sqrt{\kappa_{n,m}^{-1}} \exp(j\Phi_{n,m}^{\phi\theta}) & \exp(j\Phi_{n,m}^{\phi\phi}) \end{bmatrix} \\
 & \cdot \begin{bmatrix} F_{tx,s,\theta}(\theta_{n,m,ZOD}, \phi_{n,m,AOD}) \\ F_{tx,s,\phi}(\theta_{n,m,ZOD}, \phi_{n,m,AOD}) \end{bmatrix} \cdot \exp\left(j2\pi \frac{f_k}{c} (\hat{r}_{rx,n,m}^T \cdot \bar{d}_{rx,u} + \hat{r}_{tx,n,m}^T \cdot \bar{d}_{tx,s})\right) \\
 & \cdot \left(\sqrt{P_{n,m,k}} \cdot 10^{\frac{-(OL_{n,m}(f_k) + BL_{n,m}(f_k, t))}{20}} \right) \exp\left(j2\pi \frac{f_k}{c} \hat{r}_{rx,n,m}^T \cdot \bar{v}t\right)
 \end{aligned} \quad (113)$$

where $F_{rx,u,\theta}$ and $F_{rx,u,\phi}$ are the receive antenna element u field patterns in the direction of the spherical basis vectors, $\hat{\theta}$ and $\hat{\phi}$ respectively, $F_{tx,s,\theta}$ and $F_{tx,s,\phi}$ are the transmit antenna element s field patterns in the direction of the spherical basis vectors, $\hat{\theta}$ and $\hat{\phi}$ respectively. The delay (TOA) for ray m in cluster n for a link between Rx antenna u and Tx antenna s is given by:

$$\tau_{u,s,n,m} = \tau_n + \tau'_{n,m} - \frac{1}{c} \hat{r}_{rx,n,m}^T \cdot \bar{d}_{rx,u} - \frac{1}{c} \hat{r}_{tx,n,m}^T \cdot \bar{d}_{tx,s} \quad (114)$$

For the m -th ray within n -th cluster, $\hat{r}_{rx,n,m}$ is the spherical unit vector with azimuth arrival angle $\phi_{n,m,AOA}$ and elevation arrival angle $\theta_{n,m,ZOA}$, given by

$$\hat{r}_{rx,n,m} = \begin{bmatrix} \sin \theta_{n,m,ZOA} \cos \phi_{n,m,AOA} \\ \sin \theta_{n,m,ZOA} \sin \phi_{n,m,AOA} \\ \cos \theta_{n,m,ZOA} \end{bmatrix} \quad (115)$$

$\hat{r}_{tx,n,m}$ is the spherical unit vector with azimuth departure angle $\phi_{n,m,AOD}$ and elevation departure angle $\theta_{n,m,ZOD}$, given by

$$\hat{r}_{tx,n,m} = \begin{bmatrix} \sin \theta_{n,m,ZOD} \cos \phi_{n,m,AOD} \\ \sin \theta_{n,m,ZOD} \sin \phi_{n,m,AOD} \\ \cos \theta_{n,m,ZOD} \end{bmatrix} \quad (116)$$

Also, $\bar{d}_{rx,u}$ is the location vector of receive antenna element u and $\bar{d}_{tx,s}$ is the location vector of transmit antenna element s , $\kappa_{n,m}$ is the cross polarisation power ratio in linear scale. If polarisation is not considered, the 2x2 polarisation matrix can be replaced by the scalar $\exp(j\Phi_{n,m})$ and only vertically polarised field patterns are applied.

The Doppler frequency component is calculated from the arrival angles (AOA, ZOA), and the UT velocity vector \bar{v} with speed v , travel azimuth angle ϕ_v , elevation angle θ_v and is given by

$$\bar{v} = v \cdot [\sin \theta_v \cos \phi_v \quad \sin \theta_v \sin \phi_v \quad \cos \theta_v]^T \quad (117)$$

In case of LOS, the channel coefficient is calculated in the same way as in equation (113) except for $n=1$:

$$H_{u,s,n=1,k}(t) = \begin{bmatrix} F_{rx,u,\theta}(\theta_{LOS,ZOA}, \phi_{LOS,AOA}) \\ F_{rx,u,\phi}(\theta_{LOS,ZOA}, \phi_{LOS,AOA}) \end{bmatrix}^T \begin{bmatrix} \exp(j\Phi_{LOS}) & 0 \\ 0 & -\exp(j\Phi_{LOS}) \end{bmatrix} \begin{bmatrix} F_{tx,s,\theta}(\theta_{LOS,ZOD}, \phi_{LOS,AOD}) \\ F_{tx,s,\phi}(\theta_{LOS,ZOD}, \phi_{LOS,AOD}) \end{bmatrix} \\ \cdot \exp\left(j2\pi \frac{f_k}{c} (\hat{r}_{rx,LOS}^T \cdot \bar{d}_{rx,u} + \hat{r}_{tx,LOS}^T \cdot \bar{d}_{tx,s})\right) \cdot \left(\sqrt{P_{1,k}} \cdot 10^{\frac{-(OL_{n,m=1}(f_k) + BL_{n,m=1}(f_k,t))}{20}}\right) \exp\left(j2\pi \frac{f_k}{c} \hat{r}_{rx,LOS}^T \cdot \bar{v}t\right) \quad (118)$$

where the corresponding delay (TOA) for cluster $n=1$ for a link between Rx antenna u and Tx antenna s is given by $\tau_{u,s,n=1} = \tau_n - \frac{1}{c} \hat{r}_{rx,LOS}^T \cdot \bar{d}_{rx,u} - \frac{1}{c} \hat{r}_{tx,LOS}^T \cdot \bar{d}_{tx,s}$.

In equations (113) and (118), the oxygen absorption loss, $OL_{n,m}(f)$, for each ray m in cluster n at carrier frequency f is modelled as

$$OL_{n,m}(f) = \alpha(f)/1000 \cdot c \cdot \left[\tau_n + \tau'_{n,m} + \min_{l_{RT}}(\tau'_{l_{RT}}) \right] \text{ [dB]} \quad (119)$$

where:

- $\alpha(f)$ is the frequency dependent oxygen loss per distance (dB/km) characterized in § 5.1
- c is speed of light (m/s); and
- τ_n is the delay (s) obtained from Step 3 for deterministic clusters and from Step 5 for random clusters. $\min_{l_{RT}}(\tau'_{l_{RT}})$ is from the output of Step 3.

In equations (113) and (118), blockage modelling is an add-on feature. If the blockage model is applied, the blockage loss, $BLoss_{n,m}(f,t)$ in unit of dB, for each ray m in cluster n at carrier frequency f and time t is modelled in the same way as given in § 5.4; otherwise $BLoss_{n,m}(f,t)=0$ dB for all f and t .

Attachment 2 to Annex 1

Extension module below 6 GHz (alternative method of generating the channel parameters)

The purpose of the extension module is to generate parameters relating to the primary model below 6 GHz. The extension module provides additional level of parameter variability. In the primary module, SS and LS parameters are variables, and the extension module provides new parameter values for the primary module based on environment-specific parameters. The extension module below 6GHz is based on the time-spatial propagation model (TSP model) described in [27].

Table A1-45 shows key parameters of the TSP model and their applicable ranges.

TABLE A1-45
Key parameters in TSP model

Condition	Key parameter	Symbol	Applicable range
Frequency conditions	Carrier frequency (MHz)	f_c	400-6 000 MHz
	Bandwidth or chip rate (MHz)	B	0.5-100 MHz
City structures	Average building height (m)	$\langle H \rangle$	5-50 m:(height above the UT ground level)
	Road width (m)	W	5-50 m
	The average height of the buildings along the road	h_s	4-30m
Cell conditions	BS antenna height (m)	h_b	10-150 m:(height above the UT ground level)
	UT antenna height (m)	h_m	1-10 m
	Distance from the BS (m)	d	50-5 000 m
	The road angle	Θ	0-90 degrees:(the acute angle between the direction of the UT and the direction of the road)

1 Large scale parameters

1.1 NLOS scenarios

Formulas for NLOS scenarios, are given below:

a) Path-loss model

An empirical propagation loss formula is given as follows:

$$\begin{aligned} Loss_L(d) = & 101.04 - 7.1 \log W + 7.5 \log \langle H \rangle - \{24.37 - 3.7(\langle H \rangle / h_b)^2\} \log h_b \\ & + (43.42 - 3.1 \log h_b) \log(d / 1000) + 20 \log f_c - (3.2(\log(11.75 h_m))^2 - 4.97) \quad \text{dB} \end{aligned} \quad (120)$$

b) Power delay profile model

An empirical long-term path delay profile model $PDP_L(i, d)$ is given as follows:

$$PDP_L(i, d) = a(i) \left(-\{19.1 + 9.68 \log(h_b / \langle H \rangle)\} B^{-0.36 + 0.12 \log(h_b / \langle H \rangle)} (d / 1000)^{-0.38 + 0.21 \log(B)} \right) \log(1 + i) + 10 \log c(i) \quad (121)$$

where:

$$a(i) = \left(0.4 + (1 - 0.4) \exp \left[-0.2 \left(\langle H \rangle / h_b \right)^4 \right] \right) + \left(\left(\langle H \rangle / h_b \right) \left(1 - \exp \left[-0.4 \left(\langle H \rangle / h_b \right)^2 \right] \right) \right) (i / B) \quad (122a)$$

$$c(i) = \begin{cases} 1 & (i = 0) \\ \min \left(0.63, \left\{ 0.59 e^{-0.017B} + (0.017 + 0.0004B) \langle H \rangle \right\} e^{-\left((0.077 - 0.00096B) - (0.0014 - 0.000018B) \langle H \rangle \right) i} \right) & (0.5 \leq B \leq 50 \text{ Mcps}) \\ \min \left(0.63, \left\{ 0.59 e^{-0.0172B} + (0.0172 + 0.0004B) \langle H \rangle \right\} e^{-\left(0.0878 e^{-0.0218B} - (0.0014 - 0.000018B) \langle H \rangle \right) i} \right) & (50 < B \leq 100 \text{ Mcps}) \end{cases} \quad (i \geq 1) \quad (122b)$$

Here i represents the path number ($i = 0, 1, 2, \dots$) in the sense of an excess delay time normalized by the time resolution $1/B$.

The power delay profile normalized by the total power of all clusters is given by:

$$PDP_{LN}(i, d) = PDP_L(i, d) - 10 \log \left(\sum_{i=0} 10^{PDP_L(i, d)/10} \right) \text{ dB} \quad (123)$$

The path number i can be changed to the excess delay time τ (μs) by using the following relation:

$$\tau = i/B \Rightarrow i = \tau B \quad (124)$$

The delay profile $PDP_L(\tau, d)$ can be calculated as:

$$PDP_L(\tau, d) = a(\tau) \alpha(d) \log(1 + \tau B) + 10 \log c(\tau B) \text{ dB} \quad (125)$$

c) Departure angular profile model

An empirical long-term arrival angular profile model $AOD_L(\theta, d)$ is given as follows:

$$AOD_L(\theta, d) = 10 \log \left(1 + |\theta| / \left(-\frac{0.2d}{1000} + 2.1 \left\{ \left(\frac{\langle H \rangle}{h_b} \right)^{0.23} \right\} \right) \right)^{-((-0.015 \langle H \rangle + 0.63)d/1000 - 0.16 + 0.76 \log(h_b))} \quad (|\theta| \leq \theta_{max}) \text{ dB} \quad (126)$$

d) Arrival angular profile model

The arrival angular profile around the MT of each cluster is given as follows:

$$AOA_L(\theta, d) = \exp[-|\theta|/\theta_{AOA}] \quad (|\theta| \leq 180^\circ) \quad (127)$$

where θ_{AOA} denotes the angle spread of AOA.

e) ZOD and ZOA

The generation of ZOA and ZOD is as same as primary module.

1.2 LOS scenarios

Formulas for LOS scenarios are given in the following.

a) Path-loss model

The break point, B_p is defined by:

$$B_p = \frac{2\pi h_b h_m}{\lambda} \quad (128)$$

λ (m) denotes the wavelength and is given by $300/f_c$. An empirical propagation loss formula before the break point B_p is given as follows:

$$\begin{aligned} Loss_{LLOS}(d) \\ = 20 \log(4\pi d / \lambda) + (\min(0.03 \langle H \rangle^{1.72}, 10)) \log(d) - \min(0.044 \langle H \rangle^{1.72}, 14.77) + (0.002 \log \langle H \rangle) d \end{aligned} \quad (129)$$

An empirical propagation loss formula after the break point B_p , is expressed as follows:

$$Loss_{LLOS}(d) = 40 \log(1000d) - 20 \log h_b - 20 \log h_m + 5 \log f_c + 11 \log \langle H \rangle - 7.1 \log W - 2.45 \quad (130)$$

b) Power delay profile model

An empirical long-term delay profile model $PDP_{LLOS}(\tau, d)$ is given by:

$$PDP_{LLOS}(\tau, d) = \langle R \rangle \left(\frac{\sqrt{1+8 \cdot d \cdot (300\tau)/W^2 - 1}}{2} \right) + (-12) \cdot 10^{PDP_L(\tau, d)/10} \quad (131)$$

$\langle R \rangle$ is the average power reflection coefficient of building side wall and recommended to have value of 0.3 (−5 dB). $PDP_L(\tau, d)$ is given by the NLOS power delay profile model.

c) Departure angular profile model

An empirical long-term departure angular profile model $AOD_{LLOS}(\theta, d)$ is given by:

$$AOD_{LLOS}(\theta, d) = AOD_{L, direct}(\theta, d) + (-12) \cdot 10^{AOD_L(\theta, d)/10} \quad (132)$$

where:

- 1) BS facing right side of the street: (The formulas are interchangeable when BS facing the left side of the street.)

$$AOD_{L, direct}(\theta, d) = \begin{cases} 0 & (\theta \geq 0) \\ \langle R \rangle^{d|\theta|\pi/(180W)} & (\theta < 0) \end{cases} \quad (133a)$$

- 2) BS facing the end of the street:

$$AOD_{L, direct}(\theta, d) = \langle R \rangle^{d|\theta|\pi/(180W)} \quad (133b)$$

d) Arrival angular profile model

An empirical long-term arrival angular profile model $AOA_{LLOS}(\theta, d)$ with is given as follows:

$$AOA_{LLOS}(\theta, d) = AOA_{L, direct}(\theta, d) + (-12) \cdot 10^{AOA_L(\theta, d)/10} \quad (134)$$

where:

- 1) BS facing the right side of the street (The formulas are interchangeable when BS facing the left side of the street.):

$$AOA_{L, direct}(\theta, d) = \begin{cases} \langle R \rangle^{d|\theta|\pi/(180W)} & (\theta \geq 0) \\ \langle R \rangle^{(d|\theta|\pi/(180W))^{-1}} & (\theta < 0) \end{cases} \quad (135a)$$

- 2) BS facing the end of the street:

$$AOA_{L, direct}(\theta, d) = \langle R \rangle^{d|\theta|\pi/(180W)} \quad (135b)$$

e) ZOD and ZOA

The generation of ZOA and ZOD is as same as primary module.

1.3 XPD

XPD represents cross-polarization discrimination; its value (dB) is given by:

$$XPD_L = 15 - 10(1.5h_b / \langle H \rangle + 1)^{-0.35} \quad \text{dB} \quad (136)$$

1.4 Building penetration loss

The building penetration loss is as same as primary module.

1.5 Short-term variation

The short-term variation is generally caused by shadow effects. It can be assumed it follows a log-normal distribution with its power spectrum being:

$$P_s(f) = \begin{cases} \frac{\sigma_s^2}{2f_s} & (|f| \leq f_s) \\ 0 & (|f| > f_s) \end{cases} \quad (137)$$

where σ_s^2 is the average power of the short-term variation and is usually given by the normalized power of 1. Typical standard deviation of log-normal shadowing is set to 4.5 dB for macro-cell environments. f_s , the maximum frequency of the short-term variation, and depends on the environment and bandwidth as follows:

$$f_s = \nu / (110B^{-0.146} < H >^{0.058}) \quad (138)$$

where ν (m) is the speed of the UT.

1.6 Spreads and their variations of PDP, AOD and AOA in large scale parameters

a) The spread of PDP

The delay spread $\sigma_{PDP}(d)$ at distance d from the BS is expressed as:

$$\sigma_{PDP}(d) = \sqrt{\int_0^{\tau_{\max}(d)} \left(\tau - \frac{\int_0^{\tau_{\max}(d)} \tau 10^{PDP_L(\tau,d)/10} d\tau}{\int_0^{\tau_{\max}(d)} 10^{PDP_L(\tau,d)/10} d\tau} \right)^2 10^{PDP_L(\tau,d)/10} d\tau / \int_0^{\tau_{\max}(d)} 10^{PDP_L(\tau,d)/10} d\tau} \quad (139)$$

$\tau_{\max}(d)$ (μ s) is the maximum delay time determined from the threshold level ΔL_{th} (dB) (>0); it must satisfy the following equation:

$$PDP_L(\tau_{\max}(d), d) = -\Delta L_{th} \quad (140)$$

b) The spread of AOD

The angular spread $\sigma_{AOD}(d)$ at distance d from BS is expressed by:

$$\sigma_{AOD}(d) = \sqrt{\int_{-\theta_{\max}(d)}^{\theta_{\max}(d)} \left(\theta - \frac{\int_{-\theta_{\max}(d)}^{\theta_{\max}(d)} \theta \cdot 10^{AOD_L(\theta,d)/10} d\theta}{\int_{-\theta_{\max}(d)}^{\theta_{\max}(d)} 10^{AOD_L(\theta,d)/10} d\theta} \right)^2 \cdot 10^{AOD_L(\theta,d)/10} d\theta / \int_{-\theta_{\max}(d)}^{\theta_{\max}(d)} 10^{AOD_L(\theta,d)/10} d\theta} \quad \text{degrees} \quad (141)$$

$\theta_{\max}(d)$ (degrees) is the maximum AOD. It must satisfy the following equation:

$$AOD_L(\theta_{\max}(d), d) = -\Delta L_{th} \quad \text{and} \quad \min(60, \theta_{\max}(d)) \Rightarrow \theta_{\max}(d) \quad (142)$$

In the case of NLOS, $\theta_{\max}(d)$ can be easily obtained by equation (143):

$$\theta_{\max}(d) = \min[60, a(d)(10^{\Delta L_{th}/10\beta(d)} - 1)] \quad (\text{deg.}) \quad (143)$$

c) The spread of AOA

The angular spread $\sigma_{AOA}(d)$ at distance d from the BS is expressed as:

$$\sigma_{AOA}(d) = \sqrt{\int_{-\theta_{\max}(d)}^{\theta_{\max}(d)} \left(\theta - \frac{\int_{-\theta_{\max}(d)}^{\theta_{\max}(d)} \theta \cdot 10^{AOA_L(\theta,d)/10} d\theta}{\int_{-\theta_{\max}(d)}^{\theta_{\max}(d)} 10^{AOA_L(\theta,d)/10} d\theta} \right)^2 \cdot 10^{AOA_L(\theta,d)/10} d\theta / \int_{-\theta_{\max}(d)}^{\theta_{\max}(d)} 10^{AOA_L(\theta,d)/10} d\theta} \quad \text{degrees} \quad (144)$$

$\theta_{max}(d)$ (degrees) is the maximum AOA. It must satisfy equation (145):

$$AOA_L(\theta_{max}(d), d) = -\Delta L_{th} \quad (145)$$

In the case of NLOS, $\theta_{max}(d)$ can be easily obtained by the equation (146):

$$\theta_{max}(d) = \min[180, \phi_{AI} \ln(10^{\Delta L_{th}/10})] = \min[180, 0.23\phi_{AI}\Delta L_{th}] \text{ (deg.)} \quad (146)$$

1.7 Threshold parameter

Threshold parameter ΔL_{th} is 25dB.

1.8 Time-spatial profile in cluster

a) Delay profile in the i th cluster

An empirical delay profile model $PDP_I(l_{ik})$ normalized by the first arrival path's power in the i th cluster is given as follows:

$$PDP_I(l_{ik}) = e^{-l_{ik}/l_I} \quad (0 \leq l_{ik} \leq l_{I\max}) \quad (147)$$

where l_I and $l_{I\max}$ denote the average excess path distance and the maximum excess path distance in the cluster, respectively. On the other hand, the excess path distance l (m) can be changed to the access delay time τ (μ s) by using the relation of $l = 300\tau$. The delay profile model in the cluster, $PDP_I(\tau_{ik})$, can then be determined:

$$PDP_I(\tau_{ik}) = e^{-\tau_{ik}/\tau_I} \quad (0 \leq \tau_{ik} \leq \tau_{I\max}) \quad (148)$$

where τ_I and $\tau_{I\max}$ denote the excess average delay time and the maximum excess delay time in the cluster, respectively.

b) Departure angular profile in the i th cluster

An empirical departure angular profile model $AOD_I(\phi_{ik})$ with departure angle ϕ_{ik} in the i th cluster normalized by its central angular path's power is given as:

$$AOD_I(\phi_{ik}) = e^{-|\phi_{ik}| \left[\frac{2(300\tau_{I\max})}{(d+300\tau)} \cdot \left(\frac{180}{\pi} \right) \right]} \quad (0 \leq |\phi_{ik}| \leq \phi_{DI\max}) \quad (149)$$

c) Arrival angular profile in the i th cluster

An empirical arrival angular profile model $AOA_I(\phi_{ik})$ with arrival angle ϕ_{AI} in the i th cluster normalized by its central angular path's power is given by:

$$AOA_I(\phi_{ik}) = e^{-|\phi_{ik}|/\phi_{AI}} \quad (0 \leq |\phi_{ik}| \leq 180) \quad (150)$$

where ϕ_{AI} denotes the average arrival angle in the cluster. $\phi_{AI} = 180^\circ$ is a typical value.

2 Generation of reduced variability models based on TSP model

2.1 NLOS scenario

The reduced variability model is created by setting its key parameters. Each channel can be realized by the following procedure:

Step 1: Set test environments and key parameters

Set the Frequency conditions, City structure and Cell conditions on Table A1-45.

Step 2: Set the simulation conditions

Set the number of clusters for NLOS N_{path} and LOS N_{path}^S , level difference between the peak path's power and cut off power in NLOS scenario ΔL_{th} and LOS scenario ΔL_{th}^S .

Step 3: Generation of long-term TSP

Step 3.1: Generation of delay time

a) *Calculation of maximum delay time*

Convert excess distance l (m) into excess delay time τ (μ s) by equation (151):

$$\tau = l/(300/f_c) \text{ (}\mu\text{s)} \quad (151)$$

The maximum delay time can be calculated by considering ΔL_{th} as follows:

$$PDP_L(\tau_{LMax}, d) = -\Delta L_{th} \text{ (}\Delta L_{th} \geq 0\text{)} \quad (152)$$

b) *Dynamic delay time of each cluster*

The delay time interval $\Delta\tau_L$ is calculated as follows:

$$\Delta\tau_L = \tau_{LMax}/(N_{path} - 1) \quad (153)$$

The dynamic delay time is generated by using a random number:

$$\tau_L(i) = \begin{cases} 0 & (i=0) \\ i\Delta\tau_L + \Delta\tau_L(\text{Random}[0,1]-1/2) & (i=1,2,\dots,N_{path}-1) \end{cases} \quad (154)$$

where $\text{Random}[0,1]$ denotes a random value with uniform distribution between 0 and 1.

c) *Fixed delay time of each cluster*

Instead of the dynamic delay time, fixed delay time $\tau_L(i)$ is given as follows. Table A1-46 shows the normalized fixed delay time $\tau_L^N(i)$. The fixed delay time $\tau_L(i)$ is calculated by using Table A1-46 by:

$$\tau_L(i) = \tau_L^N(i) \left(\frac{\tau_{LMax}}{\tau_L^N(N_{path}-1)} \right) \text{ (}i=0,1,2,\dots,N_{path}-1\text{)} \quad (155)$$

TABLE A1-46
For the case of $N_{path} = 10$

Index number i	Normalized delay time $\tau_L(i)$	Normalized short term variation X_i^N with STD of 1 (dB)			
		$X_i^{N(1)}$	$X_i^{N(2)}$	$X_i^{N(3)}$	$X_i^{N(4)}$
1	0.0000	1.1458	1.2001	1.7690	0.48474
2	0.094923	0.75311	0.53053	0.060735	0.43398
3	0.19599	-0.70881	1.0645	-1.9474	0.058202
4	0.25979	1.6582	0.56882	0.20572	-2.0529
5	0.43136	-1.1183	-1.4115	-0.66017	-0.35828
6	0.50651	-0.78058	0.052757	-0.49775	0.48382
7	0.59619	-1.4302	-0.86393	1.2526	-1.0723
8	0.68790	0.91257	-0.66617	-0.33581	-0.37723
9	0.79581	-0.35092	1.0897	0.64893	1.8421
10	0.90483	-0.080880	-1.5649	-0.49588	0.55783

Step 3.2: Generation of relative power (without considering short-term variation)

The delay profile is normalized by the first cluster's power as follows:

$$PDP_L(i, d) \equiv PDP_L(\tau_L(i), d) \quad \text{dB} \quad (156)$$

Set the delay profile normalized by all clusters' power as 1(= 0 dB):

$$PDP_{LN}(i, d) = PDP_L(i, d) - 10 \log \left(\sum_{i=0}^{N_{path}-1} 10^{PDP_L(i, d)/10} \right) \quad \text{dB} \quad (157)$$

Step 3.3: Generation of departure angle

Set the departure angle of the i th cluster as follows:

$$\begin{aligned} &\theta_{LD}(i, d) \\ &= (-1)^i \left(-\frac{0.2d}{1000} + 2.1 \left\{ \left(\frac{\langle H \rangle}{h_b} \right)^{0.23} \right\} \right) (PDP_L(i\Delta\tau_L, d))^{-1/((-0.015\langle H \rangle + 0.63)d/1000 - 0.16 + 0.76 \log(h_b))} - 1 \quad \text{degrees} \quad (158) \\ &(i = 0, 1, 2, \dots, N_{path} - 1) \end{aligned}$$

Step 3.4: Generation of arrival angle

Set the arrival angle of the i th cluster as follows:

$$\theta_{LA}(i, d) = (-1)^i \cos^{-1} \left(\frac{(2d^2 + 2di\Delta\tau_L + (i\Delta\tau_L)^2) \cos \theta_{LD}(i) - 2d(d + i\Delta\tau_L)}{2d^2 + 2di\Delta\tau_L + (i\Delta\tau_L)^2 - 2d(d + i\Delta\tau_L) \cos \theta_{LD}(i)} \right) \quad \text{degrees} \quad (159)$$

Step 3.5: Generation of ZOA

The generation of ZOA is as same procedure as primary module.

Step 4: Generation of short-term variation

a) *Dynamic short term variation*

The dynamic short term variation of each cluster x_i follows an independent log-normal distribution as equation (160):

$$G(X_i) = e^{-X_i^2/2\sigma_s^2} / \sqrt{2\pi}\sigma_s \quad (160)$$

where σ_s represents the standard deviation of short term variation.

b) *Fixed short term variation*

Instead of the dynamic short-term variation, fixed short term variation X_i can be easily obtained based on Table A1-46 by using the following equation:

$$X_i = \sigma_s X_i^N \quad (i = 0, 1, 2, \dots, N_{path} - 1) \quad (161)$$

where X_i^N represents a normalized short term variation, with standard deviation of 1, obtained from Table A1-46. A typical standard deviation value for σ_s is 4.5 dB for macro-cell.

Step 5: Generation of relative power considering short-term variation

Instead of using the relative power without short-term variation as per Step 3.2, the relative power with short-term variation $PDP_{L\&S}(i, d)$ can be obtained as follows:

$$PDP_{L\&S}(i, d) = PDP_L(i, d) + X_i \quad \text{dB} \quad (162)$$

2.2 LOS scenario

Channel realizations for LOS are achieved by the following procedure:

Step 1 and Step 2: Set the conditions as per the NLOS case.

Step 3: Generation of direct clusters.

Direct clusters consist of three direct clusters, $p_{D,i}$ ($i = 0, 1, 2$). Generate delay time $\tau_{D,i}(i, d)$, arrival angle $\theta_{DA,i}(i, d)$, departure angle $\theta_{DG,i}(i, d)$ and relative power $PDP_{D,i}(i, d)$ normalized against the first cluster's power as follows:

$$\tau_{D,0}(0, d) = 0, \quad \tau_{D,1}(1, d) = W^2 / (300d), \quad \tau_{D,2}(2, d) = 3W^2 / (300d) \quad (\mu\text{s}) \quad (163)$$

$$\theta_{DA,0}(0, d) = 0, \quad \theta_{DA,1}(1, d) = 2W / d \cdot (180 / \pi), \quad \theta_{DA,2}(2, d) = -2W / d \cdot (180 / \pi) \quad \text{degrees} \quad (164)$$

$$\theta_{DD,0}(0, d) = 0, \quad \theta_{DD,1}(1, d) = W / d \cdot (180 / \pi), \quad \theta_{DD,2}(2, d) = 2W / d \cdot (180 / \pi) \quad \text{degrees} \quad (165)$$

$$PDP_{D,0}(0, d) = 1, \quad PDP_{D,1}(1, d) = 0.3, \quad PDP_{D,2}(2, d) = 0.1 \quad (166)$$

Step 4: Generation of scattering clusters

Step 4.1: Generation of delay time for scattering clusters

Scattering clusters consist of $(N_{path}^S - 3)$ clusters.

a) The PDP for scattering clusters is given by:

$$PDP_{L,scatter}(k, d) = PDP_L(k\Delta\tau_L, d) - 12 \quad \text{dB} \quad (167)$$

b) Calculation of maximum delay time

The maximum delay time is calculated to satisfy the following equation:

$$PDP_L(\tau_{LMax}, d) = -\Delta L_{th}^S \quad (\Delta L_{th}^S \geq 0) \quad (168)$$

Solving the above equation yields the maximum delay time τ_{LMax}^S . ΔL_{th}^S is generally given by $\Delta L_{th}^S = \Delta L_{th} - 12$ (dB).

Step 4.2: Generation of delay time, relative power, departure angle, arrival angle, and relative power considering short-term variation for scattering clusters.

This step is completely the same as *Step 3* to *Step 5* in the NLOS case.

Step 5: Generation of the power delay profile

Step 5.1: Generation of relative power

a) *Dynamic delay time of each cluster*

The delay time interval $\Delta\tau_L$ is calculated as follows:

$$\Delta\tau_L = \tau_{LMax} / (N_{path}^S - 3) \quad (169)$$

The dynamic delay time is generated by using a random number:

$$\tau_{LLOS}(i) = \begin{cases} \tau_{D,i}(i, d) & (i = 0, 1, 2) \\ (i-2)\Delta\tau_L + \Delta\tau_L (Random[0,1] - 1/2) & (i = 3, \dots, N_{path}^S - 1) \end{cases} \quad (170)$$

Where $Random[0,1]$ denotes a random value with uniform distribution between 0 and 1.

b) *Fixed delay time of each cluster*

Instead of the dynamic delay time, fixed delay time $\tau_L(i)$ is given as follows. Table A1-46 shows the normalized fixed delay time $\tau_L^N(i)$. When the number of clusters and the maximum delay time are given, the fixed delay time $\tau_L(i)$ is calculated by using Table A1-46 as follows:

$$\tau_{LLOS}(i) = \tau_{LLOS}^N(i-2) \left(\frac{\tau_{LLOSMax}}{\tau_{LLOS}^N(N_{path}^S - 3)} \right) \quad (i = 3, \dots, N_{path}^S - 1) \quad (171)$$

Step 5.2: Generation of relative power.

The delay profile considering the direct clusters and scattering clusters is given by:

$$PDP_{LLOS}(i, d) = \begin{cases} 10 \log(PDP_{D,i}(i, d) + 10^{PDP_{L,scatter}(0,d)/10}) & (0 \leq i \leq 2) \\ PDP_{L,scatter}(i-2, d) & (3 \leq i \leq N_{path}^S - 1) \end{cases} \quad \text{dB} \quad (172)$$

Set the delay profile normalized by the first cluster's power as follows:

$$PDP_{LLOS^N}(i, d) = PDP_{LLOS}(i, d) - PDP_{LLOS}(0, d) \quad \text{dB} \quad (173)$$

Step 5.3: Generation of departure angle

Set the departure angle of the i th cluster as follows:

$$\theta_{LDLOS}(i, d) = \begin{cases} \theta_{DD,i}(i, d) & (i = 0, 1, 2) \\ (-1)^{(i-2)} \alpha (PDP_L((i-2)\Delta\tau_L, d))^{-1/\beta} - 1 & (i = 3, \dots, N_{path}^S - 1) \end{cases} \quad \text{degrees} \quad (174)$$

Step 5.4: Generation of arrival angle

Set the arrival angle of the i th cluster as follows:

$$\theta_{LALOS}(i, d) = \begin{cases} \theta_{DA,i}(i, d) & (i = 0, 1, 2) \\ (-1)^{i-2} \cos^{-1} \left(\frac{(2d^2 + 2d(i-2)\Delta\tau_L + ((i-2)\Delta\tau_L)^2) \cos \theta_{LD}((i-2)) - 2d(d + (i-2)\Delta\tau_L)}{2d^2 + 2d(i-2)\Delta\tau_L + ((i-2)\Delta\tau_L)^2 - 2d(d + (i-2)\Delta\tau_L) \cos \theta_{LD}((i-2))} \right) & \text{degrees} \\ (i = 3, \dots, N_{path}^S - 1) \end{cases} \quad (175)$$

Step 5.5: Generation of ZOA

The generation of ZOA is as same procedure as primary module.

3 K-factor

In the NLOS case, the K -factor is basically $0 (= -\infty \text{ dB})$. In the LOS case, the K -factor of the direct cluster is determined by the ratio of the direct cluster's power to the first scattering cluster's power. On the other hand, the K -factor of the other scattering clusters is basically $0 (= -\infty \text{ dB})$.

4 Cross polarization

$PDP_{L\&S}^{VV}(i, d)$, $PDP_{L\&S}^{VH}(i, d)$, $PDP_{L\&S}^{HH}(i, d)$ and $PDP_{L\&S}^{HV}(i, d)$ express delay profiles with short-term variation due to vertical-to-vertical (VV), vertical-to-horizontal (VH), horizontal-to-horizontal (HH) and horizontal-to-vertical (HV) polarization, respectively as follows:

$$PDP_{L\&S}^{VV}(i, d) = PDP_L(i, d) + X_i^{(1)} \quad \text{dB} \quad (176a)$$

$$PDP_{L\&S}^{VH}(i, d) = PDP_L(i, d) - XPD_L + X_i^{(2)} \quad \text{dB} \quad (176b)$$

$$PDP_{L\&S}^{HH}(i, d) = PDP_L(i, d) + X_i^{(3)} \quad \text{dB} \quad (176c)$$

$$PDP_{L\&S}^{HV}(i, d) = PDP_L(i, d) - XPD_L + X_i^{(4)} \quad \text{dB} \quad (176d)$$

where $X_i^{(1)}$, $X_i^{(2)}$, $X_i^{(3)}$ and $X_i^{(4)}$ are independent random variables following log-normal distributions with standard deviation of σ_s . If these values are required to be fixed, these values can be generated by using the normalized variations $X_i^{N(k)}$ in Table A1-46 and the relation $X_i^{(k)} = \sigma_s X_i^{N(k)}$ ($k = 1, 2, \dots, 4$).

5 Generation of small scale parameters in clusters

Instantaneous time-spatial profiles can be generated by using small-scale parameters.

This process generation is applied for all NLOS clusters and all LOS scattering clusters.

Step 1: Simulation condition

N_p : number of paths in cluster.

Step 2: Generation of delay time

The delay time interval $\Delta\tau_I$ and delay time τ_I in a cluster are calculated respectively as follows:

$$\Delta\tau_I = \tau_{I\max} / (N_p - 1) \quad \mu\text{s} \quad (177)$$

$$\tau_I(k) = k\Delta\tau_I \quad (k = 0, 1, 2, \dots, N_p - 1) \quad \mu\text{s} \quad (178)$$

Here $\tau_{I\max}$ denotes the maximum delay time. It is typically $0.1 \mu\text{s}$ and $0 \mu\text{s}$ in the simplest case. Delay time $\tau_I(k)$ is recalculated at a time interval of $\Delta\tau_I$.

Step 3: Generation of relative power

The delay profile normalized by the first path's power in a cluster is expressed as:

$$PDP_I(k) = 10 \log(e^{-\tau_I(k)/\tau_{lav}}) = 10 \log(e^{-k\Delta\tau_I/\tau_{lav}}) \quad \text{dB} \quad (179)$$

where τ_{lav} is the average delay time of each cluster. τ_{lav} is typically 0.1 μs and 0 μs in the simplest case. Set the delay profile normalized by all paths' power in a cluster as follows:

$$PDP_{IN}(k) = PDP_I(k) - 10 \log\left(\sum_{k=0}^{N_p-1} 10^{PDP_I(k)/10}\right) \quad \text{dB} \quad (180)$$

Step 4: Generation of arrival angle

The arrival angle interval $\Delta\phi_{IA}$ is set as follows:

$$\Delta\phi_{IA} = 180/N_p \quad \text{degrees} \quad (181)$$

Set the arrival angle of the k th path in a cluster as follows:

$$\phi_{IA}(k) = (-1)^k k \Delta\phi_{IA} \quad (\text{deg.}) \quad (k = 0, 1, \dots, N_p - 1) \quad (182)$$

The arrival angle $\phi_{IA}(k)$ is calculated using the angular interval $\Delta\phi_{IA}$.

Step 5: Generation of departure angle

The departure angle interval $\Delta\phi_{ID}$ is set as follows:

$$\Delta\phi_{ID}(i) = \frac{\left(\frac{60}{(d+i \cdot (300/B))} \cdot \frac{180}{\pi}\right) \Delta\tau_I}{\tau_{lav}} \quad \text{degrees} \quad (183)$$

Set the departure angle in a cluster according to:

$$\phi_{ID}(i, k) = (-1)^k k \Delta\phi_{ID}(i) \quad (\text{deg.}) \quad (k = 0, 1, 2, \dots, N_p - 1) \quad (184)$$

Steps 1 to 3 yield the delay time, departure angle, arrival angle, and normalized relative power of paths in each cluster. Note that when τ_{Imax} is set to 0 μs , the fading model in the clusters becomes the well-known Clark model.

Attachment 3 to Annex 1

Channel impulse response generation when using antenna arrays

When antenna arrays are deployed at the transmitter and receiver, the impulse response of such an arrangement results in the vector channel. An example of this is given below for the case of a 2D antenna array.

$$\mathbf{H}_n^{\text{NLOS}}(t) = \sqrt{\frac{P_n}{M}} \sum_{m=1}^M \begin{bmatrix} F_{\text{rx},\theta}(\theta_{n,m,\text{ZOA}}, \phi_{n,m,\text{AOA}}) \\ F_{\text{rx},\phi}(\theta_{n,m,\text{ZOA}}, \phi_{n,m,\text{AOA}}) \end{bmatrix}^T \begin{bmatrix} \exp(j\Phi_{n,m}^{\theta\theta}) & \sqrt{\kappa_{n,m}^{-1}} \exp(j\Phi_{n,m}^{\theta\phi}) \\ \sqrt{\kappa_{n,m}^{-1}} \exp(j\Phi_{n,m}^{\phi\theta}) & \exp(j\Phi_{n,m}^{\phi\phi}) \end{bmatrix} \quad (185)$$

$$\times \begin{bmatrix} F_{\text{tx},\theta}(\theta_{n,m,\text{ZOD}}, \phi_{n,m,\text{AOD}}) \\ F_{\text{tx},\phi}(\theta_{n,m,\text{ZOD}}, \phi_{n,m,\text{AOD}}) \end{bmatrix} \mathbf{a}_{\text{rx}}(\theta_{n,m,\text{ZOA}}, \phi_{n,m,\text{AOA}}) \mathbf{a}_{\text{tx}}^H(\theta_{n,m,\text{ZOD}}, \phi_{n,m,\text{AOD}}) \exp(j2\pi\nu_{n,m}t)$$

$$\mathbf{H}_n^{\text{LOS}}(t) = \begin{bmatrix} F_{\text{rx},\theta}(\theta_{\text{LOS,ZOA}}, \phi_{\text{LOS,AOA}}) \\ F_{\text{rx},\phi}(\theta_{\text{LOS,ZOA}}, \phi_{\text{LOS,AOA}}) \end{bmatrix}^T \begin{bmatrix} \exp(j\Phi_{\text{LOS}}) & 0 \\ 0 & \exp(j\Phi_{\text{LOS}}) \end{bmatrix} \quad (186)$$

$$\times \begin{bmatrix} F_{\text{tx},\theta}(\theta_{\text{LOS,ZOD}}, \phi_{\text{LOS,AOD}}) \\ F_{\text{tx},\phi}(\theta_{\text{LOS,ZOD}}, \phi_{\text{LOS,AOD}}) \end{bmatrix} \mathbf{a}_{\text{rx}}(\theta_{\text{LOS,ZOA}}, \phi_{\text{LOS,AOA}}) \mathbf{a}_{\text{tx}}^H(\theta_{\text{LOS,ZOD}}, \phi_{\text{LOS,AOD}}) \exp(j2\pi\nu_{\text{LOS}}t)$$

where $\mathbf{a}_{\text{tx}}(\theta_{n,m,\text{ZOD}}, \phi_{n,m,\text{AOD}})$ and $\mathbf{a}_{\text{rx}}(\theta_{n,m,\text{ZOA}}, \phi_{n,m,\text{AOA}})$ are the tx and rx antenna array response vectors, respectively, of rays $m \in 1, \dots, M$ in cluster $n \in 1, \dots, N$, given by

$$\mathbf{a}_{\text{tx}}(\theta_{n,m,\text{ZOD}}, \phi_{n,m,\text{AOD}}) = \exp(j\frac{2\pi}{\lambda}(\mathbf{W}_{\text{tx}} \mathbf{r}_{\text{tx}}(\theta_{n,m,\text{ZOD}}, \phi_{n,m,\text{AOD}}))), \forall n, m, \quad (187)$$

$$\mathbf{a}_{\text{rx}}(\theta_{n,m,\text{ZOA}}, \phi_{n,m,\text{AOA}}) = \exp(j\frac{2\pi}{\lambda}(\mathbf{W}_{\text{rx}} \mathbf{r}_{\text{rx}}(\theta_{n,m,\text{ZOA}}, \phi_{n,m,\text{AOA}}))), \forall n, m, \quad (188)$$

where λ is the wavelength of carrier frequency f , $\mathbf{r}_{\text{tx}}(\theta_{n,m,\text{ZOD}}, \phi_{n,m,\text{AOD}})$ and $\mathbf{r}_{\text{rx}}(\theta_{n,m,\text{ZOA}}, \phi_{n,m,\text{AOA}})$ are the corresponding angular 3×1 spherical unit vectors of the tx and rx, respectively. \mathbf{W}_{tx} and \mathbf{W}_{rx} are the location matrices of the tx and rx antenna elements in 3D Cartesian coordinates.

The location matrices in the vectored impulse response above are provided for an antenna configuration that is a uniform rectangular array consisting of cross polarized antenna elements and arranged in the following manner.

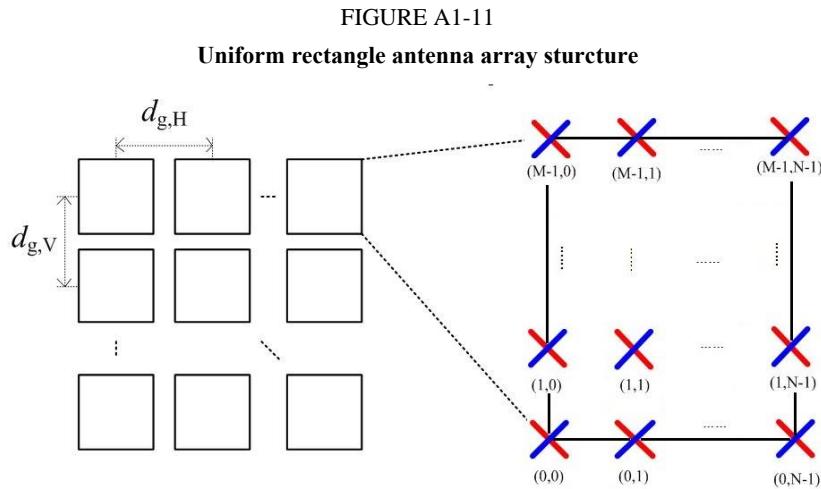
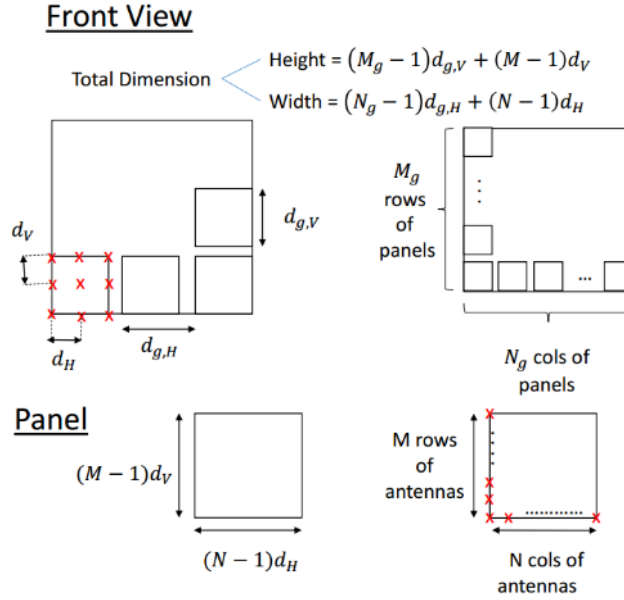


FIGURE A1-12

Illustration of distance of uniform antenna array



Here BS antenna model is a uniform rectangular panel array, comprising $M_g N_g$ panels, as illustrated above:

- M_g is number of panels in a column.
- N_g is number of panels in a row.
- Antenna panels are uniformly spaced in the horizontal direction with a spacing of $d_{g,H}$ and in the vertical direction with a spacing of $d_{g,v}$.
- On each antenna panel, antenna elements are placed in the vertical and horizontal direction, where N is the number of columns, M is the number of antenna elements with the same polarization in each column.
 - Antenna numbering on the panel illustrated in the figure assumes observation of the antenna array from the front (with x-axis pointing towards broad-side and increasing y-coordinate for increasing column number).
 - The antenna elements are uniformly spaced in the horizontal direction with a spacing of d_H and in the vertical direction with a spacing of d_v .
 - The antenna panel is either single polarized ($P=1$) or dual polarized ($P=2$).

In case of a single cross polarized antenna, $M = N = N_g = M_g = 1$. In case of a uniform rectangular array of cross polarized antennas with no sub arrays, $N_g = M_g = 1$.

For a URA configuration shown above, \mathbf{w}_{tx} or \mathbf{w}_{rx} is a matrix of $2NMN_g M_g \times 3$ dimension. Take \mathbf{w}_{tx} for example,

$$\mathbf{W}_{tx} = [\mathbf{w}_{ij}], \quad i=1,2,\dots,2NMN_g M_g, \quad j = 1,2,3. \quad (189)$$

where:

$$w_{ij} = \begin{cases} 0, & j=1 \\ \left[\left(i-1-2N \left[\frac{i-1}{2N} \right] \right) / 2 \right] \cdot d_H + \left[\left(i-1-2NN_g \left[\frac{i-1}{2NN_g} \right] \right) / (2N) \right] \cdot d_{g,H}, & j=2 \\ \left[\left(i-1-2NMN_g \left[\frac{i-1}{2NMN_g} \right] \right) / (2NN_g) \right] \cdot d_v + \left[\left(i-1-2NMN_g M_g \left[\frac{i-1}{2NMN_g M_g} \right] \right) / (2NMN_g) \right] \cdot d_{g,v}, & j=3 \end{cases} \quad (190)$$

The spherical unit vectors are:

$$\mathbf{r}_{rx,n,m} = \begin{bmatrix} \sin \theta_{n,m,ZOA} \cos \varphi_{n,m,AOA} \\ \sin \theta_{n,m,ZOA} \sin \varphi_{n,m,AOA} \\ \cos \theta_{n,m,ZOA} \end{bmatrix} \quad (191)$$

$$\mathbf{r}_{tx,n,m} = \begin{bmatrix} \sin \theta_{n,m,ZOD} \cos \varphi_{n,m,AOD} \\ \sin \theta_{n,m,ZOD} \sin \varphi_{n,m,AOD} \\ \cos \theta_{n,m,ZOD} \end{bmatrix} \quad (192)$$

The Doppler frequency component $v_{n,m}$ is calculated from the arrival angles (AOA, ZOA), UT velocity vector \bar{v} with speed v , travel azimuth angle φ_v , elevation angle θ_v and is given by

$$v_{n,m} = \frac{\mathbf{r}_{rx,n,m}^T \bar{v}}{\lambda_0} \quad (193)$$

$$\bar{v} = v \cdot [\sin \theta_v \cos \varphi_v \quad \sin \theta_v \sin \varphi_v \quad \cos \theta_v]^T \quad (194)$$

Annex 2

Linear cell layout configuration for high speed vehicular mobility at 500 km/h under Rural-eMBB test environment

1 Network layout

For high speed vehicular mobility configuration at 500 km/h which can be applied to high speed train, a linear base station placement along the rail track is considered. Two types of linear cell layout, 4 GHz/without relay and 30 GHz/with relay, are shown in Figs A2-1 and A2-2.

FIGURE A2-1

Sketch of linear cell layout for high speed vehicular mobility, TYPE 1 (4 GHz/without relay)

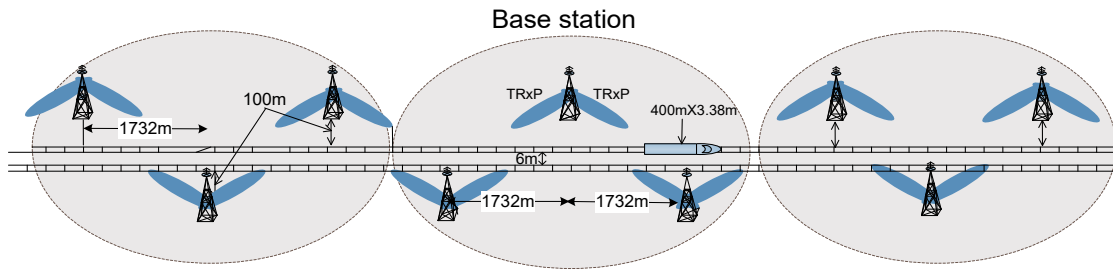
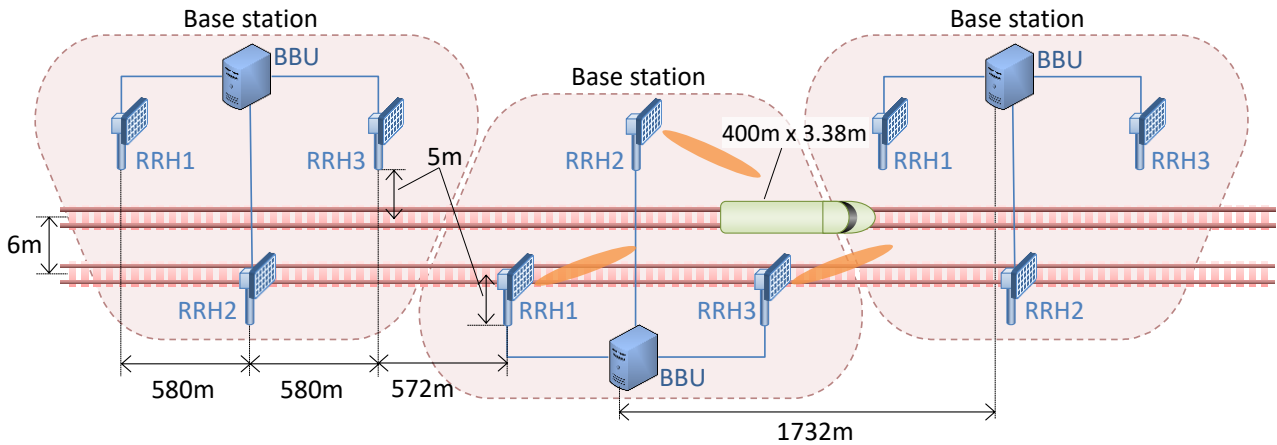


FIGURE A2-2

Sketch of linear cell layout for high speed vehicular mobility, TYPE 2 (30 GHz/with relay)



2 Additional configuration parameters

TABLE A2-1

Additional parameters for high speed vehicular mobility evaluation in linear cell layout, TYPE 1 (4 GHz/without relay)

Evaluation Parameters	Rural-eMBB linear cell, TYPE 1
Layout	High speed train layout as shown in Fig. A2-1
Carrier frequency for evaluation	4 GHz
UE speeds of interest	500 km/h
User density	20 UEs per carriage (carriage size: 400 m × 3.38 m)
UE height	2 m

TABLE A2-2

**Additional parameters for high speed vehicular mobility evaluation in linear cell layout,
TYPE 2 (30 GHz/with relay)**

Evaluation Parameters	Rural-eMBB linear cell, TYPE 2
Layout	High speed train layout as shown in Figure A2-2
Carrier frequency for evaluation	30 GHz
BS antenna height (RRH)	2.5 m
UE antenna height (Relay)	2.5 m
Total BS transmit power (RRH)	RRH 30 dBm for 80 MHz bandwidth e.i.r.p. should not exceed 69 dBm
UE power class (Relay)	27 dBm for 80 MHz bandwidth e.i.r.p. should not exceed 43 dBm
Number of UE antenna elements (Relay)	Up to 256 Tx/Rx
UE speeds of interest	500 km/h
User density	1 Relay for a train (100% of users in train 300 UEs per macro cell (assuming 1 000 passengers per high-speed train and at least 30% activity ratio))
BS Noise figure (RRH)	RRH 7 dB
UE Noise figure (Relay)	Relay 7 dB